Master's thesis

NTNU
Norwegian University of Science and Technology
Faculty of Engineering
Department of Structural Engineering

Kristin Enevoldsen

Rehabilitation of Cableway Posts, Longyearbyen

Master's thesis in Civil and Environmental Engineering
Supervisor: Anatoly Sinitsyn
Co-supervisor: Aleksey Shestov and Arne Aalberg
June 2022

Author

NTNU
Norwegian University of Science and Technology

UNIS
The University Centre in Svalbard

Kristin Enevoldsen

Rehabilitation of Cableway Posts, Longyearbyen

Master's thesis in Civil and Environmental Engineering
Supervisor: Anatoly Sinitsyn
Co-supervisor: Aleksey Shestov and Arne Aalberg
June 2022

Norwegian University of Science and Technology
Faculty of Engineering
Department of Structural Engineering

NTNU
Kunnskap for en bedre verden

Department of Structural Engineering
Faculty of Engineering
NTNU – Norwegian University of Science and Technology

ACCESSIBILITY

Open

MASTER THESIS Spring 2022

SUBJECT AREA: Frozen Ground Engineering	DATE: June 2022	NO. OF PAGES: 164

TITLE:

Rehabilitation of Cableway posts in Longyearbyen

Rehabilitering av taubanebukkene i Longyearbyen

BY:

Kristin Enevoldsen

SUMMARY:
The cableway posts of Longyearbyen are defined as cultural heritage. With increasing temperatures, the permafrost in which they are embedded is melting, causing settlements and deformations in the structures. To preserve the cultural heritage, rehabilitation of the foundations is needed. In this thesis we aim to describe the performance of the foundations in conditions of degrading permafrost and compare them to a proposed foundation solutions in which piles are used. By 2030, predictions show a permafrost temperature at 0°C near the depth of the authentic foundations. Our analysis shows that the active layer thickness of the permafrost will be above the minimum threshold of 1.5m by 2040. Findings show that within the next 40 years the active layer thickness will increase by 4m, and the ground temperature will be between -1°C and 0°C 10m below the surface. Simulations show a major shift in active layer thickness and permafrost temperatures after 2060, as changes in the hydrological regime contributes further and further into the future. A proposed functional solution wherein pile foundations are used, will have settlements increasing by 5cm for a 10m pile after 2040 for soil types
sand and silt. The functional solution of using 10m long piles will not perform well after 2040, as longer piles would need to be used by then to sufficient effective pile length. Due to the warm permafrost temperatures below the authentic foundation
(shallow foundation) rehabilitation with authentic solution is not recommended. Thereby, piles are recommended as a more reliable foundation
method due to the future scenarios.

RESPONSIBLE TEACHER:
Arne Aalberg, NTNU

SUPERVISOR(S):
Anatoly Sinitsyn, SINTEF
Aleksey Shestov, UNIS

CARRIED OUT AT: University center of Svalbard, UNIS

Preface

This master's thesis is based on the knowledge and interest gained during the Master of Civil and Environmental Engineering. The study is conducted at the Norwegian University of Science (NTNU) in Trondheim. The master thesis is conducted at the University Centre in Svalbard (UNIS) in collaboration with NTNU and SINTEF in Trondheim. Three supervisors are a part of this project, namely Aleksey Shestov (UNIS), Arne Aalberg (NTNU) and Anatoly Sinitsyn (SINTEF). The idea of studying the rehabilitation method of cableway posts in Longyearbyen was initiated by SINTEF in light of ongoing project "Polar Climate and Cultural Heritage – Preservation and Restoration Management" (PCCH-Arctic [38]).

Longyearbyen, 10-06-2022

Kristin Enevoldsen

Acknowledgements

I would like to thank my SINTEF supervisor, Anatoly Sinitsyn, for including me in his project (PCCH-Arctic) as a temporary colleague. Thank you for believing in me and guiding me through this process. Thank you, PCCH-working group, for including me in the meetings and listening to my advise regarding the project. Thank you, Yared Bekele from SINTEF, for support and guidance with Temp/W. Thank you, Christoffer Snaperud Christensen from SNSK, for trusting me with fieldwork and including me as a colleague in the project.

I would like to thank Trondheim for being such a great student town and Svalbard for opening up a new world of adventure! Thank you, Markus, for the support through the ups and downs during the thesis.

Finally, a huge thank you to my friends and family for always believing in me and encouraging me to take challenges, which led me to this amazing adventure at Svalbard.

The financial support for the fieldwork done in this thesis was obtained from Arctic Field Grant project (RiS ID 11866), via the Research Council of Norway.

Kristin Enevoldsen

Abstract

The cableway posts of Longyearbyen are defined as cultural heritage. With increasing temperatures, the permafrost in which they are embedded is melting, causing settlements and deformations in the structures. To preserve the cultural heritage, rehabilitation of the foundations is needed. In this thesis we aim to describe the performance of the foundations in conditions of degrading permafrost, and compare them to a proposed foundation solutions in which piles are used. By 2030, predictions show a permafrost temperature at 0 °C near the depth of the authentic foundations. Our analysis shows that the active layer thickness of the permafrost will be above the minimum threshold of 1.5 m by 2040. Findings show that within the next 40 years the active layer thickness will increase by 4 m, and the ground temperature will be between −1 °C and −0 °C 10 m below the surface. Simulations show a major shift in active layer thickness and permafrost temperatures after 2060, as changes in the hydrological regime contributes further and further into the future. A proposed functional solution wherein pile foundations are used, will have settlements increasing by 5 cm for a 10 m pile after 2040 for soil types sand and silt. The functional solution of using 10 m long piles will not perform well after 2040, as longer piles would need to be used by then to sufficient effective pile length. Due to the warm permafrost temperatures below the authentic foundation (shallow foundation) rehabilitation with authentic solution is not recommended. Thereby, piles are recommended as a more reliable foundation method due to the future scenarios.

Sammendrag

Taubanebukkene formidler byens gruvehistorie og er kategorisert som kulturminner. Grunnet varmere klima vil temperaturene i bakken øke og det aktive laget nå dypere. Dette fører til økte setninger og deformasjoner når permafrosten smelter. For å bevare kulturminnene er det, ved flere tilfeller, behov for rehabilitering av fundamentene. De økte temperaturene må taes hensyn til ved refundamentering av taubanebukkene. I denne oppgaven ønsker vi å beskrive ytelsen til de originale fundamentene ved økt aktivt lag, og sammenligne dem med en alternativ løsning, pele fundamentering. De originale fundamentene har en dybde på 1.5-3.0 m avhengig av størrelse på taubanebukken. Innen 2030 forventes det at temperaturen under de originale fundamentene vil øke og dermed nærme seg 0 °C. Våre beregninger viser at tykkelsen av det aktive laget vil, innen 2040, ha en minimums dybde på 1.5 m, som tilsvarer dybden av de grunneste taubane fundamentene. I løpet av de neste 40 årene vil det aktive laget øke til ca. 4 m, og temperaturen ved 10 m dybde vil være mellom −1 °C og 0 °C. Simuleringen indikerer et stort skifte i tykkelsen av det aktive laget rundt år 2060, ettersom endringer i det hydrologiske regimet bidrar ytterligere. En foreslått løsning vil være å rehabilitere med pele fundamenter. En standard pel med lengde 10 m vil ha setninger nær 5 cm i 2040, i jordtype sand og leire. En standard pel på 10 m vil ikke fungere godt etter 2040, grunnet temperaturer over −1 °C langs pelen, lengre peler er da anbefalt for å opprettholde nødvendig kapasitet. Grunnet økte temperaturer, som fører til økt aktivt lag og varmere permafrost temperaturer, anbefales det å gå vekk fra den originale fundamenteringsmetoden. Ved sammenligning av original fundamentering og pele fundamentering er peler anbefalt grunnet de fremtidige scenarioene.

Contents

List of Figures

List of Tables

Acronyms

ALT Active Layer Thickness.

HSE Health, safety and environment.

MAAT The Mean Annual Air Temperature.

MET The Norwegian Meteorological Institute.

NIKU The Norwegian Institute for Cultural Heritage.

NTNU The Norwegian University of Science and Technology.

PCCH-Arctic Polar Climate and Cultural Heritage- Preservation and Restoration Management.

SNSK Store Norske Spitsbergen Kullkompani AS.

UiO The University of Oslo.

UNIS The University Centre in Svalbard.

Symbolslist

ρ	Bulk density.
α	Thermal diffusivity.
θ	Temperature.
ν	Poisson's ratio.
ΔT	Temperature shift.
ϕ'	Friction angle.
$\tau_{a,i}$	Adfreeze friction strength of the soil material in layer i.
θ_{bf}	Freezing point depression.
θ_{bfp}	Freezing point depression for none saline soil.
ρ_d	Dry density.
γ_d	Dry unit weight.
ρ_s	Density Solids.
ρ_w	Density water.
A_S	Temperature amplitude, surface.
D_{sal}	Salinization.
E	Youngs modulus.
G_s	Specific gravity of soil materials.
L	Latent heat.
L'	Latent heat of fusion for water.
L_{eff}	Effective length of the pile.
M	Bending moment.
M	Modulus of deformation.
P_p	Adfreeze friction capacity.
Q	Force.
S_n	Salinity.
T	Moment of torsion.
$T_{S,t}$	Surface temperature at time t.
T_m	Mean annual air temperature.
T_z	Temperature at depth z.

V	Volume.
V_v	Volume voids.
V_w	Volume of water.
X	Thawing depth.
c_{vf}	Volumetric heat capacity for frozen soil.
c_{vu}	Volumetric heat capacity for unfrozen soil.
c_{vw}	Volumetric heat capacity for water.
e	Void Ratio.
e	Eccentricity.
g	Gravity of acceleration.
m	Mass.
m_s	Mass of soil.
m_w	Mass of water.
n	Porosity.
n_f	Freezing surface index.
n_t	Thawing surface index.
p	Periode.
r	Radius.
w	Water content.
a	Radius.

Chapter 1

Introduction

The town of Longyearbyen lies on the Svalbard archipelago, situated at 78 °N. Despite the harsh environment, the settlement was established in the late 19 th century due to the rich presence of coal in the area. As such, most of the infrastructure that makes up the town today was originally built to facilitate the industry involved in the mining and transportation of coal.

One of the most visible reminders of this industry throughout Longyearbyen are the cableway posts. Initially built to transport coal from the mines to the harbor, less than 200 posts remain and have become iconic symbols of the town and it's coal mining history. On Svalbard, all fixed and movable structures built before 1946 are considered cultural heritage and are automatically protected according to §39 in Svalbardmiljøloven, enacted in 2003 [24], [18]. Therefore, as the cableway posts were built to support industry existing before 1946, they are currently protected as cultural heritage.

In 2012, the Norwegian Institute for Cultural Heritage Management (NIKU) and Mycoteam conducted a condition evaluation of 50 cableway posts in Longyearbyen. The inspection revealed rot in the foundations and structural weaknesses. According to the cultural heritage Act, "If it comes to the knowledge of the authority appointed under the Act that a protected structure is falling into disrepair due to lack of maintenance, the structure may be inspected" [23] and "If there is a danger that the structure will fall into decay, the owner or user may be ordered, with the consent of the Ministry, to take steps within a reasonable time to prevent this" [23]. It was therefore necessary that rehabilitation works be undertaken by Store Norske Spitsbergen Kullkompani AS (SNSK), as the responsible body for managing cultural heritage on Svalbard on behalf of the Ministry of Trade, Industry and Fisheries. Due to the cultural heritage status of the cableway posts, it was integral that

they were reconstructed as they were originally built without any damage to the original structure in accordance with the Act which states, "no person shall initiate any measure which is liable to damage, destroy, dig up, move, change, cover conceal or in any other way unduly disfigure any monument or site that is automatically protected by law or to create a risk of this happening" [23]. From 2016-2021, SNSK received funding from the Svalbard Environmental Fund to rehabilitate and secure the cableway posts. During this time, five cableway posts were rehabilitated, but the method used was deemed both time-consuming, expensive and created some concerns regarding safety during the replacement process.

The primary goal of this thesis is to investigate the consequences of different rehabilitation solutions of the foundations of the cableway posts in Longyearbyen. In this thesis we will describe the consequences of predicted climate change, and how this potentially affects the structural design. We will also look into piles as a foundations method that might provide a superior rehabilitation solution. In order to create a general knowledge base which can be applied to future rehabilitation efforts, the calculations of settlements are done for three different generalized sizes of the cableway posts and three different soil types; sand, silt and clay. The thawing depth is calculated according to standard design calculations of ground thermal regime, and for predicted future scenarios with analytical and numerical calculations. For the authentic solution, (the original method of foundation), three foundation depths are analysed in order to visualize the importance of foundation depth. For piles, (the proposed method of foundation), the settlements are calculated while assuming a general pile length of 10m for the different thawing depths.

This thesis is a part of the PCCH-Arctic project. PCCH-Arctic, Polar Climate and Cultural Heritage- Preservation and Restoration Management is funded by the Research Council of Norway. The PCCH-Arctic project, with a project period from 2021 to 2024, aims to create a knowledge base for sustainable safeguarding and future use of cultural heritage in the Arctic under changing climate and demography conditions [38]. The project is a cooperation between SINTEF, The University of Oslo (UiO), The Norwegian Meteorological Institute (MET), The University Centre in Svalbard (UNIS) and the user partners Municipality of Longyearbyen (Longyearbyen Lokalstyre), SNSK and Kings Bay AS. One of the goals for the project is to develop and improve methodologies for restoration of foundations of the cableway posts in Longyearbyen. As this thesis is for the degree of Master of Civil and Environmental Engineering with a specialization in Structural Engineering,

the objective is to implement engineering design calculations to visualize the consequences of the choice of structural design.

The thesis is divided into 5 Chapters. The Introduction outlines the main scientific goal and scope of the thesis. Chapter 2 Background outlines the characteristics of the cableway posts and presents previous rehabilitation methods. It also describes the physics of permafrost and the calculation methods used for foundation solutions embedded in permafrost. Chapter 3 describes the fieldwork that has been conducted in cooperation with PCCH-Arctic. Chapter 4 presents the analytical and numerical calculations of the future temperature distribution in the ground. The bearing capacity of the authentic solution (shallow foundation) for frozen state is calculated. The settlements of the authentic solution and pile foundations are calculated based on the predicted thawing depths. In Chapter 5 the results and methods are discussed and recommendation for further work is given.

In addition, appendix is added. In this thesis Excel and Python were used for the analytical calculations, the python scripts are added in Appendix A. Appendix B presents data used in the calculations. Data from the fieldwork is added in Appendix C. Appendix D present the load calculations due to wind and self weight.

Chapter 2

Background

The primary goal of this thesis is to investigate the performance of different foundation solutions for the rehabilitation of the cableway posts in Longyearbyen in conditions of degrading permafrost. This chapter lays out the relevant theory related to this topic area. The chapter is divided into three sections. The first section presents the cableway posts and their foundation methods. It describes the need for rehabilitation and the previous rehabilitation processes. In section two theory of permafrost and the thermal regime are presented. The analytical and numerical approach of thawing depth calculations are introduced. The third section provides the basis of the relevant theory involved in the calculations (soil parameters, bearing capacity and settlements) performed in Chapter 4 of this thesis.

2.1 Cableway posts

There are approximately 268 cableway posts (according to SNSK) in the area of Longyearbyen. The structures were built around the third quarter of the 1900s as the coal mining industry developed. The purpose of the cableway was to transport the coal trolley from the mine to the harbor. The trolley could carry 700kg of coal [36] and was transported along the cableway via a hook. The cableway consists of several wooden structures named cableway posts, placed on a straight line from a mine to a cableway station. Height of the individual cableway post depend on the terrain profile, where each post was designed to assure desired elevation of the cableway line. From late 1980s, the practical function of the cableways has been replaced by trucks, however the structures remain in place and are protected as cultural heritage.

The cableway posts are wooden structures with steel connections, a sketch is shown in Figure 2.1. The wooden frame is constructed with steel joints in drilled holes. For simplicity, the structure is divided into an upper and lower structure as illustrated in Figure 2.1.

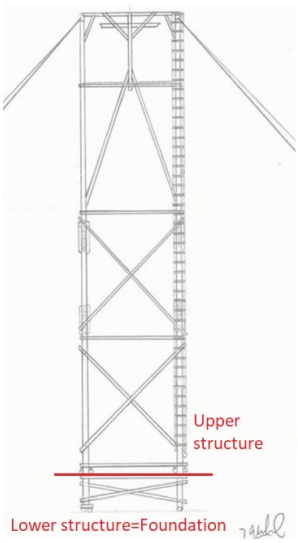

Figure 2.1: Sketch of a cableway post. The structure is divided into two sections: the upper structure and the lower structure. Figure is adapted from [7].

The upper structure consists of four vertical columns connected with horizontal beams and stiffened with diagonal struts. The upper structure is subject to wind and other weather induced actions.

The lower structure is the foundation. There are only two types of foundation [9]; a wooden frame foundation which was used on land, and concrete block foundation, which was used in rivers. The lower and the upper structures are connected in such a way that a movement in the lower section does not give an immediate effect on the upper structure. From a distance the cableway posts appear straight and in good condition, but when examined in detail, it is evident that in many cases the upper and the lower structures are tilted due to loads from different actions, from a slope process of solifluction [1]. Furthermore, several structures have large settlements in the permafrost and several structures have been destroyed by natural hazards such as avalanches, landslides and riverine flooding. In addition, the structural integrity of the posts seem to be significantly affected by timber rot in many cases. The rot mainly occurs in the area between air and ground (the zone from ground surface and ca. 30 cm down in the ground [10]). Figure 2.2 shows different cases of settlements and examples of damage to the structures.

[1]Solifluction: Gradual processes in which a mass moves down a slope related to freeze-thaw activity [44].

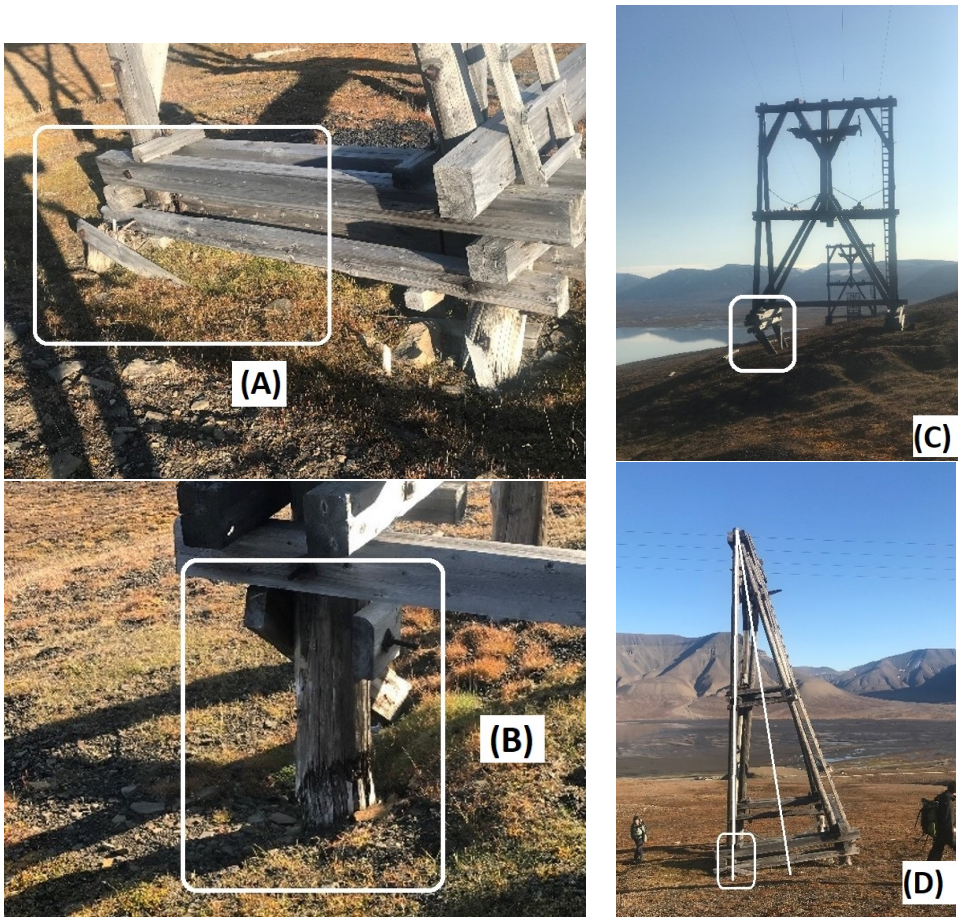

Figure 2.2: Pictures of cableway posts from field inspection, fall 2021. The pictures shows an example of vertical settlement (A), rot of the foundation (B), cableway subjected to slope processing (C) and uneven vertical settlement (D). The field inspection is further described in Section 3. Photos taken by Anatoly Sinitsyn and the author.

The cableway posts were built before geotechnical engineering was a recognized practice [26], hence the foundations were built relying solely on practical knowledge. The fact that they do not generally meet modern geotechnical standards is an important consideration in determining the most appropriate rehabilitation method.

Foundation

This thesis focuses on the the classical wooden frame foundation, which is most commonly found around Longyearbyen. The concrete block foundation used in the rivers will not be discussed in this thesis. The depth of the foundations differ. Measurements performed by SNSK when the cableway post labeled "A" in Figure 2.3 was rehabilitated, showed that it is approximately 35m tall and had a foundation depth of 2.5m [39]. For the cableway post labeled "B" in Figure 2.3, the depth was between 1-2m depending on the location relative to the slope [7]. This cableway post is approximately 24m tall. Both of these structures are among the tallest structures along the cableway. The foundation depth is only known for the structures which have been rehabilitated. For the remaining cableway posts, the depth can be assumed based on data from rehabilitated posts or by access to archive drawings, if possible.

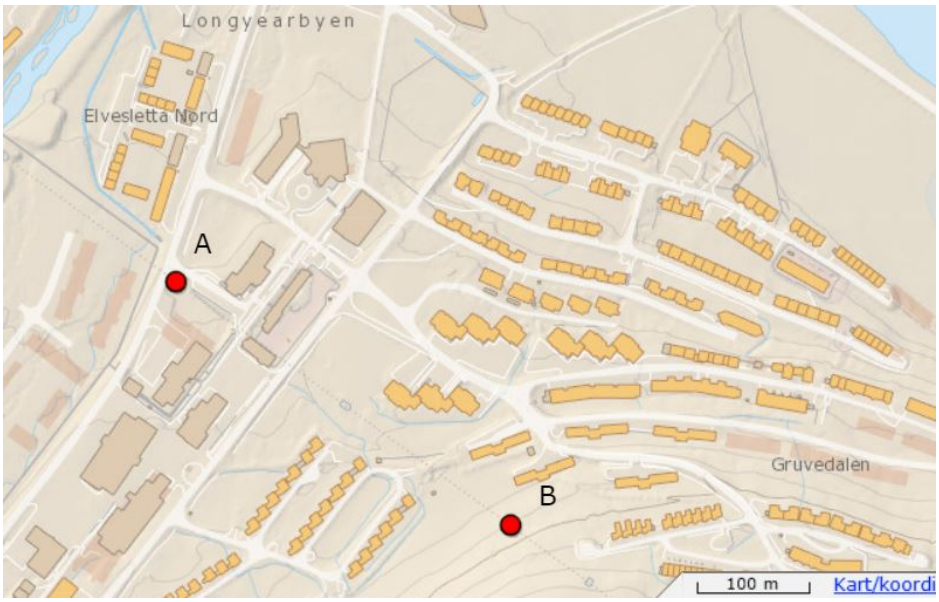

Figure 2.3: The map shows the location of two cableway posts in Longyearbyen that have been rehabilitated. Adapted from [33].

The depth of the active layer (further explained in Section 2.2) differs locally. In general it is approximately 1-2m in Longyearbyen [15]. Very limited knowledge exists regarding whether or not the foundations of the cableway posts are embedded in the permafrost layer, as illustrated with the green line in Figure 2.4. It is reasonable to assume that they were initially anchored in the permafrost layer when they where built, due to the historical knowledge of active layer depth and from the rehabilitation reports [7] [39]. The reports indicate that the depth of the foundation depends on the size of the structure, meaning it is reasonable to expect the foundation of smaller cableway posts to be shallower. Figure 2.4 presents a simplified illustration of the authentic (original) foundation of a cableway post. The coloured lines illustrates two different depths of the active layer, which is defined in Section 2.2. The foundation need to be in the permafrost (below the active layer). Foundations that are shallower than the active layer are more vulnerable to frost actions that occur due to melting and refreezing.

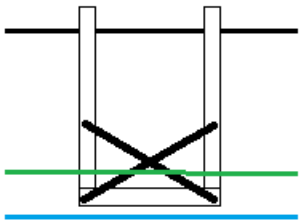

Figure 2.4: The illustration shows a sketch of the original foundation. The green and blue line illustrates the depth of the active layer for two different situations, with green representing the foundation partly embedded in the permafrost. The blue line representing the foundation embedded in the active layer, above the permafrost, which may be a situation for now or in the future (local conditions for each cableway post are unknown).

2.1.1 Previous rehabilitation

To highlight the need for discussion of different rehabilitation processes and foundation methods, this section examines the rehabilitation process for the cableway post labeled "B" in figure 2.3. The rehabilitation of the cableway post was finished in 2019, as shown in figure 2.5.

Figure 2.5: Picture of the cableway post in the alpine slope of Longyearbyen, marked with B in figure 2.3. The photo is taken after the rehabilitation. Photo taken by Author.

The cableway post is located in sloping terrain. Inspection of the terrain close to the structure indicates seasonally wet ground and soil affected by solifluction. The foundation of the cableway post was built by four beams connected to a wooden frame with backfill. The depth of the ground beams were 2 m and 1.5 m, and the diameter of the logs were approximately 30 cm [7]. The piles in the foundation had settled 20 cm to 35 cm horizontally for every 2 m in the vertical plane [7]. The bottom of the wooden frame was assumed to be below the active layer. The piles had some rot damage in the transfer zone from air to ground.

During the rehabilitation process the rotten piles and ground beams were replaced with new wooden logs, connected with angle sections of steel between the pile and the ground beams. The profiles were connected by M24 threaded rods and one-sided bulldog connections.

To carry the load during the rehabilitation process, support-piles were drilled down and connected to the original columns. Figure 2.6 shows how the support-piles were connected to the original structure with bolts of type

M24 8.8 [7]. The boreholes for the bolt connections were not accepted due to the conservation of cultural heritage. To replace the bolts, straps were used to connect the columns to the added supporting piles as shown in Figure 2.7.

Figure 2.6: Picture of a bolt connection between a column and a supporting pile. Picture adapted from [7].

Figure 2.7: The picture shows how the new solution with 8 straps as connection between the columns and the supporting piles were used. Picture adapted from [7].

After the supporting-piles were installed and connected to the columns of the cableway post, the soil around the foundation was removed. To protect the original foundation when removing the soil, only a chisel machine was used and the use of larger excavators was avoided. Piles and diagonal struts were replaced, and the structure was leveled using a jack. The original backfill

was put back in place and packed around the lower structure using a plate-vibrator.

The temporary structure needed to be designed for a horizontal wind load. Figure 2.8 presents illustrations that shows how the horizontal load Q may affect the temporary pile. The load creates a torsion when the force has an eccentricity to the cross-section as shown in the right sketch. The shear and axial forces are not shown in these sketches. The illustration in the middle shows how to calculate the bending moment for a fixed-ended beam. On the left is a sketch of the temporary structure subjected to an axial force N and a horizontal force Q.

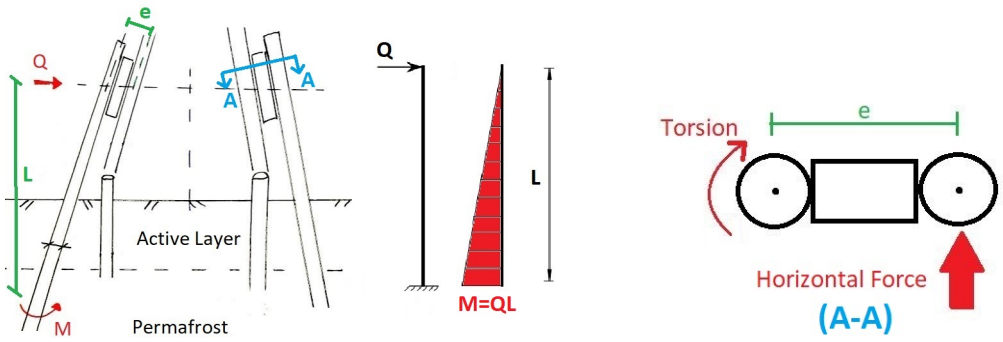

Figure 2.8: The sketches shows how the temporary structure is exposed to a bending moment and a torsion moment from a horizontal wind load. The distance between the horizontal force and the fixed end is marked with H and the horizontal wind force is marked Q. The eccentricity e due to the temporary supporting pile creates a moment of torsion T as illustrated in cross section A-A (right sketch). The sketches are adopted from [8].

The calculations done in the pre-project for this thesis (Appendix D), are summarized in Table 2.1. The table shows the bending moment capacity $M_{y,Rd}$ and torsion capacity T_{Rd} of the supporting piles. The capacities are compared to the bending moment M and moment of torsion T that the supporting piles are exposed to, due to the horizontal wind load. The utilization rate is the exposed load divided by the capacity.

	Capacity [kNm]	Load [kNm]	Utilization rate
Bending moment	17.0	66.0	389 %
Moment of torsion	5.4	13.0	245%

Table 2.1: Summary of capacity and loads in supporting piles for the cableway post in Gruvedalen (Longyearbyen).

The capacity is overloaded both due to bending moment and moment of torsion (Table 2.1). The utilization rates are above 100 % which means that the structure doesn't have adequate capacity to take the design loads, calling the safety of this method into question. This is one of the main reasons that the rehabilitation process needs to be improved. The wind calculations are based on a return period of 50 years, so whilst the rehabilitation currently remains stable, to ensure on-going safety and longevity.

The calculation of torsion capacity looked at the cross-section of the supporting piles and not at the connection between the original column and the supporting pile. Design of bolt connections are described in Eurocode 5 [29], but a connection such as the one with straps shown in Figure 2.7 is not described in Eurocode. To use that kind of connection the design might rely on experiments and tests that would prove the capacity of the connection.

The rehabilitation method as described above was deemed both time consuming and expensive. The recommendation is to find a new and improved rehabilitation solution which is designed according to Eurocode.

2.1.2 Future rehabilitation methods

Due to the aforementioned limitation of the previous rehabilitation methods, it is recommended to utilise improved solutions for future rehabilitation operations. A dialogue between SNSK and AF Decom AS has resulted in the idea of possibly separating the upper structure from the lower structure during the rehabilitation process. This will yield access to an excavator and accelerate the rehabilitation process. This approach will also remove the safety risks associated with working underneath a temporary structure. A challenging aspect of this method is ensuring the lifting operation is performed without any damage to the original structure, in accordance with the cultural heritage act. AF Decom AS have performed experiments to find an adequate method and plan to lift the upper-structure using a modified machine with a steel grid and different straps connected to the columns of the structure.

Two different solutions for foundations have been considered, by SNSK, regarding the future rehabilitation. In this thesis the two solutions will be investigated and compared, to determine which foundation design is the most suitable.

Solution A:

Rehabilitate the authentic solution with the original design, but with increased foundation depth. This option requires two lifting operations. The upper structure needs to be moved and anchored properly on a temporary place while the rehabilitation take place. With the upper structure removed, the foundation becomes accessible for an excavator. The safety conditions are improved since the risks associated with working under a temporary structure are removed. This can be expected to increase working efficiency and decrease the costs. The foundation would be restored and placed deeper if needed. When the rehabilitation is finished the upper structure would then be lifted back on the foundation and reconnected to it.

Solution B:

Replace the authentic solution with foundation on piles. Four piles would be drilled into the ground next to the original foundation (within the line of the cableway). The piles would be anchored deeper in the permafrost layer and therefore provide more stability than Solution A. The upper structure will be lifted directly to the new foundation piles. This solution only needs one lifting operation and no need of working under a temporary structure.

2.2 Permafrost

Permafrost, i.e. permanently frozen area, is characterised as areas where the ground temperature stays below zero degree Celsius throughout the whole year, for more than one year. Figure 2.9 illustrates how the ground in permafrost is divided into an active layer, a permafrost layer and unfrozen ground below. The permafrost layer is frozen and has a temperature below 0° C throughout the whole year. In Svalbard, the permafrost layer is typically about 100m thick in major valley bottoms and up to 400-500m thick in the high mountains [32].

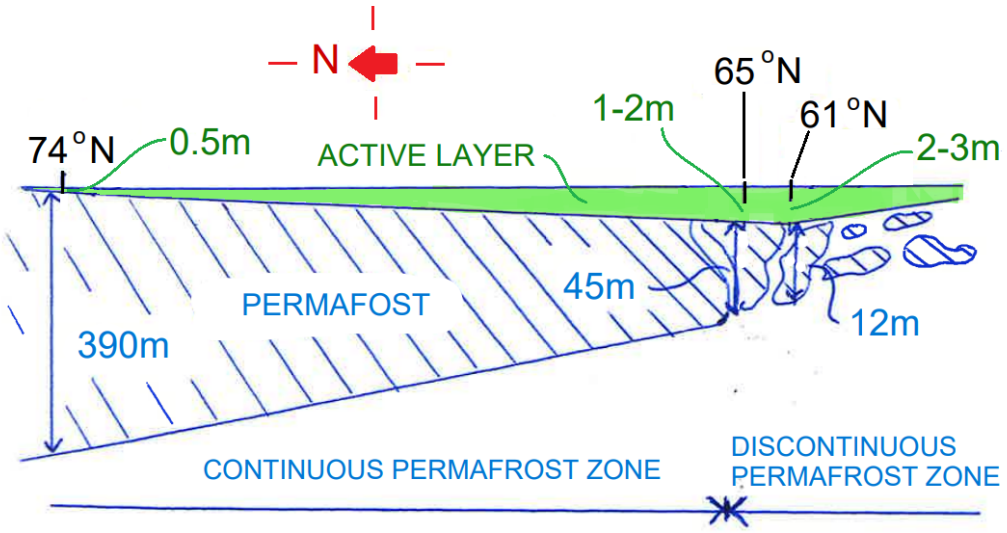

Figure 2.9: Illustration of how the thickness of the permafrost layer increases with latitude, and the difference between discontinuous and continuous permafrost. The illustration is not in scale, adapted from [2], edited by author.

In areas with permafrost, the upper layer (active layer) thaws during summer. When the soil is thawing and freezing, the bearing capacity of the active layer changes during the seasons. Due to the seasonal changes, the strength of the active layer is unreliable, therefor the strength of the active layer is neglected. This is why the depth of the active layer is important for the design of foundations in permafrost. The depth of the active layer varies locally, but in general it is approximately 1-2 m in Longyearbyen and the surrounding area. The active layer in Longyearbyen has been observed to be increasing by approximately 25-30cm since 1998 [10]. In areas close to water flows (rivers, melting rivers, lakes etc.) the heat from the unfrozen water

increases the temperature in the ground and thereby increases the depth of the active layer. This, alongside the insulating properties of snow cover, explain much of the local variation in active layer [5].

2.2.1 Snow cover

Snow acts as a thermal insulator. When covered by snow, heat-flow from the ground, from ice on the ocean, lake, or from a man-made structure, is greatly reduced. In studies of permafrost or ground freezing, accurate values of the thermal conductivity of the snow cover are essential. They are also critical in assessing the potential impact of changes in snowfall resulting from climate change. [22]

Snow provides an insulating effect on ground temperature as it is comprised of frozen water and air and thereby has a low thermal conductivity. According to [5] the insulation capacity of the snow changes little with snow depth above 0.25m. The ground is cooled down during the winter, the snow cover slows down the heat exchange between the ground and the atmosphere and hinders heat from escaping from the permafrost soils during the winter [17]. As such, increased precipitation and snow cover may increase the active layer thickness the following summer and increase the permafrost temperatures at depth. Therefore, from an engineering perspective, snow cover has a negative impact on the service lifetime of the foundation or structure founded on permafrost. [17]

2.2.2 Ground thermal regime

In the Arctic region, the mean annual ground surface temperature is warming three times as fast as the global average, the mean ground surface temperature is projected to be $10°C$ above the 1985-2014 average for a high-emission scenario by 2100 [1]. The permafrost temperature has warmed by $2-3°C$ since the 1970s and the seasonally thawed top layer continues to extend deeper [1].

The temperature in the air changes much faster than the temperature in the ground. This is due to the thermal properties of the ground. Substantial changes of air temperature affect the thermal regime in the ground, but with a time lag. Figure 2.11 visualises how the temperature range is bigger for the surface than the ground and that the temperature range through a year, decreases with depth. The ground temperatures are determined by air temperature, soil thermal properties and heat flow from the interior of the earth. The annual temperature can be represented as a sinus function (visualised in Figure 2.10):

$$T_{S,t} = T_m + A_s sin(\frac{2\pi t}{p}) \tag{2.1}$$

The surface temperature $T_{S,t}$ is time dependent and is the sum of the mean annual air temperature T_m and the air temperature amplitude A_s multiplied with a sinus function. The factor p is the period of 365 days. The factor t is the number of days from when the temperature is T_m to $T_{S,t}$. Figure 2.10 shows how temperature along the y-axis change sinusoidal over time t (x-axis). The temperature at a certain depth has the same period as the the surface temperature but with a smaller amplitude and a time lag. The size of the time lag increases with the depth. The thermal conductivity of the material decides the time lag and the amplitude at a certain depth. The time lag is the time it takes for the surface temperature to warm up/cool down the soil to the equal temperature.

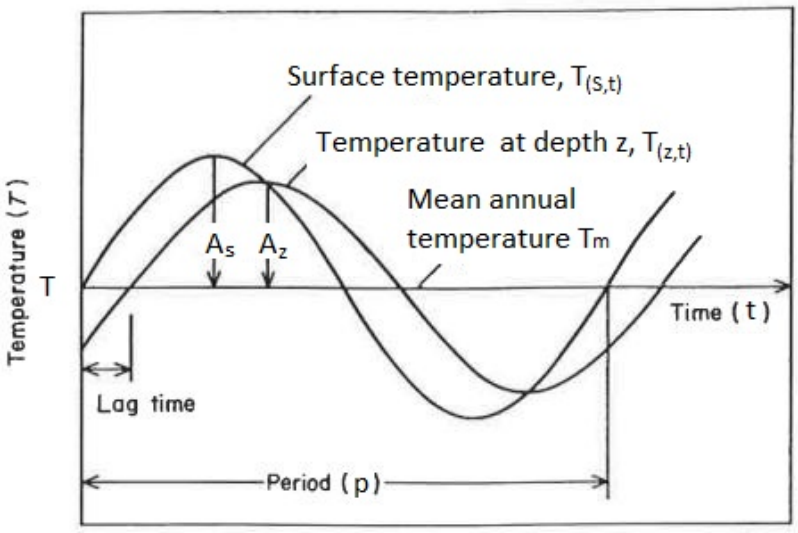

Figure 2.10: Surface and ground temperature, sinus function. The x-axis represents the time t and the y-axis represents the temperature T. The factor A is the amplitude of the temperature with index s for the surface or z for a certain depth z. Adapted from [2]

The range of annual ground temperature variations for any depth below the ground surface can be represented by a "trumpet-curve" [2]. A trumpet curve is shown in Figure 2.11, and is a plot of the warmest and coldest temperatures in the ground (through a year). At any time during the seasonal variation in temperature in the ground, the actual temperature at any depth and time, will lie between the boundaries of the trumpet curve [16]. The trumpet curve is a graph with temperature on the x-axis and depth below surface on the y-axis. In the center of the graph is the mean annual temperature T_m. The trumpet-curve is based on Equation 2.2.

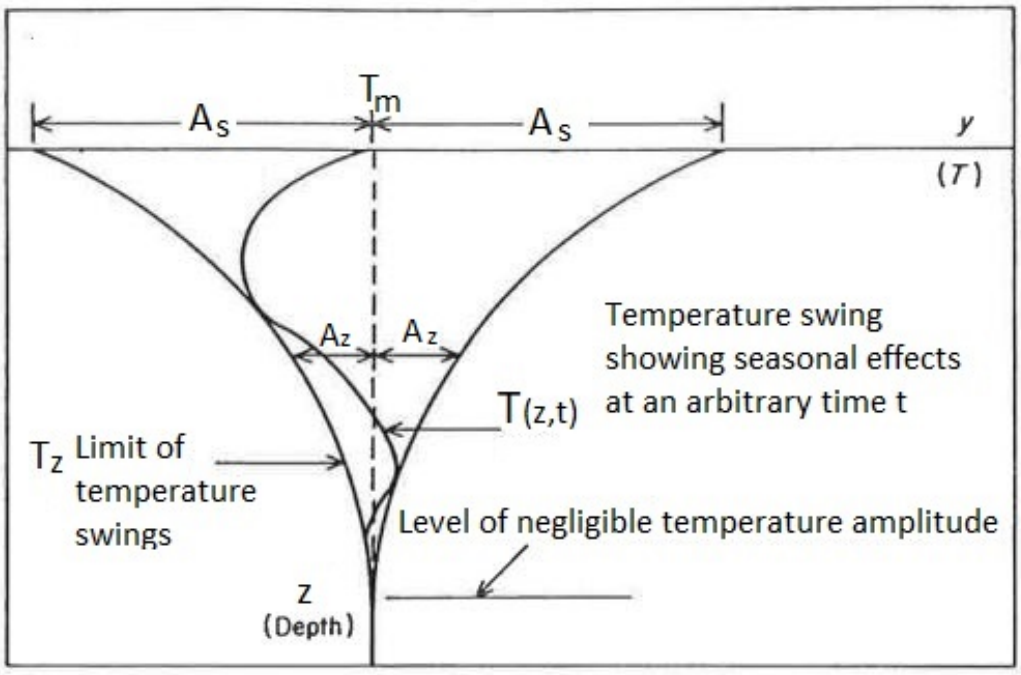

Figure 2.11: Temperature attenuation with depth. The x-axis represents the temperature and is located at the ground surface. The y-axis represents the ground depth. Adapted from [2].

Figure 2.12 shows a temperature profile in frozen soil with a geothermal gradient $\frac{dT}{dz}$. The geothermal gradient takes into account the heating from the interior of the earth. The mean temperature T_m is thereby not constant over the depth, but increases. The boundaries of the trumpet curve represent the maximum and minimum temperature curves. From an engineering design point of view, using the maximum temperature is a conservative approach since the actual temperature profile in the ground at any time during the year will be colder or equal to the calculated maximum temperature curve [16].

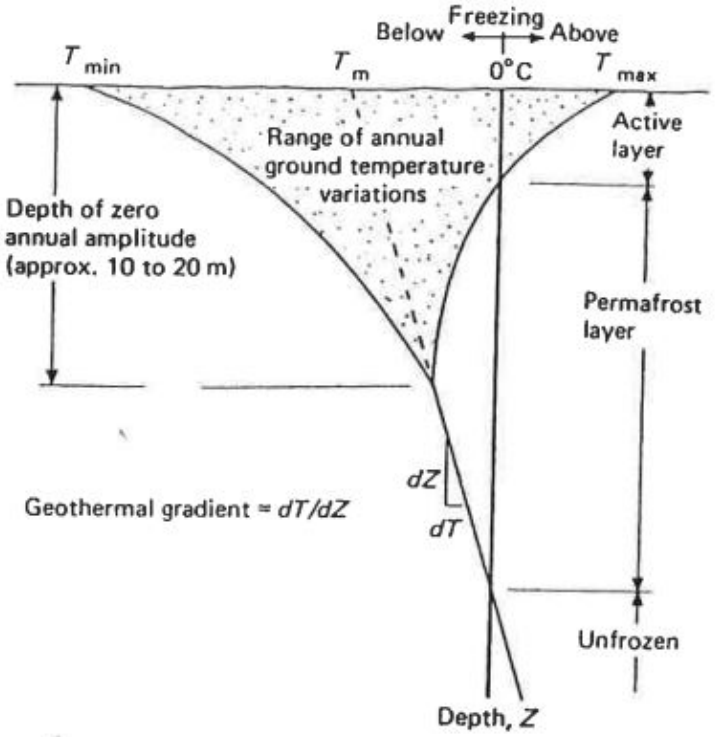

Figure 2.12: Temperature attenuation with depth, with decreasing mean ground temperature T_m due to the temperature gradient $\frac{dT}{dz}$. The x-axis represents the temperature and is located at the ground surface. The y-axis represents the ground depth. Adapted from [2].

The maximum and minimum soil temperature T_z at a certain time and depth is

$$T_z = T_m \pm A_s e^{\sqrt{\frac{\pi}{\alpha_u p}}} \tag{2.2}$$

where α_u is the soil thermal diffusivity. Equation 2.2 assumes a uniform soil with no heat flow from the earth's interior, thereby no thermal gradient. The thermal diffusivity α is further explained in Section 2.3.1.

2.2.3 Analytical solution

The depth of the active layer thickness ALT, also known as the thawing depth, can be calculated by using Stephan's formula [2]:

$$X = \sqrt{\frac{2 \cdot k_f}{L} \cdot I_{st} \cdot \alpha} \tag{2.3}$$

Here, the thawing depth X depends on the thermal conductivity of the frozen soil k_f, the latent heat of the soil L and the surface thawing index I_{st}. The factor $\alpha = 86400$ seconds/day gives the correct unit in the expression. Stephan's formula assumes a uniform soil type and doesn't consider the initial temperature of the ground. It assumes the entire ground to be frozen every year, thereby that every year is independent. This is a simplified approach. In Stephan's formula it is assumed that the latent heat of soil moisture is the only heat that must be added when thawing the soil [2]. Thermal energy stored in the form of volumetric heat, which need to increase as soil temperatures increases above freezing point, is neglected.

The air thawing index I_{at},

$$I_{at} = \sum_{days}^{season} (T_{T>0}) \tag{2.4}$$

is the degree days with air temperature above $0°C$ ($T_{T>0}$), summarized over a year. The opposite of the air thawing index is the air freezing index I_{af}:

$$I_{af} = \sum_{days}^{season} (T_{T<0}) \tag{2.5}$$

The air freezing index is an index that describes how cold a winter has been. It can be calculated by summarizing mean temperature for days with temperature ($T_{T<0}$) below 0° C over a winter season. The unit of air freezing/ thawing index is degree-days.

The freezing index can be useful in evaluating permafrost, seasonally frozen ground distribution and depth of the frost line. Permafrost will remain frozen if the absolute value of the air freezing index, I_{af}, is above 3900 freezing degree days annually, and the Mean Annual Air Temperature (MAAT) is below or equal to $-3°$ C [2].

The standard design index is defined as the average air thawing (or freezing) index of the three warmest summers (or coldest winters) during the most

recent 30 years of record [2]. The design thawing index is used to calculate the depth of the active layer which is further used in settlement calculations. To calculate the thawing depth in Equation 2.3, the surface thawing index I_{st} is used instead of the air thawing index I_{at}. The mean annual ground surface temperature (1cm depth) differs from mean annual air temperatures with no constant difference [2]. Air temperature data is generally more accessible than surface temperature data. Thereby is an empirical based n-factor approach, to simulate the complex relation of air temperature and climate, commonly used when sufficient site-specific data is not available [17]. The air freezing/thawing indexes can be transformed into surface freezing/thawing indexes by use of n-surface factors:

$$n_t = \frac{I_{st}}{I_{at}} \tag{2.6}$$

$$n_f = \frac{I_{sf}}{I_{af}} \tag{2.7}$$

The surface factors are defined as the ratio between the surface thawing/freezing index and the air thawing/freezing index. Approximate n-factors for different surface conditions, are presented in Table 2.2. The radiation from the sun contributing to warming of the surface is governed by the surface albedo[2] [14]. The albedo differs for different conditions and thereby influence the n-factor.

Surface	n_t	n_f
Snow	-	1.0
Pavement free of snow and ice	-	0.9
Sand/Gravel	2.0	0.9
Gravel	1.3-2.0	0.6-1.0
Asphalt pavement	1.4-2.3	0.29-1.0
Turf	1.0	0.5
Vegetation and 6-cm soil stripped, mineral surface	1.22	0.33

Table 2.2: Approximate n-surface factors for several surface types. Adapted from [2].

[2]Albedo is the measure of diffuse reflection of solar radiation out of total solar radiation. The albedo scale from 0, corresponding to a black body that absorbs all incident radiation, to 1, corresponding to a body that reflects all incident radiation [42].

2.2.4 Numerical simulation, Temp/W

Models can be divided by temporal, thermal and spatial criteria [14]. The choice of model depends on the availability of data and the research question. For this study, a local site-specific model, simulating the transient development of the thermal regime from an initial condition to the future is of interest. Reasonable assumptions and/or simplifications of the reality are often inevitable.

The finite element software product Temp/W, delivered by GeoStudio Products [11], is used for this study. Temp/W is used to model the thermal changes in the ground due to environmental changes [11]. The temperature profile, thereby the thawing depth, is calculated with Temp/W. In a numerical geotechnical simulation the soil space is discretized into many small elements [4]. The points forming the geometry are defined as nodes. The unknowns (temperature in this case) have to be calculated at all the nodes [4]. The governing differential equations are transformed into algebraic equations that must be written as many times as there are nodes in the discretized soil space [4]. This usually yields a large number of equations organized in matrix form. From this matrix equations, the unknowns must be extracted and solved for, this often requires an inverse process of the main matrix and can only be done by computers [4].

In addition, boundary conditions often change with time and cannot always be defined with certainty at the beginning of an analysis [11]. The analysis is described in Section 4.3 and more information about the program can be read in the manual for Temp/W [11].

2.3 Design calculations

Geotechnical design in Europe is based on Eurocode, a standardized set of codes and regulations developed by the European Commission for Standardization [17]. The main design philosophy in the Eurocode is that the structure should function according to the design assumptions during the service lifetime of the structure [17].

In permafrost regions, design service lifetime is typically shorter than the general requirement of Eurocode, due to creep effect in ice-rich foundation soils [17]. On Svalbard, a 30-year design service-life of foundations is standard engineering practice [17]. The purpose of the Eurocode is to create a safe and approved design strategy for structures. The loads and resistances are represented with characteristic values. Characteristic values are specified fractile-values of the corresponding probability distribution functions. Eurocode 0 presents the basis of structural design, while Eurocode 1 describes forces exerted onto structures[19].

Eurocode 7 presents the basis of geotechnical design. The Eurocode does not include a frozen ground approach. Thereby frozen ground engineering need to be based on knowledge from other sources. There are different approaches and studies of frozen ground engineering. In this study an European approach based on creep parameters and a Russian approach based on deformation modulus is used.

The lifetime of a structure depends on its design working life category as defined by Eurocode 0. The design lifetime of structures are presented in Table 2.3 [27].

Design working life category	**Design service lifetime**	**Type of structures**
1	10 years	Temporary structures
2	10 to 25 years	Replaceable structural parts, for example gantry girders and bearings
3	15 to 30 years	Agricultural or similar structures
4	50 years	Buildings and other common structures
5	100 years	Monumental buildings or structures, bridges and other civil engineering structures

Table 2.3: Design service lifetime of structures from [27]. Temporary structures have the lowest defined working life, while monuments and important infrastructure have the longest defined design lifetime.

The design values of geotechnical parameters are given by Equation 2.2 of Eurocode 7:

$$X_d = \frac{X_k}{\gamma_M} \tag{2.8}$$

Here, the factor X_k is the characteristic value and γ_M is the partial factor for the soil parameter. According to Table NA.A.4 in Eurocode 7, the partial factors are equal to 1.0 for resistance of piles and anchors. [30]

2.3.1 Soil parameters

A soil sample consists of a certain amount of minerals, liquids and gases. The ratio of these depends on the grain size and how graded the soil is, this affects the soil strength and behavior, thereby the soil parameters. The soil parameters are divided into physical, thermal and mechanical properties.

Physical properties

The density, ρ, is the mass per volume of the soil [kg/m^3]. The unit weight γ is the weight of the soil per volume [N/m^3]. The density and unit weight for a specific part of the soil sample are usually marked with an index, as shown in the equation for dry density, ρ_d:

$$\rho_d = \frac{\gamma_d}{g} = \frac{m_s}{V} \tag{2.9}$$

Here the index d indicates that the density only takes into account the part of the sample that is dry, i.e. no liquid or gas. The factor g is the gravity acceleration (9.81 m/s^2) and γ_d is the dry unit weight of the soil. The factor m with index s is the mass of the solids and V is the total volume of the sample. The solids density is given by:

$$\rho_s = G_s \cdot \rho_w = \frac{m_s}{V_s} \tag{2.10}$$

where G_s is the specific gravity of soil materials and ρ_w is the density of water. A common value for G_s is 2.65 for granular soil and 2.7 for clay [2]. The factor V_s is the volume of the solids within the sample. Table 4.2 shows typical values of dry unit weight, γ_d for three different soil types.

Soil	$\boldsymbol{\gamma_d}$ [kN/m^3]
Clean uniform sand	18.1
Standard Ottawa sand	16.0
Silty sand	19.2
Clay	16.5
Colloidal clay	14.1

Table 2.4: Dry unit weight γ_d for various soil types. Table adapted from [2].

The porosity n express how much of the total volume that is void. It is given by the following equation:

$$n = (1 - \frac{\rho_d}{\rho_s}) \cdot 100\% \tag{2.11}$$

The voids can be filled with gasses or liquids. Table 2.5 shows the expected range of porosity for sand, silt and clay. Adding Equation 2.9 and Equation 2.10 into Equation 2.11 the porosity can be expressed as $n = \frac{V_v}{V}$ where V_v is the volume of voids.

Soil	$\boldsymbol{n}$ [%]
Sand	30-50
Silt	40-55
Clay	40-60

Table 2.5: Experiential range of values of the porosity, n, for sand, silt and clay. Adapted from [12].

The water content,

$$w = \frac{m_w}{m_s} \cdot 100\% \tag{2.12}$$

is a mass ratio. The factor m_w is the mass of water in the soil sample. Typical values for Norwegian clays are $20 - 40\%$ [12].

The density ρ is the mass per volume, but can also be expressed by the dry density ρ_d and the water content as shown in the following equation:

$$\rho = \rho_d \cdot (1 + w) \tag{2.13}$$

Salinity

Water within soil pores may contain dissolved salts which increase the freezing-point depression[3] and will increase the unfrozen water content [2]. Increased salinity reduces the ice content, thereby reducing the frozen soil strength and increasing its creep rate at a given temperature [2].

As water freezes, solutes are forced into a smaller and smaller volume of solution. The temperature shift, ΔT, for a salinity, S_n, can be estimated using the following equation [2]:

$$\Delta T = T_k(\frac{S_n}{1.00 + S_n}) \tag{2.14}$$

Here S_n is the salinity in [g/l] (or ppt) and T_k is a reference temperature equal to 57 °C for sea salt [2]. Since the salinity leads to an decreased freezing point, saline soil might contain unfrozen water even though the temperature is below 0 °C. The unfrozen water content w_u can be calculated according to the following equation adapted from [2]:

$$w_u = w(1 - ln(\frac{\theta/\theta_{bf}}{0.72 \cdot \theta/\theta_{bf}} + 1)) \tag{2.15}$$

Here θ is the temperature of the frozen soil and θ_{bf} is the freezing point depression for the saline soil. Figure 2.13 illustrates how the salinity affects the unfrozen water content at different temperatures. The freezing point depression θ_{bf} can be expressed by the following equation:

$$\theta_{bf} = 1.86 \sum m_i i_i \theta_{bfp} \tag{2.16}$$

where m_i is the molarity of pore moisture, conditioned due to salt i. The molarity m_i can be defined from concentration of pore solution, salinity C_{pc} and molecular weight of salt M:

$$m_i = \frac{C_{pc} \cdot 1000}{M}$$

For salt, NaCl, the molecular mass is 58 g/mol and the isotonic coefficient i of salt is 2. The factor θ_{bfp} is the freezing point depression temperature of non-saline soil and depends on the water content. Table 2.6 shows the freezing point depression θ_{bfp} for different types of soil with specific water contents.

[3]Freezing-point depression is a drop in the temperature at which a substance freezes, caused when a smaller amount of another, non-volatile substance is added, such as salt [43].

Soil	$\boldsymbol{w}$	$\boldsymbol{\theta_{bfp}}$[°C]
Sand	0.10	-0.05
Silty clay 1	0.30	-0.10
Silty clay 2	0.20	-0.90
Clay poly-mineral	0.35	-0.25

Table 2.6: Freezing point depression θ_{bfp} of non-saline soil. SIlty clay 1 and 2 are two ypes of silty clay with different water content w. Values adapted from [20].

In Russian literature the amount of salt is expressed by salinization, D_{sal}, instead of salinity, S_n, as in North-American practice [41]. These two index properties, may, however, convert to each other by using the following equations:

$$D_{sal} = \frac{m_{salt}}{m_s} \tag{2.17}$$

$$S_n = \frac{m_{salt}}{m_w} \tag{2.18}$$

Both expressions are a mass ratio where the indexes express what it is a mass m of. The total mass of the solution $m_{solution}$ is a sum of the mass of fresh water m_w and mass of salts m_{salt}. The correlation between the salinity S_n and the salinization D_{sal} is,

$$S_n = \frac{D_{sal}}{D_{sal} + w} \tag{2.19}$$

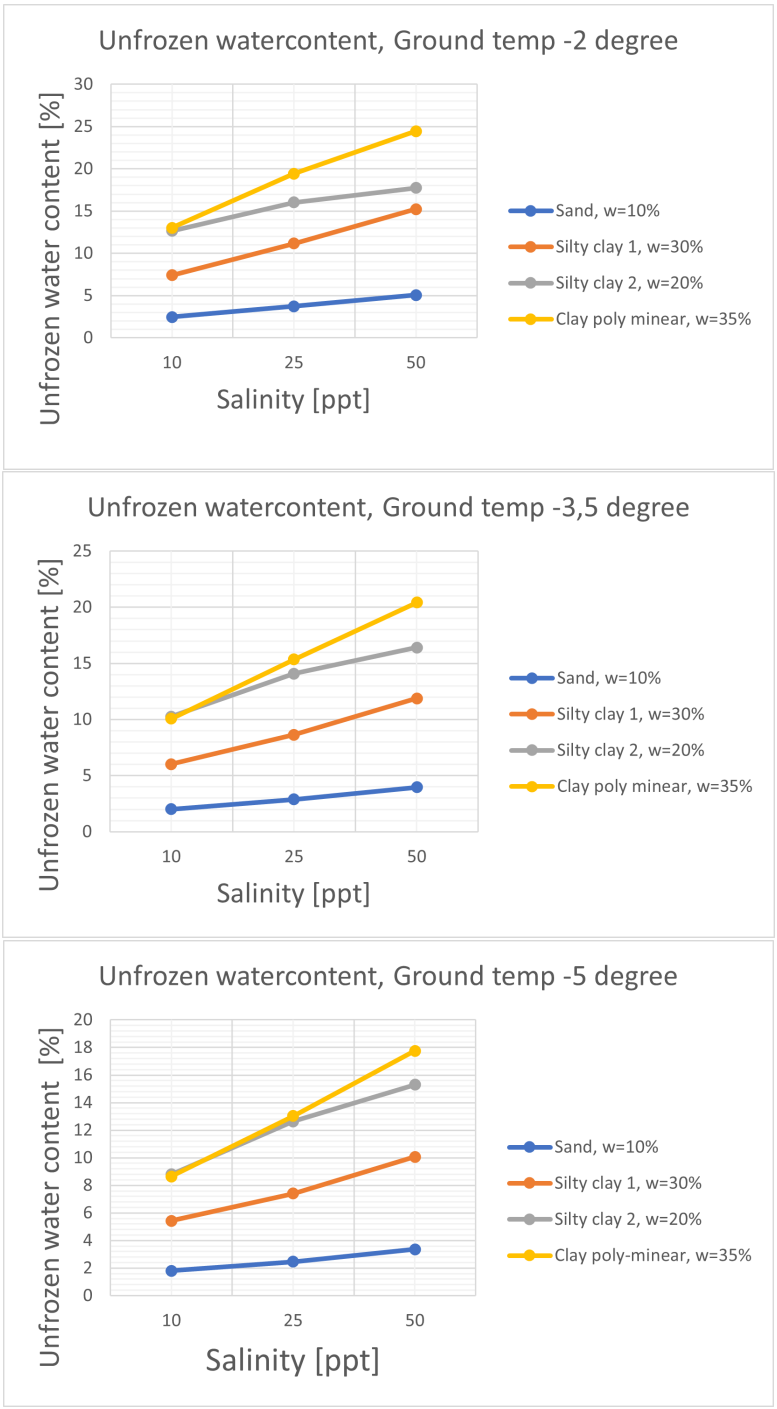

Figure 2.13: The graphs shows how the unfrozen water content w_u change due to salinity S_n and temperature θ for the soil types presented in Table 2.6. .

Thermal properties

The response of soil materials to thermal changes require an understanding of their thermal properties; heat capacity c, thermal conductivity k, latent heat L and thermal diffusivity α [2].

Specific heat capacity c_p [kJ/kg °C] describes the amount of energy needed to raise the temperature of one kilo of soil by one degree Celsius. The changes in temperature are greater for a material with low heat capacity for the same amount of supplied energy. The specific heat capacity of a material increases with increasing temperature. Also, with increasing density the heat capacity of a given soil increases. Furthermore, the heat capacity increases as the moisture content increases. This can be explained by comparing the specific volumetric heat capacity of water which is 4.2 [MJ/(m^3 °C)] to most dry soils which have a heat capacity between 1 and 1.5 [MJ/(m^3 °C)] around 0 °C [14]. The volumetric heat capacity of unfrozen and frozen soils can be estimated by the following equations [2]:

$$c_{vf} = \frac{\rho_d}{\rho_w} \cdot (0.17 + 1.0 \cdot \frac{w_u}{100} + 0.5 \cdot \frac{w - w_u}{100}) \cdot c_{vw} \tag{2.20}$$

$$c_{vu} = \frac{\rho_d}{\rho_w} \cdot (0.17 + \frac{1 \cdot w}{100}) \cdot c_{vw} \tag{2.21}$$

where w_u is the unfrozen water content. The factor c_{vw} is the volumetric heat capacity of water at 0 °C, 4.187 MJ/m^3 °C. The factor 0.17, 1.0 and 0.5 correspond to specific heats of soil, water and ice.

The amount of heat energy absorbed when a unit mass of ice is converted into a liquid at the melting point is defined as its latent heat of fusion [2]. The latent heat of fusion for water at 0 °C, L', is 333.7 kJ/kg. The latent heat L of the soil is described by the following equation:

$$L = \rho_d \cdot L'(\frac{w - w_u}{100}) \tag{2.22}$$

The thermal conductivity k is the rate of heat transferred through a material. The amount of heat transferred by conduction[4] in soil increases as dry density increases and as its degree of saturation increases. Similarly, the process of freezing and thawing leads to soil composition and structural changes with consequent changes in the soil's thermal conductivity [2]. Figure 2.14 and Figure 2.15 show how the thermal conductivity changes due to water content w, saturation S_r and dry unit weight γ_d, for frozen and unfrozen state.

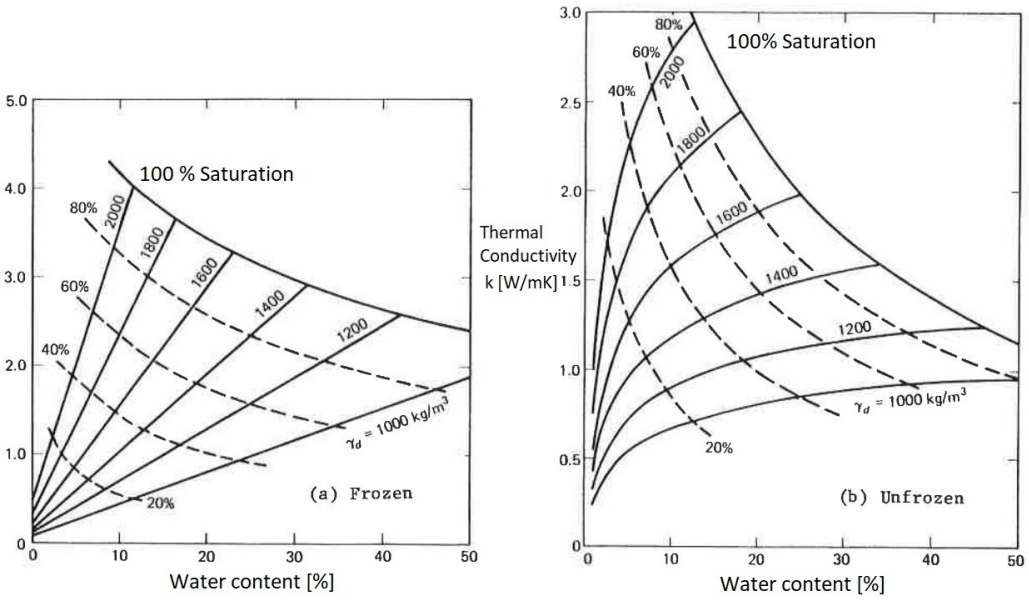

Figure 2.14: Average thermal conductivity for Sand and gravels. The y-axis in the left and right Figure represent the thermal conductivity k [W/mK] for frozen k_f and unfrozen k_u state. Adapted from [2].

[4]Conduction is the process where heat energy is transmitted through collisions between neighbooring atoms of molecules [2].

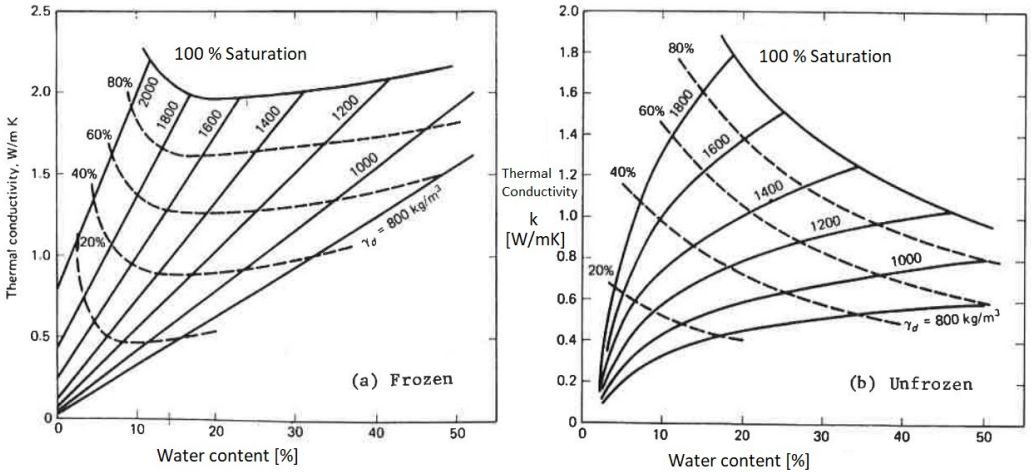

Figure 2.15: Average thermal conductivity for silt and clay soils. The y-axis in the left and right Figure represent the thermal conductivity k [W/mK] for frozen k_f and unfrozen k_u state. Adapted from [2].

The rate at which heat is transferred in a soil mass is dependent on the thermal conductivity k. The rise in temperature that a specific amount of heat will produce will vary with the heat capacity c and the bulk density ρ [2]. The ratio of these quantities is defined as the thermal diffusivity α:

$$\alpha = \frac{k}{c\rho} \tag{2.23}$$

Table 2.7 presents reference values of thermal diffusivity for different materials.

Material	$\boldsymbol{\alpha}$ [m^2/s $\cdot$ 10^{-7}]
Dense saturated sand	8.0
Soft saturated clay	4.0
Fresh snow	3.3
Dry soil	2.5
Water	1.4
Organic solids	1.0
Air	0.2

Table 2.7: Thermal diffusivity, α, of several materials adapted from [2].

Mechanical properties

When a frozen soil specimen is subjected to a load, it will respond with an instantaneous deformation and a time-dependent deformation; if the load is big enough, it will display a limiting strength [2]. Basic creep consist of primary, secondary and tertiary creep. For stresses lower than the long-term strength of frozen soil, the secondary and tertiary creep may be neglected [2]. Table 2.8 presents some creep parameters b, n, w and σ_{c0} from [2].

Soil	**b**	**n**	**w**	$\sigma_{\mathbf{c0}}$ **[kPa]**
Suffield clay	0.33	2.38	1.20	170
Bat-Baioss clay	0.45	2.50	0.97	180
Hanover silt	0.15	2.04	0.87	2 250
Callovian loam	0.37	3.70	0.89	310
Ice-rich silt	1.00	3.00	0.60	71
Ottawa sand	0.45	1.28	1.00	1 050
Manchester fine sand	0.63	2.63	1.00	160
Karlsruhe silty sand	0.40	2.00	1.00	300
Very ice-rich soil or polycrystalline ice	1.00	3.00	0.37	103

Table 2.8: The factors n, b and σ_0 are creep parameters determined from laboratory tests. Creep parameters are adapted from [2].

Methods for evaluating creep settlement for shallow foundation and pile foundation are described in Section 2.3.3. The effect of temperature on creep of a frozen soil can, according to [2], be included in the value of the creep modulus by means of an empirical formula:

$$\sigma_{c\theta} = \sigma_{c0}(1 + \frac{\theta}{\theta_c})^w \tag{2.24}$$

where θ is the temperature in the soil and θ_c is an arbitrary reference temperature equal to $-1\,^{\circ}\mathrm{C}$. The factor σ_{c0} is the value of $\sigma_{c\theta}$ extrapolated back to $0^{\circ}C$ in an unconfined compression creep test [2]. The parameter w is obtained from the unconfined compression creep test.

In Russian literature the settlement calculations are approached by the modulus of deformation, also known as the constrained modulus M. The modulus of deformation M is defined as,

$$M = E\frac{1-\nu}{(1+\nu)(1-2\nu)} \tag{2.25}$$

Here E is the Youngs modulus and ν is Poisson's ratio. The modulus of deformation is obtained when a soil sample is subjected to a vertical normal stress in a cylinder that prevents any lateral movement; it is defined as the ratio of the normal stress applied over the vertical strain obtained [4]. Table 2.9 and Table 2.10 presents the deformation modulus M for unfrozen and frozen state.

Material	E [MPa]	ν	M [MPa]
Sand	15.0	0.25	30.0
Silt	6.0	0.35	12.0
Clay	1.8	0.25	4.0

Table 2.9: Youngs modulus E, Poissons ratio ν and modulus of deformation M for unfrozen soil. Adapted from [4].

For frozen state, the modulus of deformation M depends on the soil type, the salinisation D_{sal}, the water content w and the temperature. Results from laboratory tests performed by Askenov [41] on frozen soil resulted in the M modulus of frozen soil presented in Table 2.10. Report[40] describes in situ field tests of frozen none-saline soil. These tests determined a multiplication factor that the frozen soil M modulus from laboratory tests should be multiplied with in order to represent in situ soil. The multiplication factors are presented in Table 2.11.

Modulus M is defined by an oedometer test [41]. Coefficients are developed based on comparison of laboratory tests and full-scale tests. Modulus M in this case includes instantaneous (elastic) deformations, and some of the long-term deformations, i.e. primary creep. It does not include secondary creep as the oedometer restricts expansion of a sample. Those oedometer tests were long-term (up to three weeks), but did not include any correction for longer duration of tests. Tests were run in the range of loads, with the highest load corresponding to long-term strength of frozen soils, which corresponds to the primary creep and to increasing/decreasing rate of deformations. The tests ran until the rate of deformations would drop to 0.005 mm/24h, which is accepted as the condition of stabilization of settlements.

Material	θ [$°C$]	D_{sal}[%]	w [-]	M [MPa]
Sand	-4	0.5	0.20	3.0
Sand	-4.2	0.5	0.33	1.5
Silt	-3	0.5	0.33	8.6
Clay	-2	0.5	0.37	2.0
Clay	-3	0.5	0.37	25.0
Clay	-4	0.5	0.37	10
Clay heavy	-4	0.6	-	30
Clay heavy	-6	0.6	-	10
Clay light	-3	0.4	0.34	7
Clay light	-4	0.5	0.34	12
Clay light	-6	0.5	0.34	30
Clay light	-4	0.5	-	10
Clay light	-5	0.5	-	20

Table 2.10: Reference values for module of deformation M, for different soil types at different temperatures θ, salinization D_{sal} and water content w, from Table 6.1-6.5 and Figure 6.3-6.4 in [41].

Soil	Multiplication factor
Sand	3.5
Silt	3.8
Clay	4.2

Table 2.11: Multiplication factors to transform laboratory deformation modulus M to in situ values. Adapted from [40].

According to [2] the friction angle ϕ for the soil types in frozen state have the range as presented in Table 2.12.

	ϕ [°]
Sand	29-37
Silt	15-25
Clay	0-10

Table 2.12: Range of friction angle ϕ for frozen soils according to [2].

The friction angle and cohesion depends on the salinity, water content, density and temperature of the frozen soil. A table of friction angles of the soil due to soil type, salinization and temperature is added in Appendix B.

2.3.2 Thaw Behavior of Frozen Soils

Volume change of thawing soil will result from both phase change (ice to water) and flow of excess water out of the soil [2]. Settlement due to melting of ice in the soil below the foundation is,

$$\delta_{melt} = \Delta h \cdot n \cdot 0.1 \tag{2.26}$$

where n is the porosity of the soil, assuming fully saturated soil when frozen. When ice melts the volume decreases with 10%. This settlement develops in summer time when active layer penetrates deeper than the base of the foundation. We assume that this settlement will not recover in the subsequent winter when the active layer refreezes. We also assume that the active layer will refreeze completely in the subsequent winter. Drainage of thawed soil leads to additional volume change, the amount depending on consolidation and soil structural changes that occurred during the previous freezing cycle [2].

For cableway posts located in sloping terrain, drainage of water from the active layer occur, hence the assumptions above are applicable in these circumstances. For conditions where drainage is restricted, i.e. for flat ground surfaces, the assumptions above are not valid, i.e. there will be some rebound of settlements of the active layer. In such cases, use of the assumptions will provide more conservative results, i.e. it will provide settlements which are bigger than one should expect. Such overestimation of settlements may, however, be preferred for management practice as it may give more severe than in reality values, hence the management authorities (SNSK) will have to react sooner on those.

2.3.3 Foundations

The foundation need to have sufficient bearing capacity and not cause unacceptable settlements within the service life time [30]. Acceptable settlement is dependent on the structure's sensitivity to smaller settlements [16]. As a general design rule, less than 5 cm of settlements in a foundation of ice-rich permafrost after 30 years of load application is considered "good". Less than 10 cm settlement is considered acceptable, while more than 10 cm is considered to indicate failure of the foundation [16].

When a foundation load is applied to a frozen soil, several short-term phenomena occur and some long-term deformations start developing [2]. According to [2] five sources of settlement for foundation in frozen ground will occur:

1. Instantaneous-elastic (reversible), due to the elastic deformation of the soil skeleton, ice, unfrozen water, and gasses.
2. Instantaneous-plastic (irreversible), due to either the structural collapse of unsaturated frozen soil under load with the expulsion of air, or to the plastic bearing capacity failure of the foundation soil.
3. Viscoelastic (reversible), as a consequence of the reversible phase transition in ice.
4. Consolidation (irreversible), due to the delayed processes of air and unfrozen water migration under pressure gradients.
5. Creep or Viscoplastic (irreversible), arising from irreversible displacements of solid particles governed by the flow of pore ice. Depending on load level and boundary conditions, creep settlement of a foundation may be attenuating, stationary, or accelerating, and may lead to a delayed bearing failure.

In frozen soil, distortional creep is considered to be the main source of the delayed response to stress increase.

The following sections describe the calculation procedure for bearing capacity of shallow foundations, creep settlement analysis for shallow foundation and pile foundations.

Shallow foundation

Shallow foundations are normally defined as footings having a width, B, equal to or greater than their depth, D_f (see Figure 2.16 for illustration). In Permafrost areas, shallow foundations are placed at a depth governed by the thickness of the active layer [2]. The bearing capacity analysis of shallow foundations in frozen soils and rock is general based on an evaluation of the safety against failure of the soil and rock, and evaluation of tolerable foundation settlements [16].

Bearing capacity of shallow foundation

Figure 2.16 illustrate the load distribution for shallow foundations. The foundation need to be in the permafrost to prevent freezing and thawing issues.

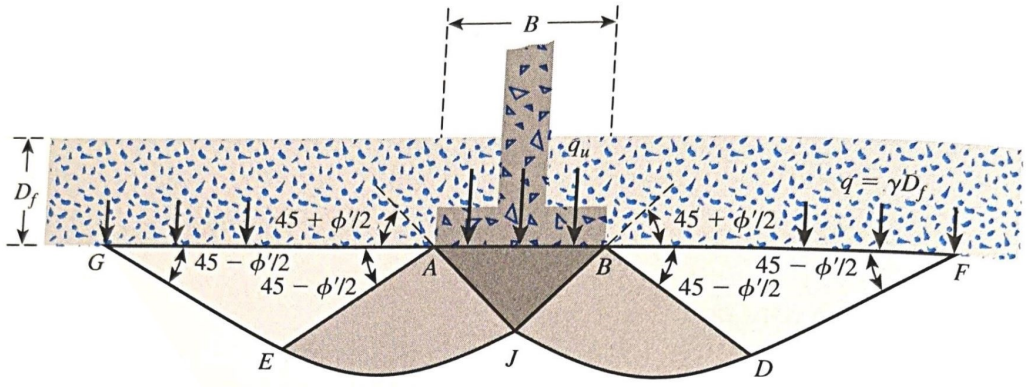

Figure 2.16: Soil-bearing capacity sketch of shallow foundations. The lines AJDF and BJEG, depending on the friction angle of the soil ϕ', marks the failure surface of the soil. The weight of the overlying soil q suport the bearing capacity q_u. Adapted from [6].

The ultimate bearing pressure q_{ult} for frozen soil can be expressed in the form used by Therzaghi, which includes three terms: cohesion, surcharge and self-weight terms [2]:

$$q_{ult,v} = cN_c s_c d_c i_c + \bar{q} N_q s_q d_q i_q + 0.5\gamma' B N_\gamma s_\gamma d_\gamma i_\gamma \tag{2.27}$$

where N_c, N_q and N_γ are bearing capacity factors. The factors s_c, s_q and s_γ are shape factors and the factors d_c, d_q and d_γ are depth factors. The factor $\bar{q}$ is the surcharge [kPa] and γ' is the natural unit weight of soil/rock [kN/m^3].

The unit weight γ is the unit weight of the soil. The bearing capacity factors are defined as:

$$N_q = e^{\pi \tan \phi'} \tan^2(45 + \frac{\phi'}{2}) \tag{2.28}$$

$$N_c = (N_q - 1)\cot(\phi') \tag{2.29}$$

$$N_\gamma = (N_q - 1)\tan(1.4\,\phi') \tag{2.30}$$

$$N_\phi = \tan^2(45 + \frac{\phi'}{2}) \tag{2.31}$$

The shape factors are given by

$$s_c = 1 + 0.2 N_\phi \frac{B}{L} \tag{2.32}$$

For ϕ bigger than 10°:

$$s_q = s_\gamma = 1 + 0.1 N_\phi \frac{B}{L} \tag{2.33}$$

For ϕ equal to 0:

$$s_q = s_\gamma = 1 \tag{2.34}$$

The shape factor will determine the bearing capacity of rectangular and circular footings [6].

The depth factors are

$$d_c = 1 + 0.2\sqrt{N_\phi}\frac{B}{L} \tag{2.35}$$

For ϕ greater than zero:

$$d_q = d_\gamma = 1 + 0.1\sqrt{N_\phi}\frac{D}{B} \tag{2.36}$$

For ϕ equal to zero $d_q = d_\gamma = 1$.

The depth factor will take into account the shearing resistance developed along the failure surface in soil above the base of the footing [6].
The inclination factors are

$$i_c = i_q = (1 - \frac{\theta}{90^\circ})^2 \tag{2.37}$$

For ϕ bigger than 10° the inclination factor is

$$i_\gamma = (1 - \frac{\theta}{\phi'})^2 \tag{2.38}$$

For ϕ equal to zero i_γ is equal to 0.
The inclination factor will determine the bearing capacity of a footing on which the direction of load application is inclined at a certain angle to the vertical [6].

Settlement analysis of shallow foundation

The authentic solution settles due to three mechanisms:

- Settlement in unfrozen ground below the foundation.
- Melt of ice in the ground below the foundation (described in section 2.3.2).
- Creep of the frozen ground below the foundation.

Settlements can be calculated by different approaches. Here we introduce settlements based on creep parameters and the deformation modulus.

The settlement of the foundation calculated based on creep parameters, which is the European approach, is:

$$s = aI(\frac{q}{\sigma_{c\theta}})^n(\frac{\dot{\varepsilon_c}}{b})^b t^b \tag{2.39}$$

where a is the width B of the foundation divided by two, q is the weight above the foundation (in our case the weight of the structure and the weight of the soil above the foundation). Factor $\dot{\varepsilon}_c$ is the strain rate (10^{-5} hour) and t is time. The influence factor I for strip footings is defined as:

$$I = (\pi\frac{\sqrt{3}}{4})(\frac{\sqrt{3}}{n})^n \tag{2.40}$$

The parameters n, b and $\sigma_{c\theta}$ are creep parameters, presented in section 2.3.1. This method calculate the settlement s, based on cavity expansion theory and is valid for homogeneous frozen soil conditions below the footing.

If the soil is not homogeneous, the soil below the footing can be divided into a convenient number of individual layers each corresponding to a specific soil type and temperature. The creep behavior varies due to temperature. [2] The settlement of any layer i of thickness Δz_i is then

$$s = \sum \Delta z_i \varepsilon_i \tag{2.41}$$

where ε_i is the creep strain in layer i. [2]

The total settlement from this approach is:

$$\delta_{tot} = s + \delta_{melt} \tag{2.42}$$

where the creep settlement s is either from Equation 2.39 or Equation 2.41 and δ_{melt} is from Equation 2.26.

Another method is the Russian approach of settlement calculation, calculated based on modulus of deformation. The settlement of the thawed ground below the foundation is:

$$\delta_{unfrozen} = (\frac{\Delta p}{M_{unfrozen}})\Delta h_{unfrozen} \tag{2.43}$$

where $\Delta h_{unfrozen}$ is the thickness of unfrozen soil below the foundation, M is the modulus of deformation presented in Equation 2.25 and Δp is the pressure from above (load from structure and load of the soil above the foot of foundation).

For frozen soil the upper boundary of stresses corresponding to primary creep is defined by long-term strength[5]. The settlement of the frozen ground below the foundation is:

$$\delta_{frozen} = (\frac{\Delta p}{M_{frozen}})\Delta h_{frozen} \tag{2.44}$$

where Δh_{frozen} is assumed to be 1m.

The total vertical settlement is

$$\delta_{total} = \delta_{unfrozen} + \delta_{melt} + \delta_{frozen} \tag{2.45}$$

[5]Long-term strength of frozen saline soils under the foot of shallow foundations is presented in Tables 7.8 and 7.10 in [41].

Settlement analysis of Pile foundation

The axial settlement of a pile due to primary creep is

$$s = \frac{3^{\frac{n+1}{2}}}{n-1} a (\frac{\tau_a}{\sigma_{c\theta}})^n (\frac{\dot{\varepsilon}_c t}{b})^b \tag{2.46}$$

where $\sigma_{c\theta}$ is the temperature dependent creep modulus for the soil, corresponding to the reference strain rate $\dot{\varepsilon}_c$ (10^{-5} hour). The factors n, b and w are creep parameters. Table 2.8 presents reference values of the creep parameters adapted from [16].

The shear stress τ_a along the pile is

$$\tau_a = \frac{P}{2\pi \cdot a \cdot L_{eff}} \tag{2.47}$$

where P is the axial load on the pile, a is the radius of the pile and L_{eff} is the effective length of the pile. The effective length of the pile is the pile length with temperatures below -1°C. The settlement of the pile depends on the average temperature θ which is the average of the temperature along the effective length L_{eff} of the pile.

Figure 2.17 illustrates how the active surface layer affects a pile during the seasonal changes.
In the summer when the soil in the active layer thaws, the soil gives a downwards load P_n to the pile in the active layer. During the fall and winter the soil freezes, and due to the expansion of water in the soil within the active layer a lifting force is applied to the pile P_a (due to adhere forces when freezing takes place). To decrease the lifting force, the friction between the pile and the soil in the active layer can be decreased by using a steel sleeve in the active layer and/or by using a oil-wax backfill. The pile needs to be anchored properly to prevent deformations due to the lifting force P_a. The axial load on the pile is P and the equilibrium of the forces require a strength of the pile equal to P_P.

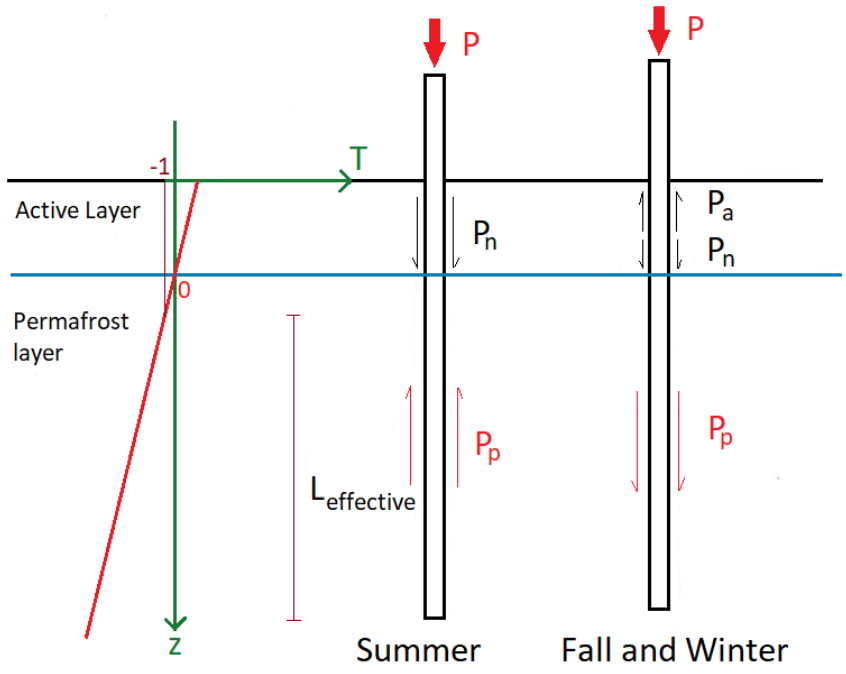

Figure 2.17: A sketch of two piles shows the change of load directions due to seasonal changes in the active layer ALT. The plot on the left side shows the temperature profile (red line) of the ground (during summer). The axis, marked in green represents the temperature and the depth in the ground. The top of L_{eff} is marked where the temperature is $-1°C$.

Piles in permafrost ground are assumed to derive their axial load-bearing capacity from the adfreeze bond between the pile lateral surface and the soil or backfill material. Due to the seasonal changes in actions only the length L_{eff} is used in calculations of the bearing length of the pile.

Chapter 3

Fieldwork

During this thesis, the following fieldwork has been done:

- Field inspection of cableway posts.
- Installation of thermistor-string and downloading data from already installed thermistor-string.
- I-buttons were installed under and around cableway posts, to measure surface temperatures.
- Time-lapse cameras were installed to measure snow accumulation.
- Snow thickness was measured around the cableway posts.

To be able to do fieldwork close to cultural heritage, permission, including locations for installations and actions, was given by an application with three levels of approval: SNSK, recommendation of Sysselmesteren and final approval from Riksantikvaren.

The fieldwork is described in the following subsections.

Field inspection

In September 2021, a field inspection of the cableway posts took place as a part of Work package 1 in PCCH-Arctic. The purpose of the inspection was to reveal the status of the cableway posts and the need of rehabilitation (see Figure 2.2 in Section 2.1). The inspection included a visual control where mapping the status of the structures was the main goal. After the fieldwork, an overview of the status was developed by SINTEF. The inspection revealed cases where the structures were exposed to solifluction, permafrost degradation and other natural hazards (i.e. avalanches, landslides etc.), the numbers

of cases within each category are presented in Table 3.1. The mapping also divided the need of restoration into different categories as shown in Table 3.2.

Type of natural hazards	**Number of cases, approximately**
Permafrost degradation	115
Solifluction	47
Gravitational slope processes	34
Surface wash and gravitational processes	2
Snow avalanches	4
"Special" cases	1
Additional evaluation is needed	8

Table 3.1: An overview of the status of the cableway posts on Svalbard. Based on field inspection during the fall 2021.

Need of immediate restoration	**Number of cases, approximately**
Restored	7
Structures are gone	36
Situation is not clear	97
To be evaluated	25
Needed	26
Needed/urgent	7
Urgent	7

Table 3.2: An overview of the need of rehabilitation for the structures evaluated. Based on field inspection the fall 2021.

The categorization "Needed" in Table 3.2 is defined as a structure with some displacement of the foundation or observable damage or ruptures of some elements, yet structural performance is visually maintained. Structures in a presence of natural hazards, which may affect the structure or permafrost under the structure. For instance, presence of adjacent eroding slope which may compromise stability of the structure, or a seasonal creek, which may cause surface erosion and may increase degradation of permafrost under the structure are also categorized as "Needed".

Structures in the category "Urgent" suffer from large displacements of foundation elements, large tilt of the whole structure, large settlement of the whole structure in vertical direction or/and potential danger due to HSE

considerations (Health, Safety, Environment).

Structures that "are gone" are structures that are already absent in their original state, for instance capsized, yet may be restored due to historical, cultural, and other considerations.

Thermistor-string

The thermistor-string is a string with sensors (from "Geo precision" [34]) used to measure temperatures at different levels in the ground (see Figure 3.2). The thermistor-string was installed in a borehole, within a plastic-pipe, at the location shown in Figure 3.1.

Figure 3.1: The red dot represent the position of the thermistor string.

Figure 3.2: Picture of a thermistorstring adapted from [34].

The thermistor string installed at the location marked in Figure 3.1 will provide temperature data for further use in the PCCH-Arctic project.

In April 2022 data from the thermistor string (logger A5387C) located at UNIS EAST, borehole E5, was downloaded. To load the data, a receiver was connected to the computer and the data was downloaded from the transmitter. The borehole was 28 m long. The thermistor string had the following sensor depths [m]: 0.00, 0.25, 0.50, 0.75, 1.00, 1.25, 1.50, 2.0, 2.5, 3.0, 3.5, 4.0, 4.5, 5.0, 6.0, 7.0, 8.0, 9.0, 10, 11, 12, 14, 16, 18, 20, 22, 24, 26, 28.
Figure 3.3 shows a Picture of the location of the thermistor-strings at UNIS EAST.

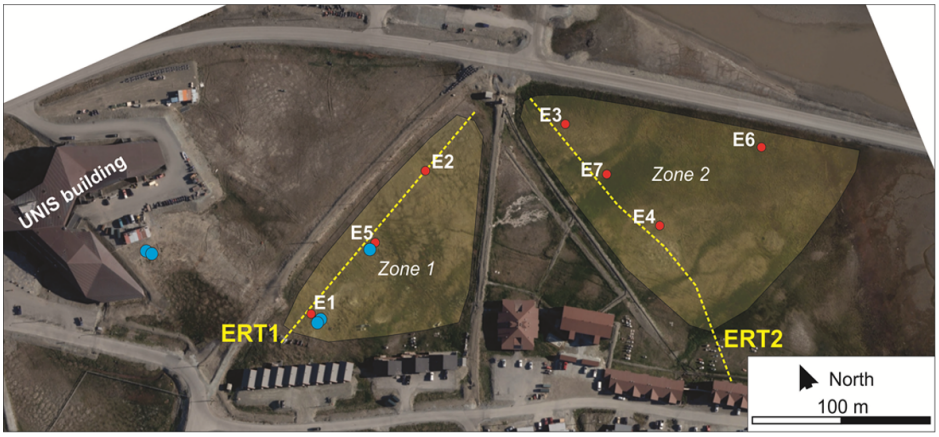

Figure 3.3: Picture of UNIS EAST. Thermistor string marked with E1-E6. Adapted from [33].

The data from the thermistor string downloaded from E5 is presented in Figure 3.4. The red sensor has the biggest range in temperature, therefor it is from the upper sensor (active layer, close to the surface). The sensors with temperatures in the range below zero are from the permafrost. As described in Section 2.2 the temperatures change in a sinusoidal function as shown in Figure 3.4.

The soil at UNIS EAST consists of clay at the depth of 3 m to approximately 20 m [13]. The soil investigation from the specific site (UNIS EAST) is adapted from the report of Gilbert [13] and added in Appendix B. The temperature data is used to calibrate the numerical simulation in Section 4.3 for soil type Clay. From 2020 the thermistor-string had several sensor errors. The calibration data was therefore chosen from year 2019.

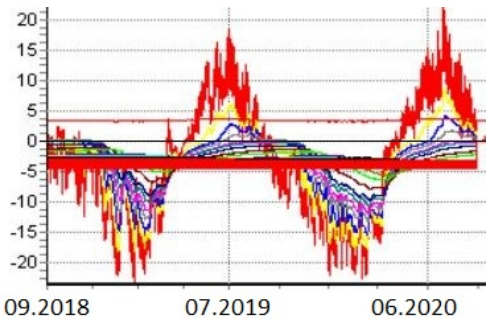

Figure 3.4: Plot of downloaded temperatures from E5. The different colours represent different sensors. The axes represent temperature [°C] and date.

I-buttons

I buttons are temperature sensors to measure ground temperature. In this case they have been used to measure the surface temperature of the ground under and next to several historical objects in Svalbard. The sensors will provide data for further use in the PCCH-Arctic project. The data will be used to model permafrost degradation, and based on that: stability of the objects of cultural heritage during the climate change. The i-buttons were installed during February 2022.

Installation

Figure 3.5 presents an illustration of the installation. At first the snow was shoveled away to get access to the surface. Then, a hole was drilled in the ground with a concrete drill bit of ca. 50-80 mm in diameter and the sensor was placed in the hole and covered. The location of the i-buttons were marked with a small stick and a label attached with a thin wire, as shown in the picture in Figure 3.6. Number of i-buttons and location is described in Appendix C.

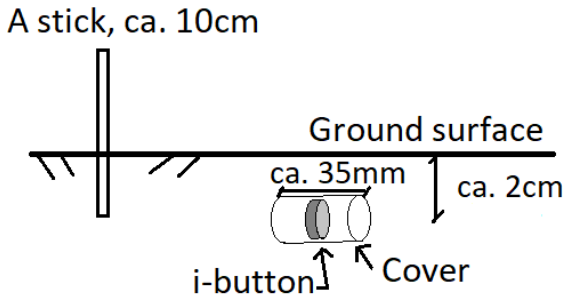

Figure 3.5: Sketch of installation of i-buttons.

Figure 3.6: Installed i-button, from installation in February 2022. Picture taken by author.

Time-Lapse-Camera

To measure snow thicknesses over time, time-lapse cameras were installed at specific positions pointing toward a stick with marks on, see Figure 3.7 and Figure 3.8. The camera records one picture a day at 12:00 every day. The snow thickness can be read from the stick on the picture. The daily differences are also observable in the pictures. Location of installed time-laps camera is added in Appendix C.

Figure 3.7: Installed time-laps-camera at Hiorthamn. Picture taken by author.

Figure 3.8: Installed measure pole for time-lapse camera at Hiorthamn. Picture taken by author.

The data from the time-lapse cameras will be used for further work in PCCH-Arctic project.

Snow measurement

In order to measure snow depth under and around the cableway posts fieldwork took place 4th April 2022. The purpose of measuring the snow depth was to collect data that will be used as input parameters for a bigger model developed by the PCCH- arctic project. April was chosen as the measuring period since it is late in the winter, therefore should represent the high snow accumulation. It is important to note that a short melting period ($> 0°C$) occurred in late March, which must be considered when interpreting the results.

The snow depth measurements were performed with an avalanche probe (see Figure 3.10). The blue dots in Figure 3.9 represent the probe locations around the structure, which is illustrated with a black square. Measure point A is in the center of the frame of the structure. The B-measure points were measured approximately 1 m from the frame and measure point C was approximately 10 m from the frame. The structures that were measured were the same as the structures where the i-buttons got installed.

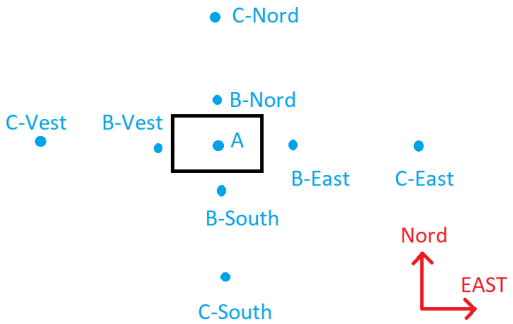

Figure 3.9: Sketch of measuring points for snow depth. The black rectangle represents the frame of a cableway post. Measure points B are approximately 1 m from the edge of the frame, measure points B and C are approximately 1m and 10 m from the edge of the frame.

Figure 3.10: Snow measurements using avalanche probe. Picture taken by author.

The data from the measurements (added in Appendix C) will be used for further work in PCCH-Arctic project.

Chapter 4

Calculations and Results

We aim to create a knowledge base for restoration of the cableway posts. To create a general knowledge base that is suitable for different cableway posts the analysis is based on general situations for different scenarios. In this thesis three different soil types are taken into account: Sand, Silt and Clay. The cableway posts have different sizes, as a generalization three different sizes are analysed, defined as small, medium and big cableway posts. The big cablewaypost is approximately 28 m high, as one of the cablewaypost in Longyearbyen. The category "medium" and "small" are 75% and 50 % of the weight of the "big" structure. This simplifications were done in lack of documentation of the cableway posts. The volume and pressure of the structures are presented in Table 4.1. The weight of the upper structure is calculated from Python Script A.5 in Appendix A, with assumed density of wood 490 kg/m^3 from [25]. The weight from a simplified foundation of 1.5m is added to the weight of the upper structure and presented in Table 4.1. Since the assumed density is high and the weight in general is based on simplifications the weight of the structures are not adapted for the different foundation depths.

	V [m^3]	ΔP [kN/m^2]
Big	31	83
Medium	23	62
Small	16	41

Table 4.1: Generalized volume V and pressures ΔP of three different sized cableway posts. The volume and pressure includes the upper and lower structure.

The foundation depths of the structures differs, to consider that the analysis differs between three foundation depths: 1.5 m, 2.0 m and 2.5 m. The settlements are calculated based on standard approach with design index and based on predicted future temperatures. The standard approach is based on historical data. This approach accounts for the three warmest years during the last 30 years as described in Section 2.2. As a standard approach the structures need to be designed for a lifetime of 30 years according to Table 2.3 in Section 2.3.

In the following Section the soil parameters are calculated based on theory presented in Section 2.3. The thawing depths are calculated according to analytical calculations in Section 4.2 and numerical calculations in Section 4.3 based on Section 2.2. Temp/W is used in the numerical calculations. The bearing capacity of the authentic solution is calculated in Section 4.4 based on shallow foundation theory. The settlement of piles and settlement for the authentic solution are calculated in Section 4.5.

4.1 Soil Parameters

The soil parameters are calculated according to the Equations in Section 2.3.1 with Python Script A.3 in Appendix A. Input for the calculations are the unit weight γ_d of the soil and the specific gravity of soil materials G_s. The input values are adapted from reference values presented in Table 4.2. If the unfrozen water content w_u is assumed to be zero and the three soil types is assumed to be fully saturated, the calculations give the soil parameters presented in Table 4.3.

Soil	γ_d [kN/m^3]	G_s [$-$]
Clean uniform sand	16.0	2.65
Silty sand	16.0	2.65
Clay	16.5	2.70

Table 4.2: This Table shows the dry unit weight γ_d and the specific gravity of soil materials G_s for three different soil types. The Table is adapted from [2].

Soil	ρ [kg/m^3]	n [%]	w[%]	L[kJ/m^3]
Sand	2015.5	38.5	23.6	128318.5
Silt	2015.5	38.5	23.6	128318.5
Clay	2059.0	37.7	22.4	125822.6

Table 4.3: Physical soil properties for frozen soil, when unfrozen water content w_u is zero.

To find the thermal conductivity of the soil types, the soil parameters from Table 4.3 are added into Figure 2.14 and Figure 2.15. The frozen and unfrozen thermal conductivity (k_u and k_f) can be read from the y-axis. The Figures are repeated with markings in Figure 4.1 and Figure 4.2. The colored marks in the Figures describe how the graphs are read. In Figure 4.1 the red mark represent soil type sand with the soil properties from Table 4.3. The blue mark in Figure 4.2 represents soil type Silt and the green mark represent soil type Clay. The thermal conductivity is presented in Table 4.5 and Table 4.6.

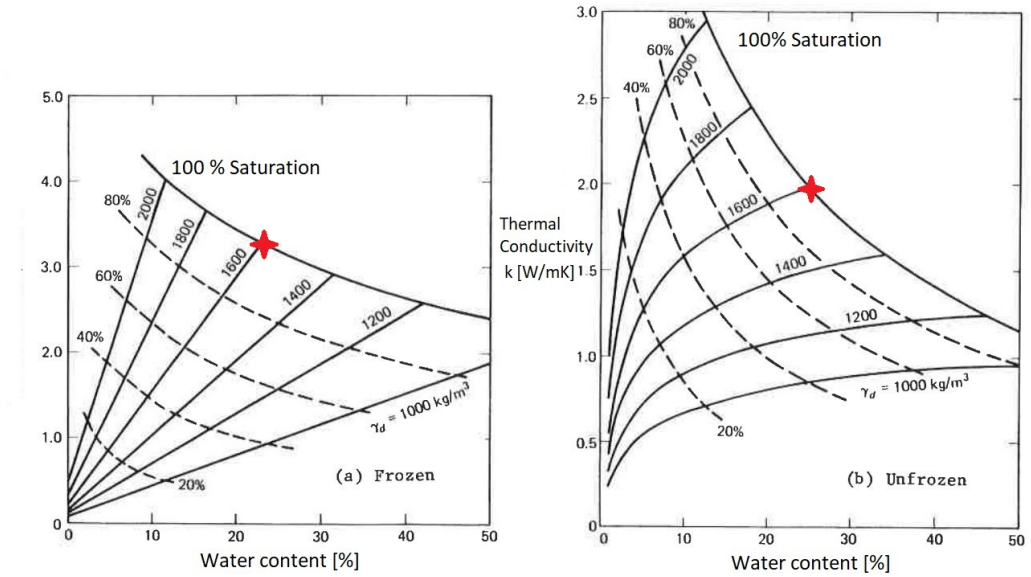

Figure 4.1: Average frozen and unfrozen thermal conductivity for Sand and gravels. The red mark represent soil type Sand. Adapted from [2].

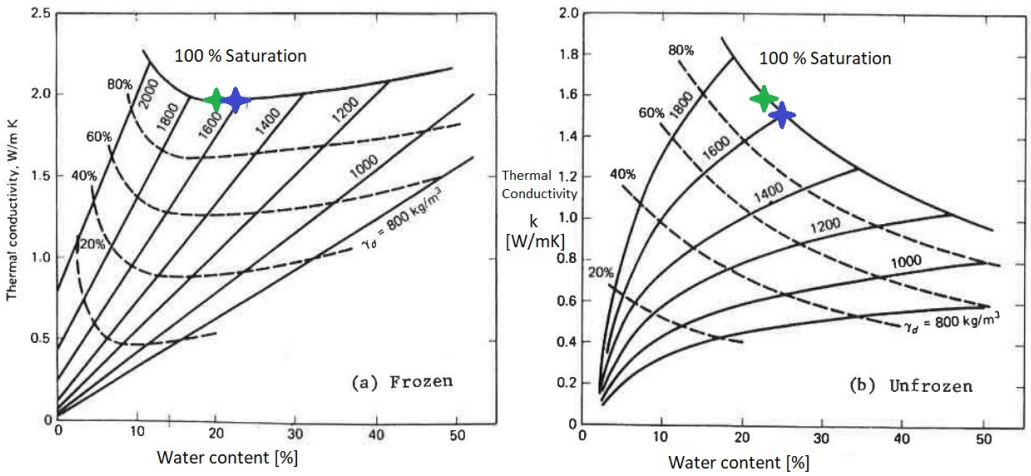

Figure 4.2: Average frozen and unfrozen thermal conductivity for silt and clay. The blue mark represent soil type Silt and the green mark represent soil type clay. Adapted from [2].

The unfrozen water content depends on the salinity and the temperature in the soil layer. No unfrozen water content for a soil just below the active layer might be an unrealistic assumption through the summer. Figure 2.13 shows how the unfrozen water content differs for different salinities for the different soiltypes presented in Table 2.6. The salinity used in these calculations are based on soil investigation at UNIS EAST from Gilberts report [13] (See Appendix B) at the depth of approximately 7 m. The result of Gilbert gives a approximately salinity of 25 ppt. The salinisation D_s depends on the water content w and the salinity S_n as shown in Equation 2.17. The calculations of the unfrozen water contents w_u presented in Table 4.4 are based on the Equations in Section 2.3.1. The values of θ_{bfp} are -0.5 °C for sand and silt, and -0.25 °C for clay, based on reference values from [20].

Soil	θ	θ_{bf}	w_u[%]	ρ [kg/m^3]	w[%]	L[kJ/m^3]	D_{sal}[%]
Sand	-2.0	-0.08	6.40	2015.5	23.6	93 485.8	0.605
Silt	-2.0	-0.08	6.40	2015.5	23.6	93 485.8	0.605
Clay	-2.0	-0.40	12.42	2059.0	22.4	56 225.2	0.574
Sand	-3.5	-0.08	5.11	2015.5	23.6	100 506.8	0.605
Silt	-3.5	-0.08	5.11	2015.5	23.6	100 506.8	0.605
Clay	-3.5	-0.40	9.82	2059.0	22.4	70 706.0	0.574

Table 4.4: Soil properties when unfrozen water content w_u unequal zero (for salinity equal to 25 ppt) at a ground temperature θ of -2 °C and -3.5 ∘C.

For the following calculation the unfrozen water content due to a ground temperature of -2 °C are used. The unfrozen water content decrease when the temperature decreases.

Latent heat L is affected by the unfrozen water content, as shown in Equation 2.22, and are presented in Table 4.4 for unfrozen water content w_u unequal to zero. The heat capacity for unfrozen c_{vu} and frozen c_{vf} soil and thermal diffusivity α are calculated according to the Equations in Section 2.3.1 with Python Script A.3 in Appendix A and are presented in Table 4.5 and Table 4.6 for frozen and unfrozen state.

Soil	c_{vf} [kJ/m^3 °C]	k_f [W/m°C]	α_f[m^2/s]
Sand	2184.5	3.2	$1.46 \cdot 10^{-6}$
Silt	2184.5	1.9	$0.90 \cdot 10^{-6}$
Clay	2423.2	1.9	$7.87 \cdot 10^{-7}$

Table 4.5: Thermal soil properties for frozen soil when unfrozen water content w_u unequal zero.

Soil	c_{vu} [kJ/m^3 °C]	k_u [W/m°C]	α_u[m^2/s]
Sand	2771.0	1.9	$6.86 \cdot 10^{-7}$
Silt	2771.0	1.5	$5.41 \cdot 10^{-7}$
Clay	2776.0	1.6	$6.84 \cdot 10^{-7}$

Table 4.6: Thermal soil properties for unfrozen soil when unfrozen water content w_u unequal zero.

4.2 Analytical Calculation

In this Section the thawing depth also known as the active layer depth ALT are calculated for the three different soil types Sand, Silt and Clay. Temperature data from Longyearbyen airport is presented in Section 4.2.1. The design ALT is calculated in Section 4.2.2, based on historical weather data at Longyearbyen airport from the last 30 years. The predicted future ALT calculated in Section 4.2.3 are based on predicted future forecast data for Longyearbyen. The active layer thicknesses are calculated according to Stephans Equation presented in Section 2.2.

4.2.1 Temperature measurements

In this thesis the local variations in air temperature for the areas around Longyearbyen are neglected. The data used to illustrate the temperature trends from the last decades is collected from a weather station at Svalbard airport [37] with data from 1976 until today. The mean annual air temperature MAAT on Svalbard increases as shown in Figure 4.3.

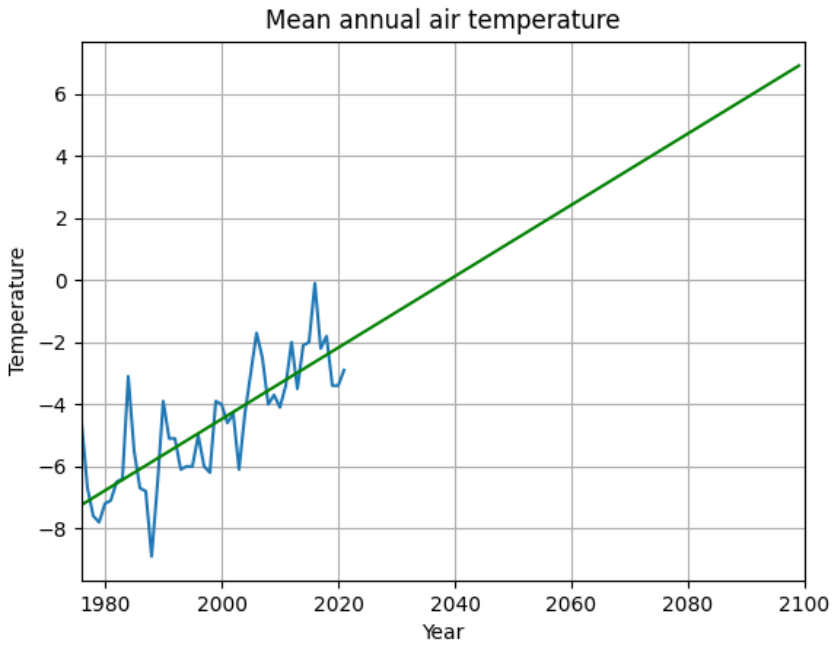

Figure 4.3: The temperature is measured in degree Celsius based on temperature data from [37]. The blue plot represents measured data from 1976 to 2021. The green line is a linearization based on the historical MAAT.

The linearization of the MAAT data gives the following equation:

$$T_m = 0.1151x - 234.6$$

The linearization expect that the MAAT will be positive at year 2039. The mean annual air temperatures for 1980, 2000 and 2020 are:

- 1980: $-7.2\,°C$
- 2000: $-4.0\,°C$
- 2020: $-3.4\,°C$

4.2.2 Historical ALT and permafrost temperatures

The air thawing index I_{at} and freezing index I_{af} for Svalbard airport based on air temperatures from the last 30 years gives the indexes presented in Table 4.7, calculated due to Equation 2.4 and Equation 2.5 in Section 2.2. The fourth column in the table presents the number of days of missing data, this might affect the results.

The design index is the average of the three warmest summers during the last 30 years. The three warmest years, marked in red (in Table 4.7), are the following:

- 2006: $I_{at} = 770\,°C$ days
- 2016: $I_{at} = 938\,°C$ days
- 2020: $I_{at} = 860\,°C$ days

The average of the three warmest summers gives a design thawing index I_{at} equal to 856 °C days.

Year	I_{at}	I_{af}	Missing data
1992	525	-2376	0
1993	603	-2818	0
1994	402	-2552	0
1995	569	-2760	0
1996	478	-2252	0
1997	464	-2643	0
1998	597	-2819	0
1999	551	-1950	0
2000	565	-2014	1
2001	643	-2302	0
2002	682	-2231	0
2003	586	-2807	0
2004	602	-2160	1
2005	670	-1743	0
2006	**770**	-1364	0
2007	697	-1609	0
2008	578	-2015	1
2009	631	-1971	0
2010	595	-2089	0
2011	753	-1962	0
2012	647	-1361	1
2013	725	-1980	8
2014	673	-1426	3
2015	669	-1463	14
2016	**938**	-902	17
2017	770	-1525	5
2018	740	-1388	0
2019	696	-1934	4
2020	**860**	-2084	3
2021	528	-1575	28

Table 4.7: Summary of thawing and freezing index for 1992 to 2021. Column four presents the number (days) of missing data. The three warmest years are marked in red.

The design thawing depth is based on the design air thawing index. To improve more reasonable results surface temperatures are recommended instead of air temperatures. Transferring air temperatures to surface temperatures can be done by adding surface factors as shown in Equation 2.7 and Equation 2.6. The surface factors in Table 2.2 are assumed to be too extreme, in the absence of more reliable values no surface factors are used in this calculations. The i-buttons described in the Fieldwork Section, in Section 3, measures surface temperature in order to recommend more reliable surface factors than the ones presented in Table 2.2 and will be used in further work in PCCH-Arctic. Some computational approaches are based on define surface temperature via air temperature by applying n-factors.

The thawing depth calculated according to Stephans Equation presented in Equation 2.3 depends on the latent heat and the frozen thermal conductivity of the soil. The latent heats from Table 4.3 and thermal conductivity from Table 4.5 are used in the following calculation. When the soil starts thawing after a cold winter the soil is deeply frozen and thereby it is assumed that the unfrozen water contents w_u are zero for all the three soil types: Sand, Silt and Clay, even though the soil contains some salt. To illustrate how the thawing depth increases due to increased thawing index, a plot is added in Figure 4.4.

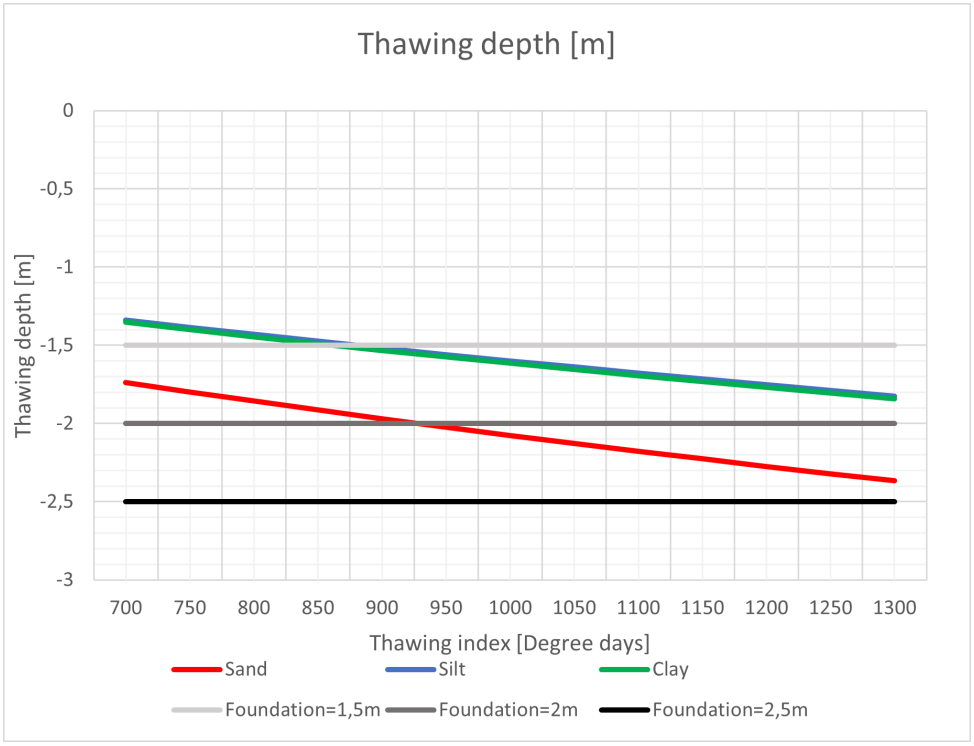

Figure 4.4: Plot of thawing depth (based on Stephan's Equation) for different air thawing index I_{at}. The ALT for Sand is marked with a red line. The ALT for Silt, marked in blue, might be hard to see since it is close to the ALT of Clay, marked with green. The three foundation depths (1.5 m, 2.0 m and 2.5 m) are marked with three horizontal lines to illustrate when the thawing depth will increase the foundation depth.

The three foundation depths that we are evaluating are illustrated as three horizontal lines in the plot. The plot visualize how the thawing depth also known as the active layer thickness (ALT) react to an increased thawing index I_t for the three different soil types. According to the calculations shown in the plot in Figure 4.4 the ALT will not reach 2.5 m for thawing indexes I_t within the range from 700 degree days to 1300 degree days.

For a design thawing index equal to 856 °C Days, which is the calculated design thawing index I_t, the thawing depths ALT are:

- SAND: 1.92 m
- SILT: 1.48 m
- CLAY: 1.49 m

According to the calculations above, the foundation depth should be at least 2m in order to be anchored in the permafrost due to the design active layer thickness for the analytical approach.

To visualise the ground temperature distributions, plots of the trumpet curves are shown in Figure 4.5, 4.6 and 4.7 for Sand, Silt and Clay. The calculations are based on historical temperature data from Svalbard airport, in Appendix B, and the average of the frozen and unfrozen thermal diffusivity α for each soil type, from Table 4.5 and Table 4.6. The calculations are done according to Equation 2.2.

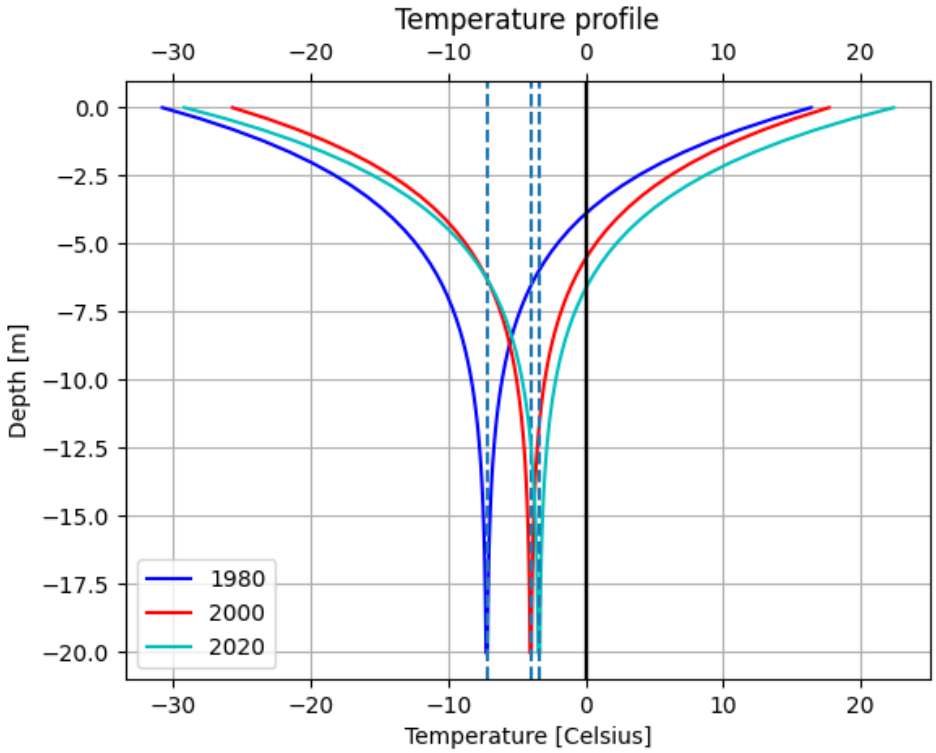

Figure 4.5: Trumpet curve for Sand with $\alpha = 1.07 \cdot 10^{-6}\,\mathrm{m}^2/\mathrm{s}$ with data input for 1980, 2000 and 2020. The dotted line is the mean annual air temperature T_m. The x-axis represents temperature [°C] and the y-axis represents depth in the ground [m].

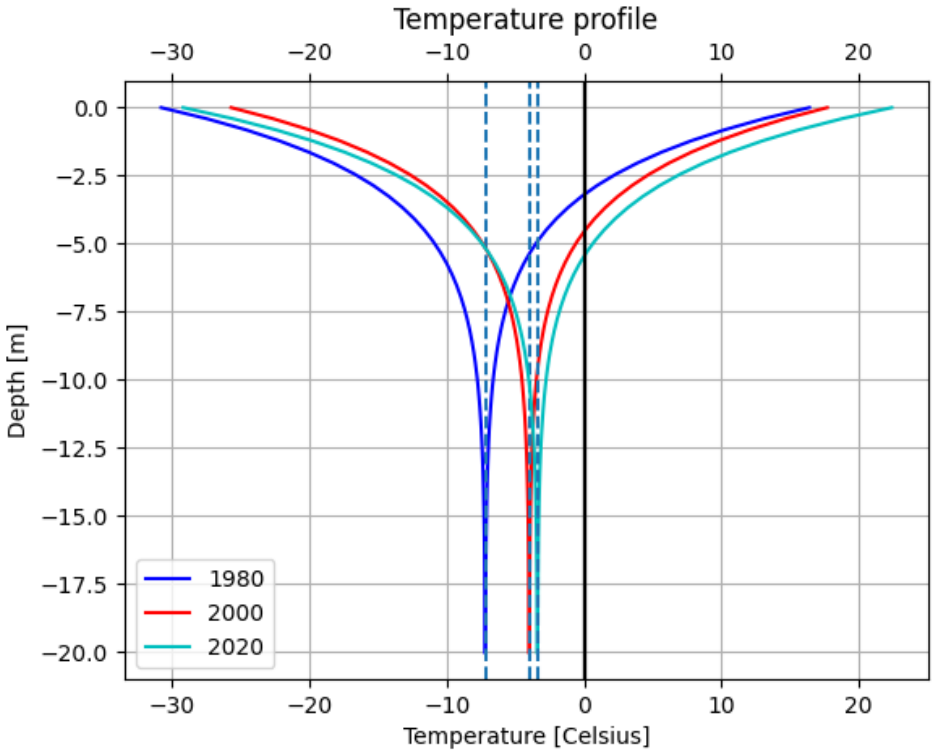

Figure 4.6: Trumpet curve for Silt with $\alpha = 7.21 \cdot 10^{-7}\text{m}^2/\text{s}$ for 1980, 2000 and 2020. The dotted line is the mean annual air temperature T_m. The x-axis represents temperature [°C] and the y-axis represents depth in the ground [m].

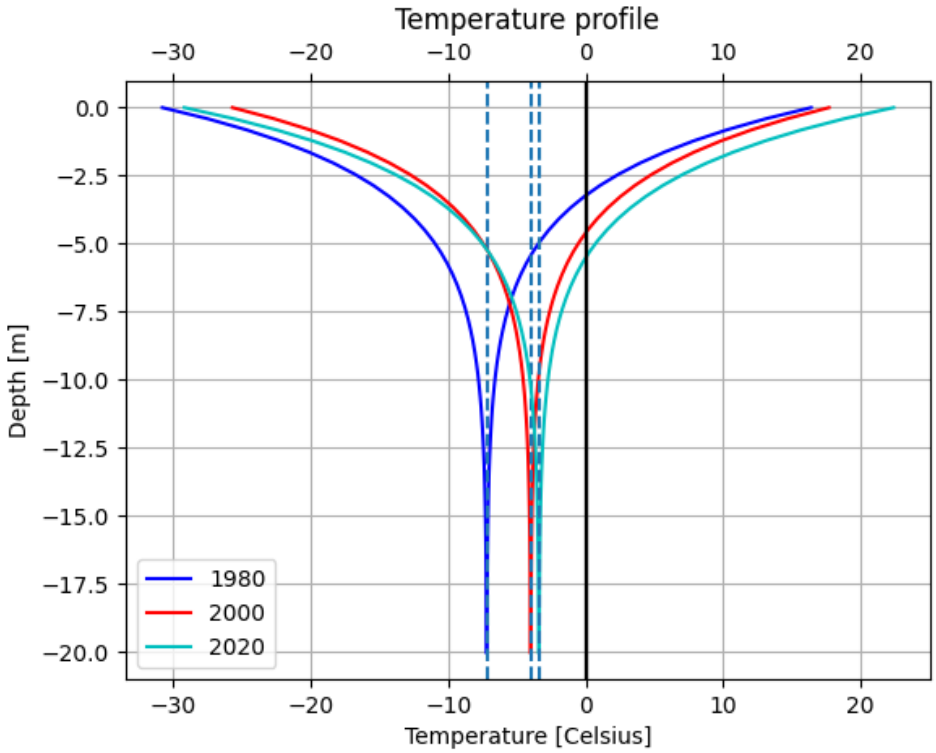

Figure 4.7: Trumpet curve for Clay $\alpha = 7.36 \cdot 10^{-7}\,\mathrm{m}^2/\mathrm{s}$ for 1980, 2000 and 2020.The dotted line is the mean annual air temperature T_m. The x-axis represents temperature [°C] and the y-axis represents depth in the ground [m].

4.2.3 Future thawing depths

The temperature data used in the following calculation is based on future temperature forecasts for Longyearbyen obtained from The Norwegian Meterological Institute, MET [3]. The downscaled seasonal mean temperatures for Longyearbyen is based on RCP8.5. RCP8.5 is the scenario with highest greenhouse gas concentrations, which provides the highest projection of global warming increase. The seasonal mean temperatures and standard deviations are obtained and these are believed to provide more robust estimates as the mean is better estimated for a seasonal sample than for a monthly or daily sample. The daily temperatures are inferred from the seasonal means and standard deviations by assuming a normal distribution. [3]

The air thawing index I_{at}, air freezing index I_{af} and active layer depth ALT are calculated based on the predicted daily temperatures. The calculations are done according Stephan's Equation (presented in Equation 2.3), based on soil parameters from Section 4.1, and presented in Script A.6 in Appendix A. The air thawing index I_{at}, air freezing index I_{af} and active layer depth ALT are plotted for Sand, Silt and Clay in the following Figures.

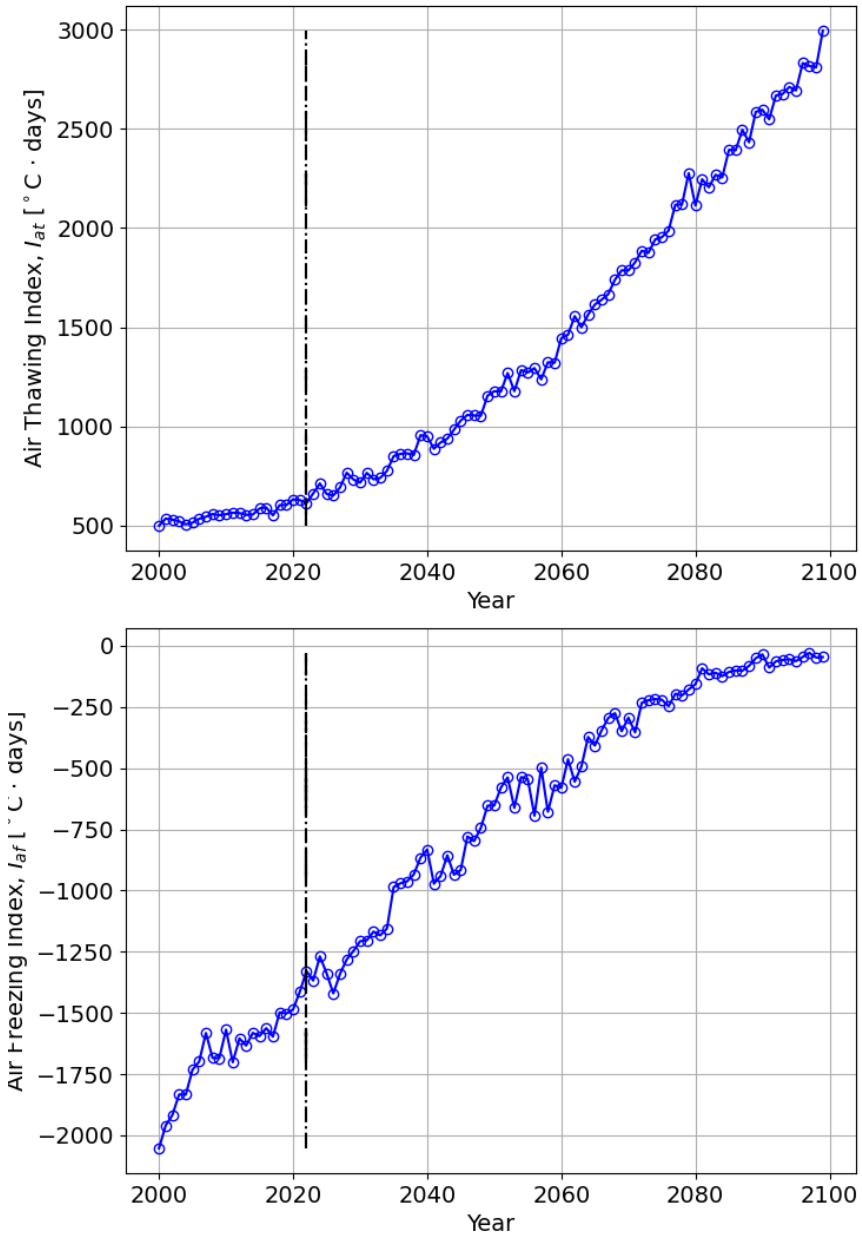

Figure 4.8: This plots show the estimated air thawing index I_{at} and air freezing index I_{af} in the period from 2000 to 2100. The vertical line indicates 2022. The future scenarios are based on predicted future temperatures from MET.

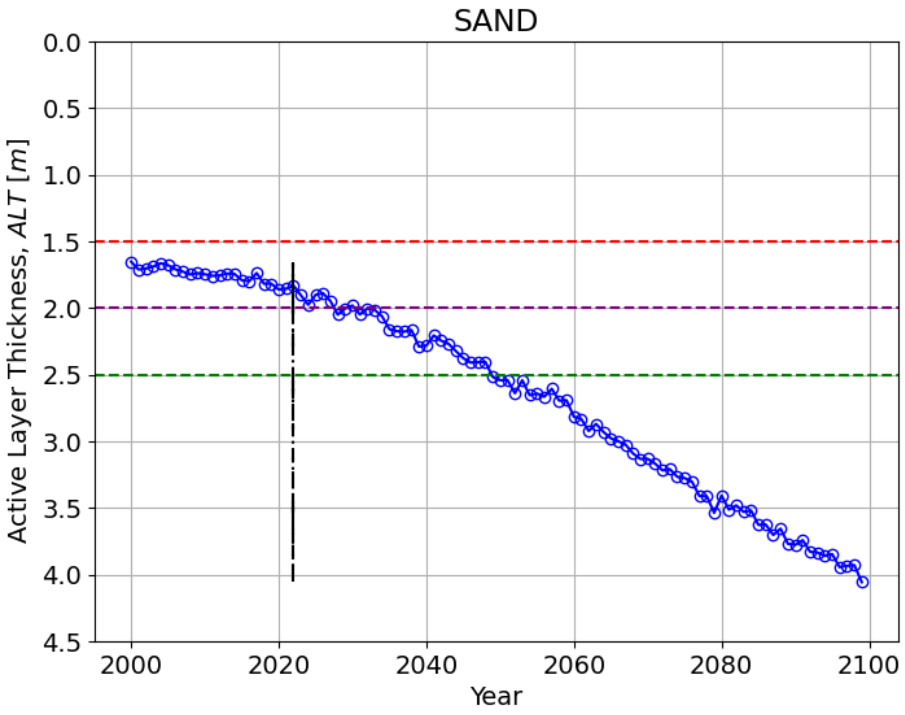

Figure 4.9: This plot shows the estimated active layer depth ALT for Sand from 2000 to 2100. The vertical line indicates 2022. The horizontal lines indicate the three different foundations depths 1.5 m (red line), 2.0 m (purple line) and 2.5 m (green line).

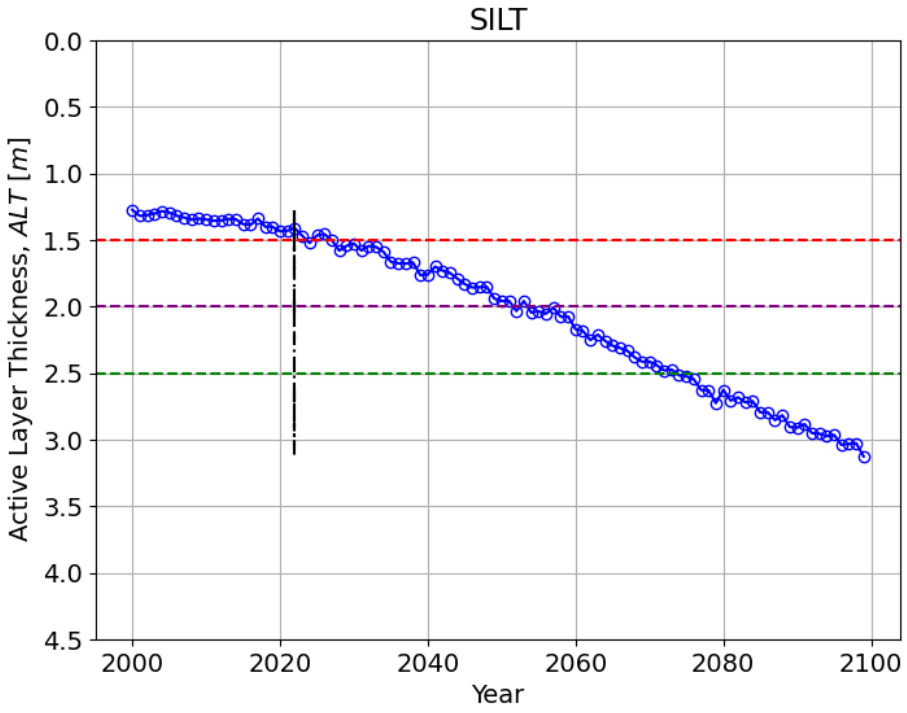

Figure 4.10: This plot shows the estimated active layer depth ALT for Silt from 2000 to 2100. The vertical line indicates 2022. The horizontal lines indicate the three different foundations depths 1.5 m (red line), 2.0 m (purple line) and 2.5 m (green line).

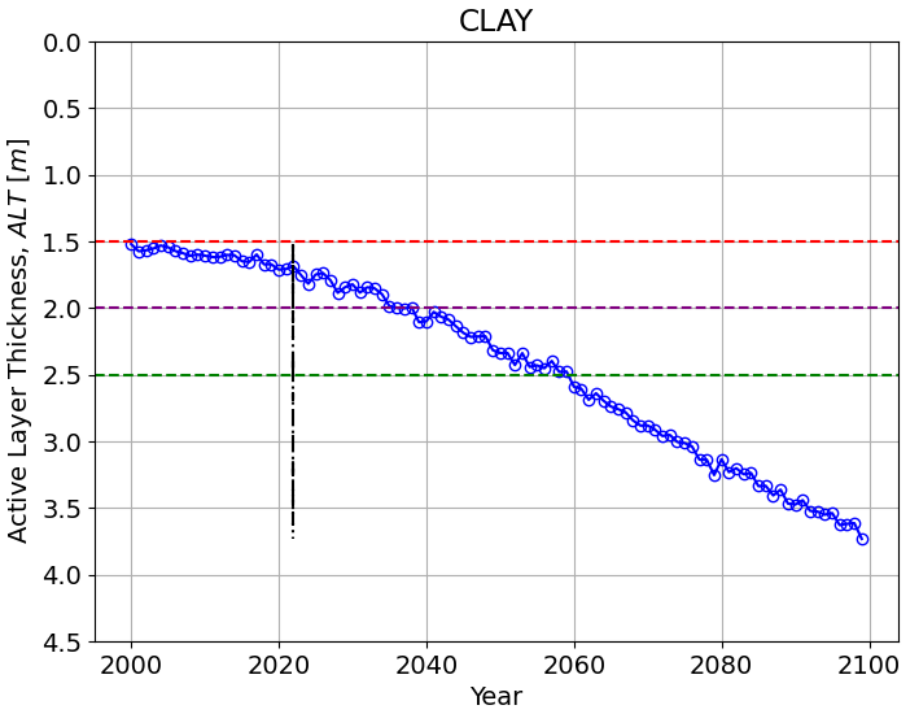

Figure 4.11: This plots show the estimated active layer depth ALT for Clay from 2000 to 2100. The vertical line indicates 2022. The horizontal lines indicate the three different foundations depths 1.5 m (red line), 2.0 m (purple line) and 2.5 m (green line).

A summary of the predicted active layer depths ALT from the Figure 4.9, Figure 4.10 and Figure 4.11 are presented in Table 4.8.

	ALT_{SAND}[m]	ALT_{SILT}[m]	ALT_{CLAY}[m]
2030	1.98	1.53	1.82
2040	2.28	1.76	2.10
2050	2.54	1.96	2.34
2060	2.81	2.17	2.60
2080	3.41	2.63	3.13
2100	4.00	3.10	3.60

Table 4.8: Future active layer depth ALT for Sand, Silt and Clay, based on analytical calculation with Stephan's Equation.

4.3 Numerical Simulation: Temp/W

In this section the numerical analysis of the temperature distribution is calculated for the three soil types: Sand, Silt and Clay. A Transient analysis type is used to analyse the temperature distribution [11]. The simulations aim to show the evolution of the ground temperatures in the active layer and the permafrost based on the predicted temperature data. To demonstrate this, the thermal analyses are performed for the period 2019 – 2100.

Model geometry and mesh

A rectangular soil sample with a width of 50 m and a depth of 28 m are created as a 2D model, as shown in Figure 4.12.

The model is spatially discretized with an average element size of 0.5 m. As the current problem set up does not involve complex initial/boundary conditions and material properties, numerical problems are not anticipated and a uniform mesh size is used throughout the model.

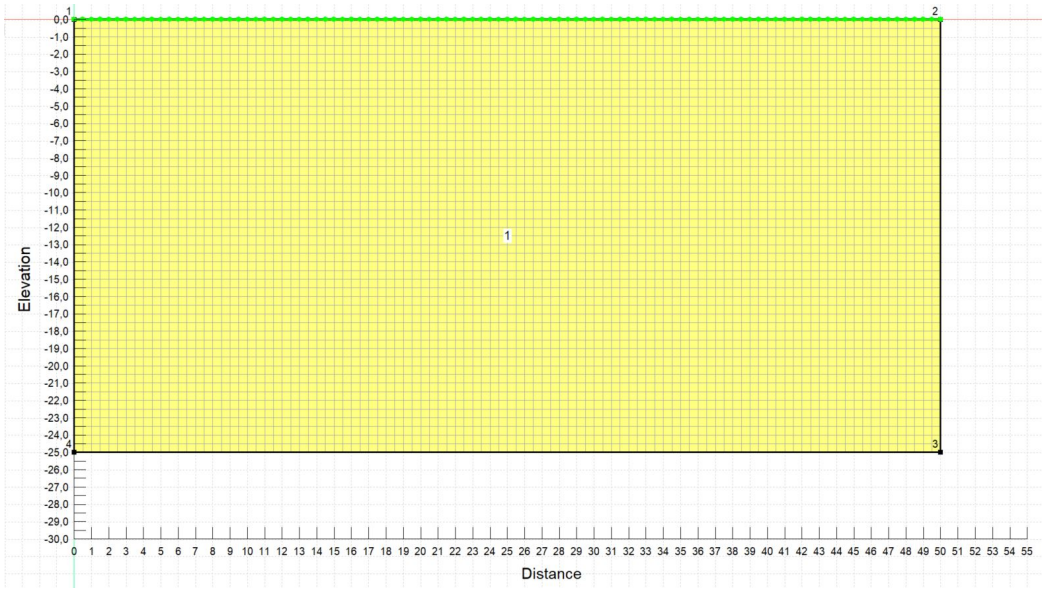

Figure 4.12: Model geometry and mesh used for the representative thermal analysis. The x-axis represent the distance, the y-axis represents the depth from the surface.

Material Properties

A full thermal model is used to model the thermal properties in Temp/W. The material properties are given in Section 4.1. A homogeneous soil body is assumed for the model. The material model is a Full Thermal Model. The thermal conductivity k is added as a Spline Data Point Function so as the function for unfrozen water content w_u.

Initial and boundary conditions

The initial temperature is set to be a spatial function with the initial temperature equal to the measured temperature at UNIS EAST borehole 5 at the top and at 28m from the 01.January.2019. The initial settings are presented in Figure 4.13.

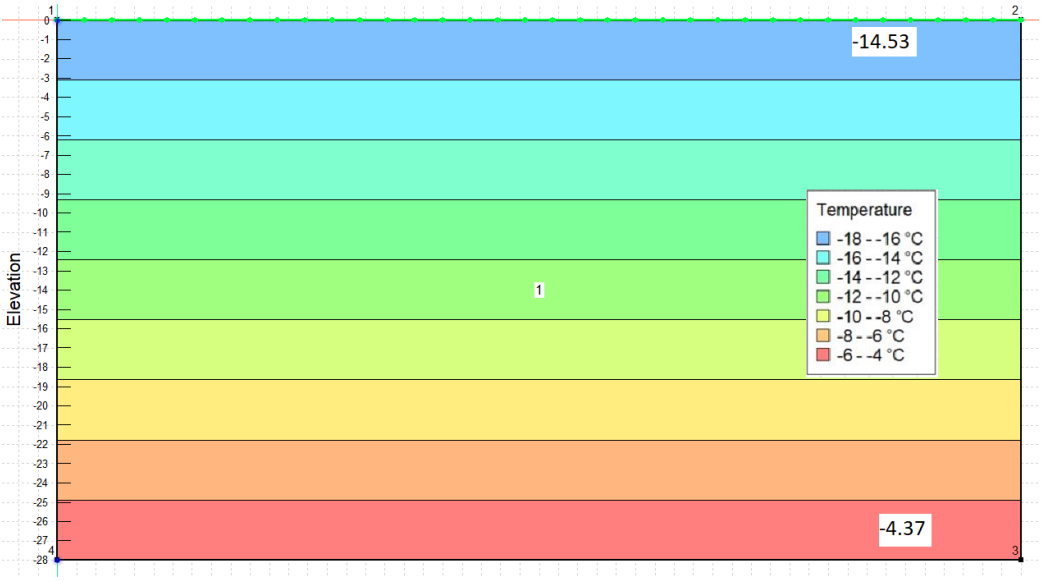

Figure 4.13: Initial temperature distribution for the thermal analysis. The y-axis represent the depth from ground surface (0 m) to 28 m. The temperature distribution is linearly distributed, from $-14.53\,^{\circ}\mathrm{C}$ at the top to $-4.37\,^{\circ}\mathrm{C}$ at the bottom, marked with colours as explained in the figure.

The predicted daily air temperature from 2019-2100 is added as a upper boundary condition to the ground surface. The data is added as a step function and presented in Figure 4.14. Natural thermal boundary conditions are assumed at the left, right and bottom boundaries of the model [3]. The simulation runs for 81 years (from 2019 to 2100) with a time step of two days.

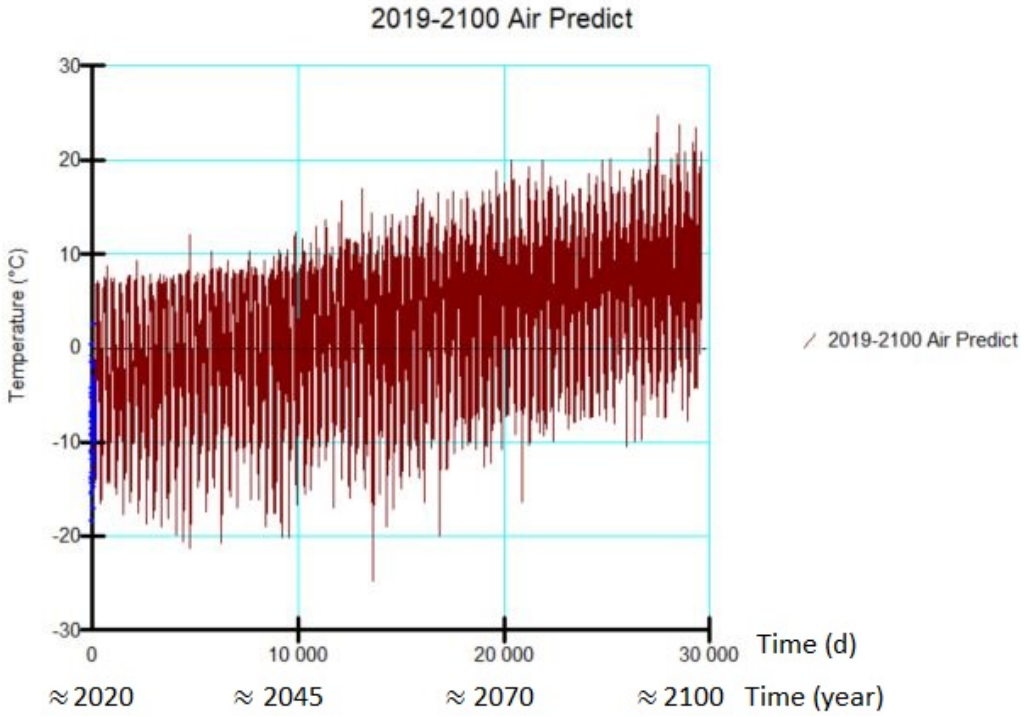

Figure 4.14: Predicted future Temperature for Longyearbyen. The y-axis represent the temperature and the x-axis represent the time (in days and year).

Calibration

The simulation of soil type Clay is calibrated towards the measured temperatures from the thermistor string data from Chapter 3. The adapted soil parameters are presented in Table 4.9.

Calibrated soil parameters for Clay		
c_{vu}	3700	kJ/m^3/°C
c_{vf}	1440	kJ/m^3/°C
w	30	%
k	1.7	J/sec/m/°C

Table 4.9: Soil parameters for calibrated clay: Frozen and unfrozen heat capacity, water content and thermal conductivity.

Sand and Silt are based on the soil parameters as calculated in Section 4.1.

Results

The analysis results in a temperature distribution curve for each time step. The simulation is computed for the three different soil types: Sand, Silt and Clay, for every second day.

To illustrate how the active layer thickness ALT is expected to change in the future the ground temperature from the end of the thawing seasons are plotted in Figure 4.15, 4.16 and 4.17. The depth of the active layer is detected for every decade from 2020 to 2060 and every second decade from 2060 to 2100 for the three soil types. From 2020 to 2050 the ALT increases approximately 1m. For 2060-2100 the ALT increases drastically, this is discussed in Chapter 5. The plots are marked with the number of years from 2019, as described in brackets in the caption of the Figures.

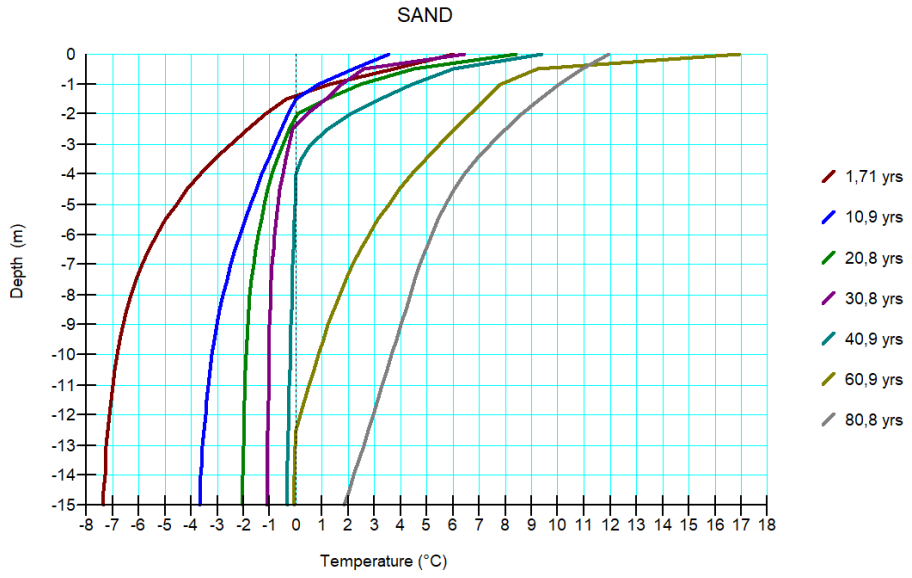

Figure 4.15: This Figure shows plots of the temperature distribution for Sand. The temperatures are plotted for the deepest ALT for 2020 (1.71 yrs), 2030 (10.9 yrs), 2040 (20.8 yrs), 2050 (30.8 yrs), 2060 (40.9 yrs), 2080 (60.9 yrs) and 2100 (80.8 yrs).

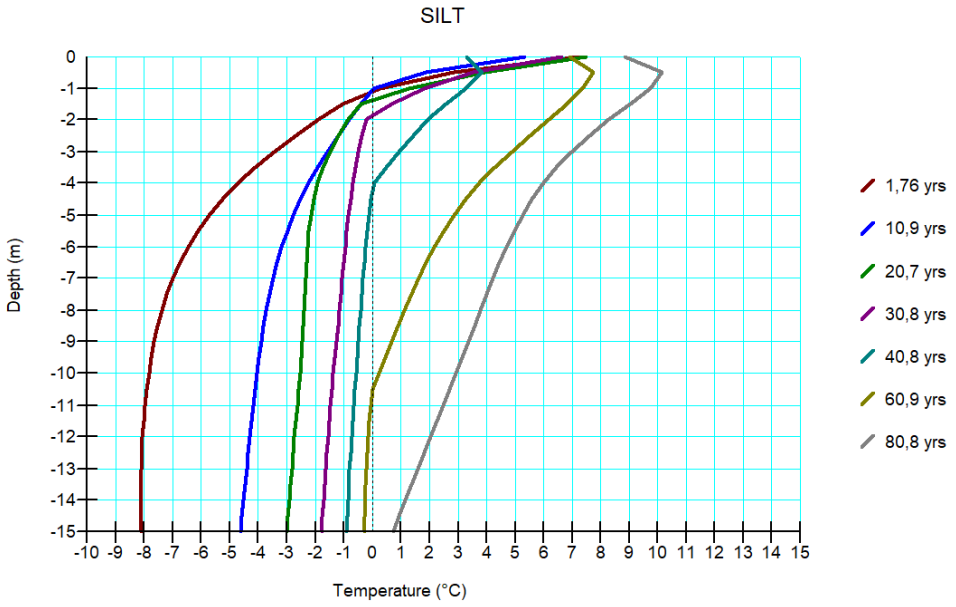

Figure 4.16: This Figure shows plots of the temperature distribution for Silt. The temperatures are plotted for the deepest ALT for 2020 (1.76 yrs), 2030 (10.9 yrs), 2040 (20.7 yrs), 2050 (30.8 yrs), 2060 (40.8 yrs), 2080 (60.9 yrs) and 2100 (80.8 yrs).

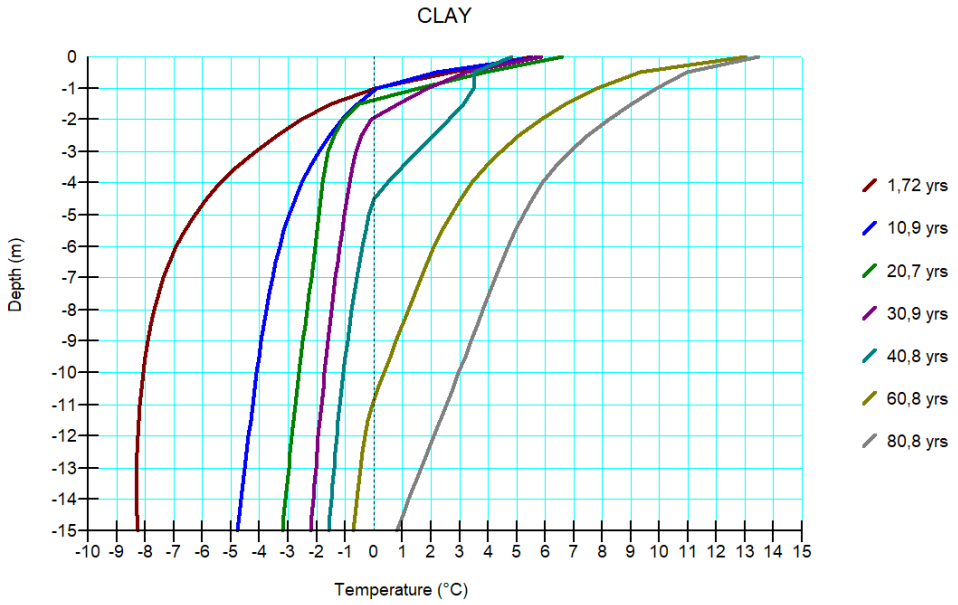

Figure 4.17: This Figure shows plots of the temperature distribution for Clay. The temperatures are plotted for the deepest ALT for 2020 (1.72 yrs), 2030 (10.9 yrs), 2040 (20.7 yrs), 2050 (30.9 yrs), 2060 (40.8 yrs), 2080 (60.8 yrs) and 2100 (80.8 yrs).

The permafrost temperature increases, as shown in Figure 4.18. The Figure presents three contour plots for Silt for year 2020, 2030 and 2040. The permafrost temperature increases from -7 $°C$ to -3 $°C$ in 20 years. A sketch of a pile and the authentic solution are drawn in the contour plots. The sketches are not in scale, but the depths are approximately 10m for the pile and between 2.0-2.5m for the authentic solution. The intention of the sketches is to visualize how the effective length of the pile and the temperature below the foundation changes. Already in year 2030 the sketch of the foundation of the authentic solution is in very warm permafrost (-1 °C). The temperatures at the depths of the foundations are summarised in Table 4.11 for the three soil types.

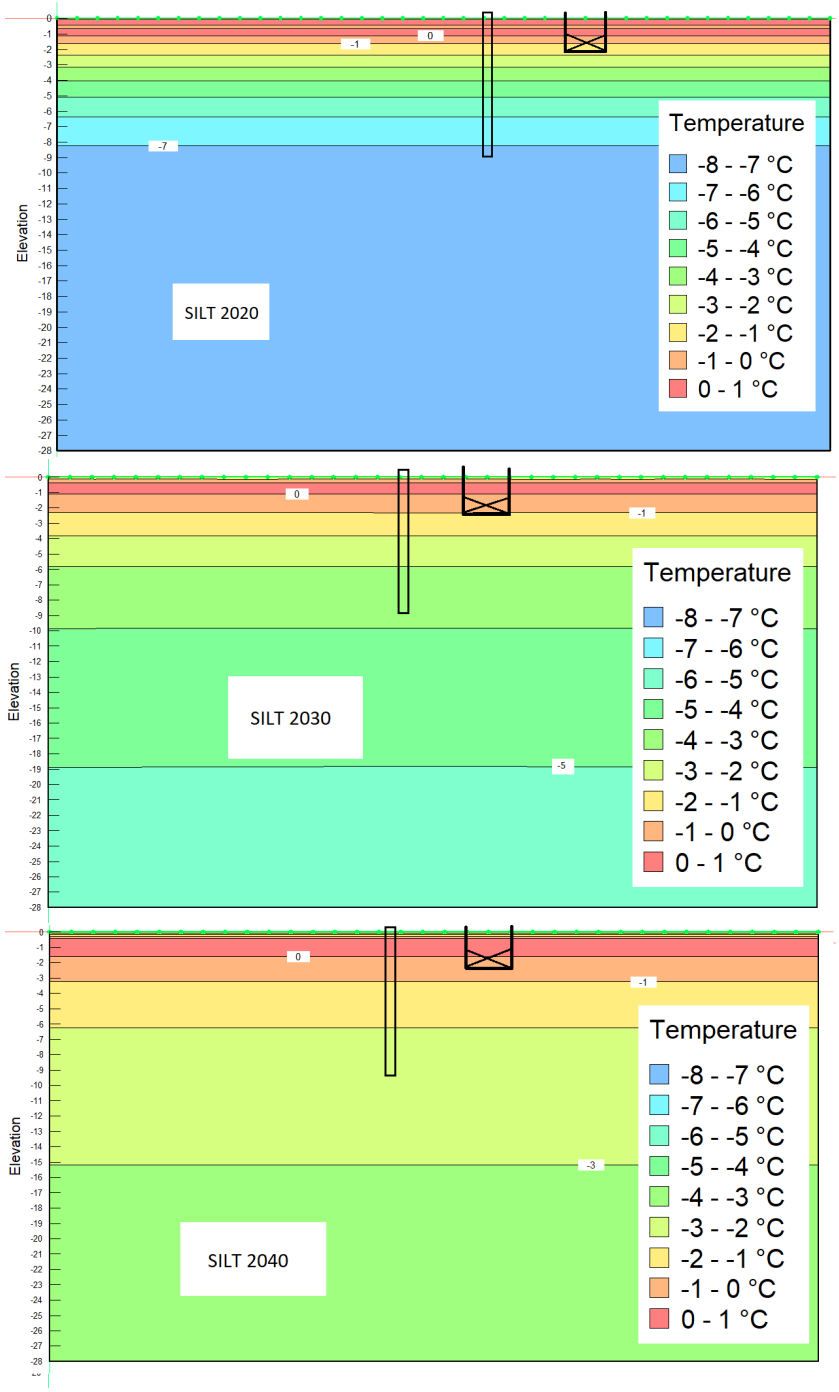

Figure 4.18: Ground temperature at the end of the thawing season for year 2020(1.9 years), 2030 (10.9 years) and 2040 (20.9 years) for soil type Silt. The two foundation types are sketched as an illustration, not in scale.

Summary

The contour plots in Figure 4.18 illustrates increase of the active layer depth and permafrost temperatures due to a warmer climate in the nearest future, i.e in 2020-2040.

The active layer depths from Figure 4.15, 4.16 and 4.17 are summarized in Table 4.10. The active layer thickness increases from 4.0-4.6 m to 20.5-16.9 m between 2060 and 2080. From the plot of the predicted temperatures in Figure 4.14 the predicted mean temperature increase 0 °C around day 10 000, which corresponds to approximately year 2045. At day 20 000, ca. year 2070 most of the temperature data is above zero (see Figure 4.14). This is the cause of the suddenly increase in the predicted active layers in Table 4.10.

	SAND	SILT	CLAY
2020	1.4	1.1	1.0
2030	1.5	1.1	1.1
2040	2.1	1.4	1.4
2050	2.3	1.8	1.9
2060	4.0	4.4	4.6
2080	12.5	10.5	16.9
2100	20.5	16.9	16.9

Table 4.10: Active layer depth ALT from the analysis without any n-factors.

The temperatures at the three foundation depths are presented in Table 4.11.

	Ground temperature [θ]								
	d_f 1.5m			d_f 2.0m			d_f 2.5m		
	SAND	SILT	CLAY	SAND	SILT	CLAY	SAND	SILT	CLAY
2030	>0	-0.4	-0.6	-0.2	-0.8	-1.1	-0.7	-1.2	-1.6
2040	>0	-0.4	-0.5	>0	-0.8	-1.1	-0.3	-1.2	-1.4
2050	>0	>0	>0	>0	-0.2	-0.8	-0.2	-0.4	-0.4
2060	>0	>0	>0	>0	>0	>0	>0	>0	>0

Table 4.11: Temperatures below footings from Temp/W for foundation depth d_f 1.5 m, 2.0 m and 2.5 m fot the three soil types.

The analysis is run for different surface conditions. The results in Table 4.10 shows the ALT from a simulation with n-factors equal to 1.0, which corresponds to a surface temperature equal to the air temperature. As described in Section 2.2 the type of ground surface affects the surface temperature. The

cableway posts are located in a big area and the individual cableway posts has different ground surfaces. The simulation of the temperature distributions are done for different surface conditions, i.e.:

- Snow: $n_f = 1$
- Pavement free of snow and ice: $n_f = 0.9$
- Sand and gravel: $n_f = 0.9$, $n_t = 2.0$
- Vegetation and 6 cm soil stripped, mineral surface: $n_f = 0.33$, $n_t = 1.22$

The surface factors are adapted from from Table 2.2. Results are summarized in Table 4.12, Table 4.13 and Table 4.14. The surface factors are added as a modification function to the air temperature boundary condition at the surface.

	Snow	Free of snow	Sand/Gravel	Vegetation
	$n_f = 1.0$	$n_f = 0.9$	$n_f = 0.9$ $n_t = 2.0$	$n_f = 0.33$ $n_t = 1.22$
2020	1.4	1.5	2.0	1.9
2030	1.5	1.6	2.6	2.2
2040	2.1	2.0	2.9	3.5
2050	2.3	2.3	4.5	6.0
2060	4.0	4.5	9.0	9.0
2080	12.5	12.5	19.0	16.4
2100	20.5	20.5	>28	24

Table 4.12: Predicted future ALT for Sand based on numerical simulation.

	Snow	Free of snow	Sand/Gravel	Vegetation
	$n_f = 1.0$	$n_f = 0.9$	$n_f = 0.9$ $n_t = 2.0$	$n_f = 0.33$ $n_t = 1.22$
2020	1.1	1.1	1.9	1.5
2030	1.1	1.1	2.1	1.7
2040	1.4	1.4	2.5	3.2
2050	1.8	1.8	5.5	5.5
2060	4.4	4.5	8.9	8.2
2080	10.5	11.0	16.5	13.9
2100	16.9	17.0	24.5	20.0

Table 4.13: Predicted future ALT for Silt based on numerical simulation.

	Snow	Free of snow	Sand/Gravel	Vegetation
	$n_f = 1.0$	$n_f = 0.9$	$n_f = 0.9$ $n_t = 2.0$	$n_f = 0.33$ $n_t = 1.22$
2020	1.0	1.0	1.5	1.4
2030	1.1	1.1	1.7	1.7
2040	1.4	1.4	3.0	3.5
2050	1.9	2.1	5.9	5.9
2060	4.6	4.9	9.0	8.0
2080	10.8	11.0	16.6	13.8
2100	16.9	17.0	25.5	20.0

Table 4.14: Predicted future ALT for Clay based on numerical simulation.

4.4 Bearing Capacity of Authentic solution

The bearing capacity of the authetic solution, presenting a shallow foundation, is calculated according to Therzaghis theory (See section 2.3.3, Equation 2.27). The foundation can be simplified to strip footings (creating a frame of ground beams) with width equal to the diameter of the log approximately 0.3 m and the length of the log approximately 5 m. The unit weight of the soil γ is calculated from the density ρ in Table 4.4.

The cohesion and friction angle are presented in Table 4.15 (based on values from Table 7.10 in [41], which includes strength parameters for temperature range -8 °C to -1 °C). The strength parameters for temperatures (at the foundation depth) equal to -1°C are chosen. This calculation is not current for warmer temperatures and conservative for lower temperatures. The input in Equation 2.27 are calculated according to the Equations in Section 2.3.3 based on the values from Table 4.15 and presented in Table 4.16.

	γ [kN/m^3]	ϕ' [°]	c[kPa]
Sand	19.8	29	28
Silt	19.8	16	50
Clay	20.2	7	42

Table 4.15: Calculated unit weight of Sand, Silt and Clay. Friction angle and cohesion from [41] for Sand, Silt and Clay at temperature -1°C.

	N_ϕ	N_c	N_q	N_γ	s_c	s_q	s_q	d_c	d_q
Sand	2.9	27.9	16.4	13.2	1.0	1.0	1.0	1.0	1.8
Silt	1.76	11.6	4.3	1.4	1.0	1.0	1.0	1.0	1.7
Clay	1.3	7.2	1.9	0.1	1.0	1.0	1.0	1.0	1.6

Table 4.16: Bearing capacity factors, shape factors and depth factors calculated due to Equations in section 2.3.3, based on input from Table 4.15

The pressure from the three structural sizes from Table 4.1 does not exceed the bearing capacity p_u for any of the values in Table 4.17. The safety factors are bigger than 3 for all cases.

Bearing capacity p_u [kN/m^2]			
d_f	1.5 m	2.0 m	2.5 m
Sand	1815	2319	2917
Silt	826	938	1068
Clay	400	444	496

Table 4.17: Calculated bearing capacity p_u [kN/m^2] based on Equation 2.27 for three different foundation depths d_f and three different soil types.

4.5 Settlements

In this Section settlements of the authentic solution (shallow foundation) and functional solution (pile foundation) are calculated. The settlements of the authentic solution are calculated based on an European approach, based on creep parameters, and a Russian approach, based on modulus of deformation. The creep parameters for the three different soil types: Sand, Silt and Clay are presented in Table 4.18.

Soil	b	n	w	σ_{c0}
Sand	0.4	2.0	1.0	300
Silt	1.0	3.0	0.6	71
Clay	0.4	2.5	1.0	175

Table 4.18: Creep parameters from Table 2.8 for Sand, Silt and Clay. Values adapted from [16].

The settlement of pile foundation is calculated based on creep parameters with two different approaches: Effective pile length L_{eff} based on maximum settlement and settlement for a standard pile of 10 m.

4.5.1 Settlement of Pile foundation

The calculations of settlements of a pile foundation are done according to the description in Section 2.3.3. From calculations done in the preproject for this thesis (added in Appendix D). The dimensional axial compression force $N_{d,c}$ for a 28 m tall cableway post was estimated to be 220 kN [8]. This compression force is used in the following pile settlement calculation. In this calculation the pile radius is set to be 0.1 m. Table 4.18 shows the input parameters for Equation 2.46.

Effective length of pile for maximum settlements

The settlement due to creep after 30 years is calculated according to Equation 2.46 and gives the effective lengths L_{eff} as presented in Figure 4.19 and Figure 4.20, for an average temperature θ equal to $-2\,^{\circ}$C and $-3.5\,^{\circ}$C. The effective lengths are calculated for maximum settlements of 10 cm, 20 cm and 30 cm.

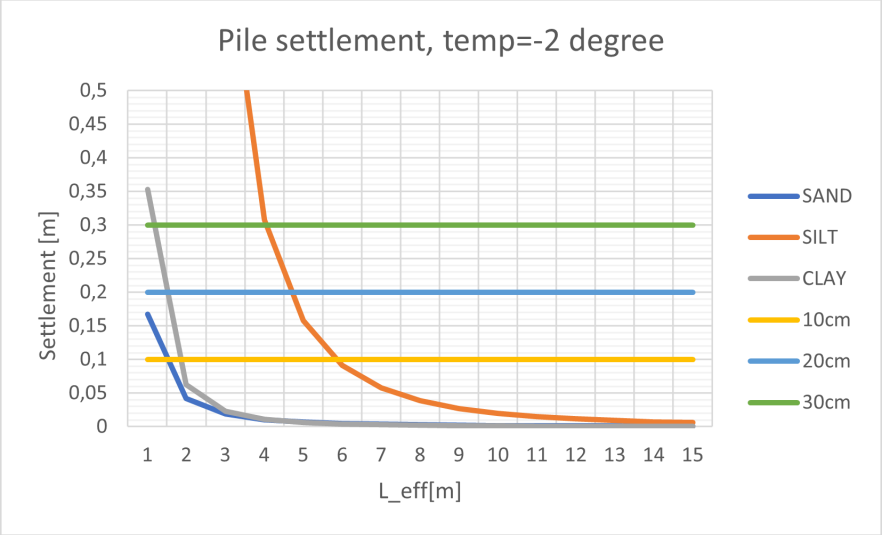

Figure 4.19: Plot of pile settlement for increased effective pile length L_{eff}, with the average temperature θ along the effective length equal to $-2\,°C$. The dark blue graph represents Sand, the orange graph represents Silt and the gray graph represents Clay. The horizontal lines represent the maximum settlements 10 cm, 20 cm and 30 cm.

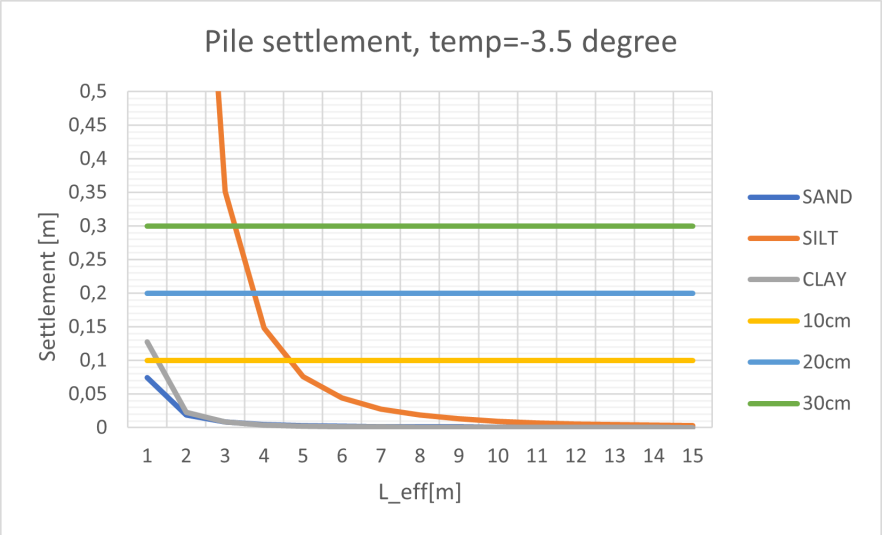

Figure 4.20: Plot of pile settlement for increased effective pile length L_{eff}, with the average temperature θ along the effective length equal to $-3.5\,°C$. The dark blue graph represents Sand, the orange graph represents Silt and the gray graph represents Clay. The horizontal lines represent the maximum settlements 10 cm, 20 cm and 30 cm.

From Table 4.18 silt has a quit low σ_{c0} compared to sand and clay. This gives large settlements. The effective length L_{eff} that reaches the maximum required settlement are presented in Table 4.19.

$\boldsymbol{L_{eff}[m]}$ **for 10 cm settlement**		
θ	$-2\,^{\circ}\mathrm{C}$	$-3.5\,^{\circ}\mathrm{C}$
Sand	1.29	0.86
Silt	5.82	4.54
Clay	1.65	1.10

$\boldsymbol{L_{eff}[m]}$ **for 20 cm settlement**		
θ	$-2\,^{\circ}\mathrm{C}$	$-3.5\,^{\circ}\mathrm{C}$
Sand	0.92	0.61
Silt	4.62	3.62
Clay	1.26	0.84

$\boldsymbol{L_{eff}[m]}$ **for 30 cm settlement**		
θ	$-2\,^{\circ}\mathrm{C}$	$-3.5\,^{\circ}\mathrm{C}$
Sand	0.75	0.50
Silt	4.03	3.16
Clay	1.08	0.71

Table 4.19: Effective length L_{eff} [m] of piles based on two different average temperatures along the effective length, three settlement limits and three soil types.

Standard Pile

In this section the settlements due to creep are calculated for a standard pile of 10 m. Table 4.20 shows the depths of −1 °C isotherm, from the simulations in Section 4.3. When the depth of −1 °C, $d_{(-1°C)}$, increases 10 m the pile have no effective length, and thereby no bearing according to this approach.

	$d_{(-1°C)}$ [m]			θ [°C]		
	Sand	Silt	Clay	Sand	Silt	Clay
2030	3.5	2.3	1.9	-2.4	-2.5	-2.5
2040	5.5	3.2	2.5	-1.5	-1.8	-1.9
2050	>10	6.5	4.9	-	-1.3	-1.4
2060	>10	>10	9.5	-	-	-1.1

Table 4.20: Predicted depth $d_{(-1°C)}$ of −1 °C from simulations in Temp/W without n-factor and average temperature θ from TempW simulation of L_{eff} of a 10 m standard pile during year 2030, 2040, 2050 and 2060.

The Settlements are calculated according to Equation 2.46 with creep parameters presented in Table 4.18 and with L_{eff} equal to the difference between the length of the pile (10 m) and the depth of $-1\,°C$ from Table 4.20. For Sand in year 2050 and 2060, and Silt in year 2060, the effective length of the pile is neglected, and thereby it is not sufficient capacity of the pile.

Settlements [m] of 10 m standard pile									
	Big structure			Medium structure			Small structure		
	Sand	Silt	Clay	Sand	Silt	Clay	Sand	Silt	Clay
2030	0.002	0.011	0.001	0.001	0.005	0.000	0.000	0.001	0.000
2040	0.010	0.049	0.002	0.005	0.021	0.001	0.003	0.006	0.004
2050	-	0.771	0.010	-	0.32	0.005	-	0.096	0.002
2060	-	-	5.5	-	-	2.7	-	-	1.0

Table 4.21: Settlement [m] of a 10m pile in Sand, Silt and Clay for three different structure sizes. The settlements are based on the future scenarios from the numerical temperature simulations in Section 4.3.

When the temperature along the entire pile increase −1 °C the effective length is zero. Calculations are not performed for the cases were L_{eff} is zero.

4.5.2 Settlement of Authentic solution

In this Section the calculations of settlement of the authentic solution are presented. The calculations are done according to the description in Section 2.3.3 with an European approach, based on creep parameters, and a Russian approach based on modulus of deformation. In this calculation we will look at the settlements for three different foundation depths and three different sizes of the structure. The pressure ΔP used in Equation 2.43 and Equation 2.44 includes the weight of the structure from Table 4.1 and the weight of the overlaying soil as illustrated in Figure 4.21.

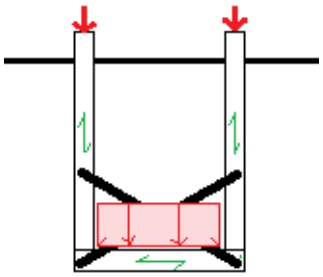

Figure 4.21: Sketch of authentic foundation.

The stresses due to the load of a cableway post are lower than the long-term strength of frozen clay, silt and sand (according to Table 7.8 and Table 7.9 in [41]). Therefore there is no conditions for development of the settlement due to secondary creep. The settlements are calculated due to Equation 2.45 and due to Equation 2.42.

The settlement due to the decrease of volume due to melt of water δ_{melt} when the soil thaw and the water shifts from solid (ice) to liquid, is calculated according to Equation 2.26. The settlement δ_{melt} increase linearly due to the increase of thawing depth below the foundation.

The modulus of deformation used in this calculations are presented in Table 4.22. The modulus of deformation for frozen sand is assumed to be equal to the unfrozen value, as the saline sand values from Table 2.9 are lower than expected.

Soil	M_u [MPa]	M_f [MPa]
Sand	30	30
Silt	12	3
Clay	4	4

Table 4.22: Unfrozen and frozen modulus of deformation for Sand, Silt and Clay used in the settlement calculations. Adapted from [41] and [40].

The settlement of the authentic solution due to vertical settlements calculated according to Section 2.3.3 are presented in the following Figures, the legends are presented in Figure 4.22. Each Figure represents one soil type and contains two plots, with thawing depth based on the analytical approach (A) (from Section 4.2) and numerical approach (B) (from Section 4.3).

As illustrated in Figure 4.22 the green markers in the plots represents the settlements due to the category "Big" structure, blue markers represents the "Medium" structure and red markers represents the "Small" structures (from Table 4.1). The columns represent the settlement for a specific thawing depth. In each column there are three different markers representing the foundation depths. The markers are square, triangle and cross, which represents foundation depth 2.5 m, 2.0 m and 1.5 m.

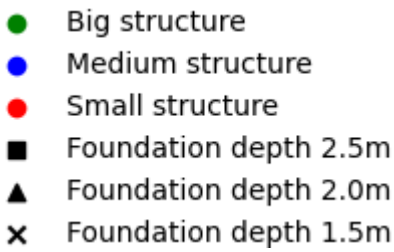

Figure 4.22: Labels in following settlement plots. The three colours differ between the sizes of the structure, the three markers differ between the foundation depth.

The settlement based on the active layer depth from the analytical design approach is labeled "design" in the following Figures. The design thawing depth is based on the three warmest summers during the last 30 years as described in section 2.2, and calculated by Stephans Equation. The design approach is added to all the Figures to compare the design approach to predicted future senarios. The numerical calculations presents the settlements based on ALT from 2030-2060, while for the analytical calculations settlements for 2080 and 2100 are added.

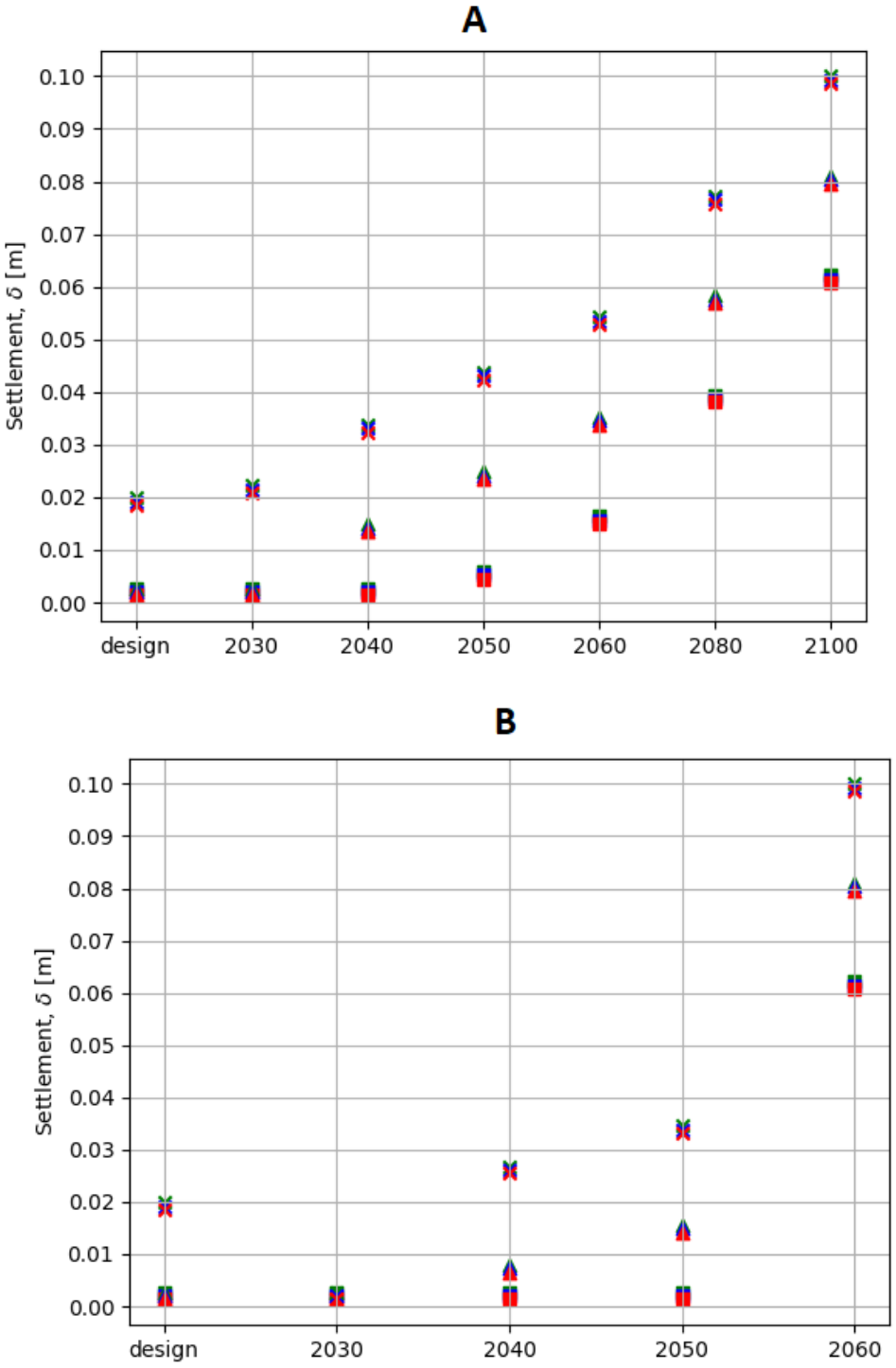

Figure 4.23: Settlement in Sand based on modulus of deformation and melt of ground ice. Active layer thickness is based on analytical (A) and numerical (B) solution. Markers are described in Figure 4.22.

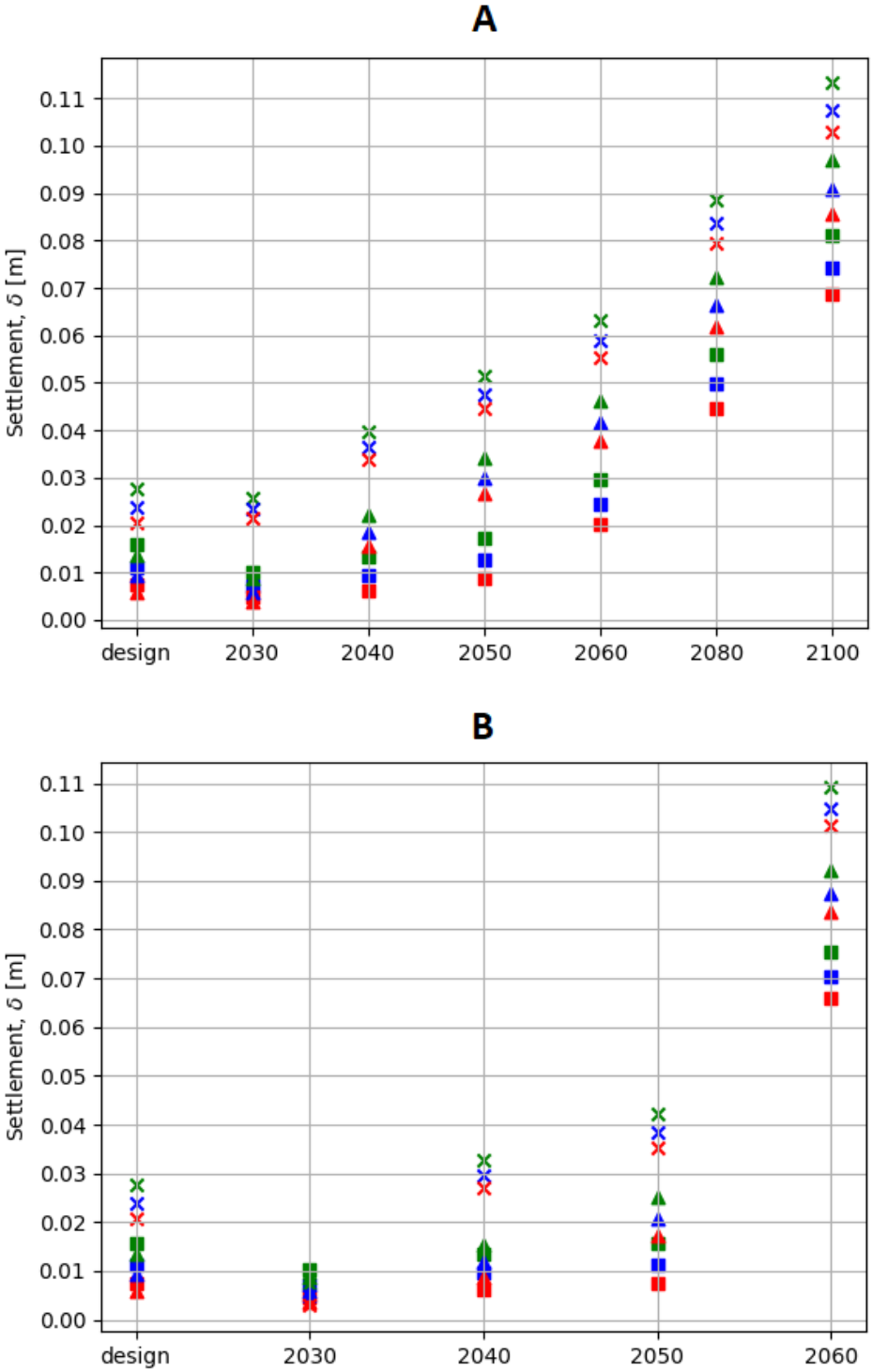

Figure 4.24: Settlement in Sand due to melt of ground ice and creep in frozen soil. Active layer thickness is based on analytical (A) and numerical (B) solution. Markers are described in Figure 4.22.

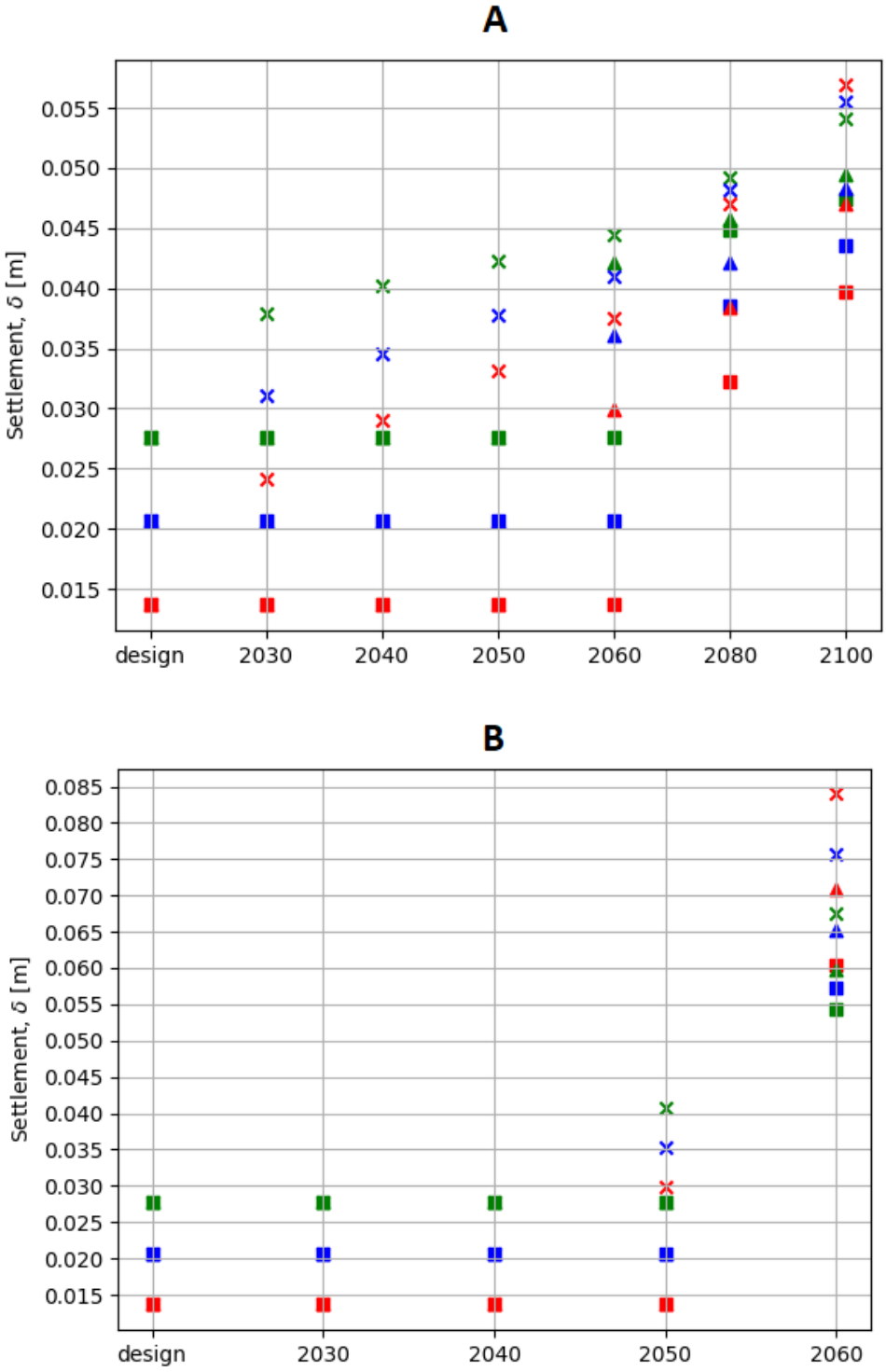

Figure 4.25: Settlement in Silt based on modulus of deformation and melt of ground ice. Active layer thickness is based on analytical (A) and numerical (B) solution. Markers are described in Figure 4.22.

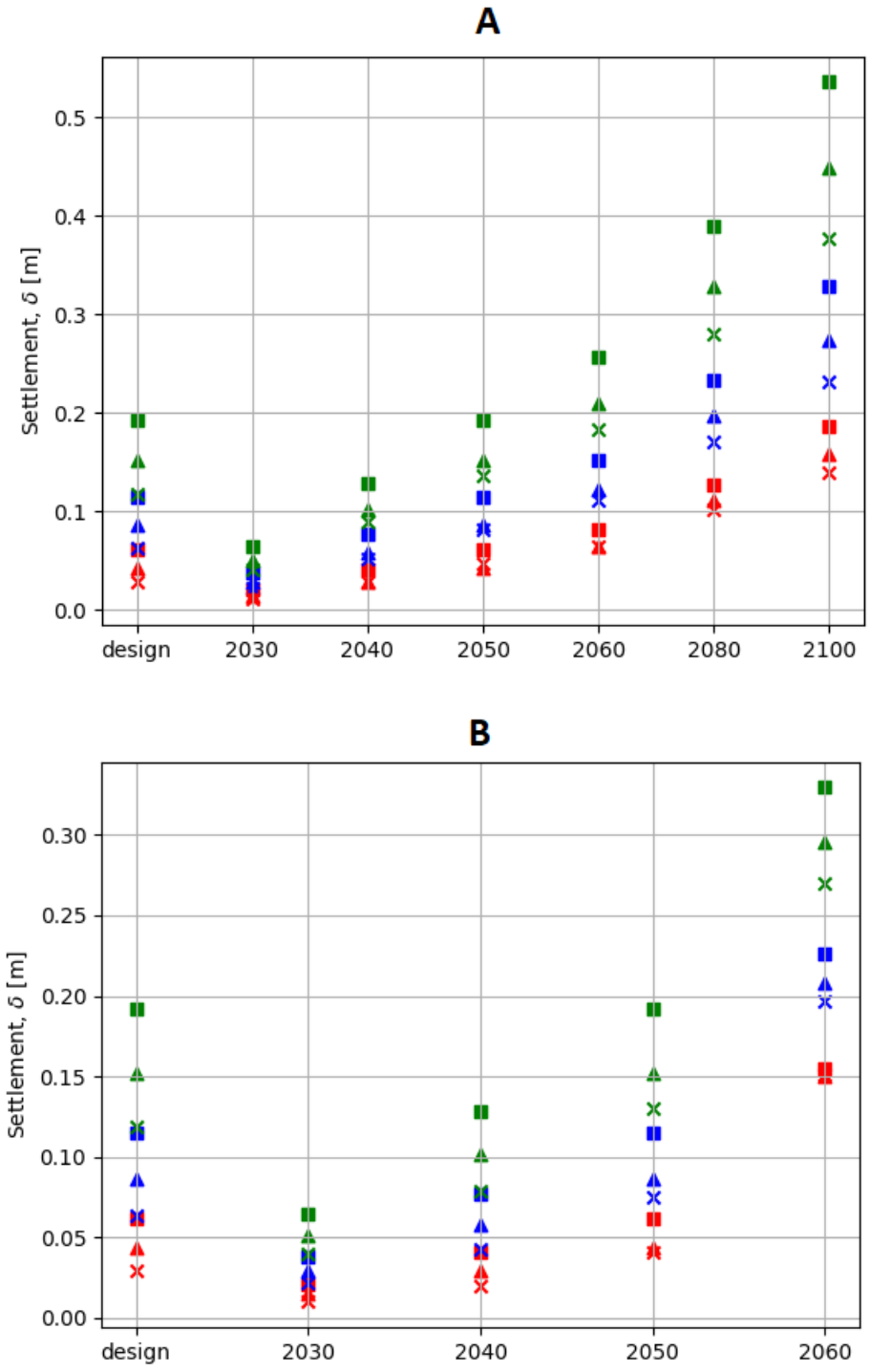

Figure 4.26: Settlement in Silt due to melt of ground ice and creep in frozen soil. Active layer thickness is based on analytical (A) and numerical (B) solution. Markers are described in Figure 4.22.

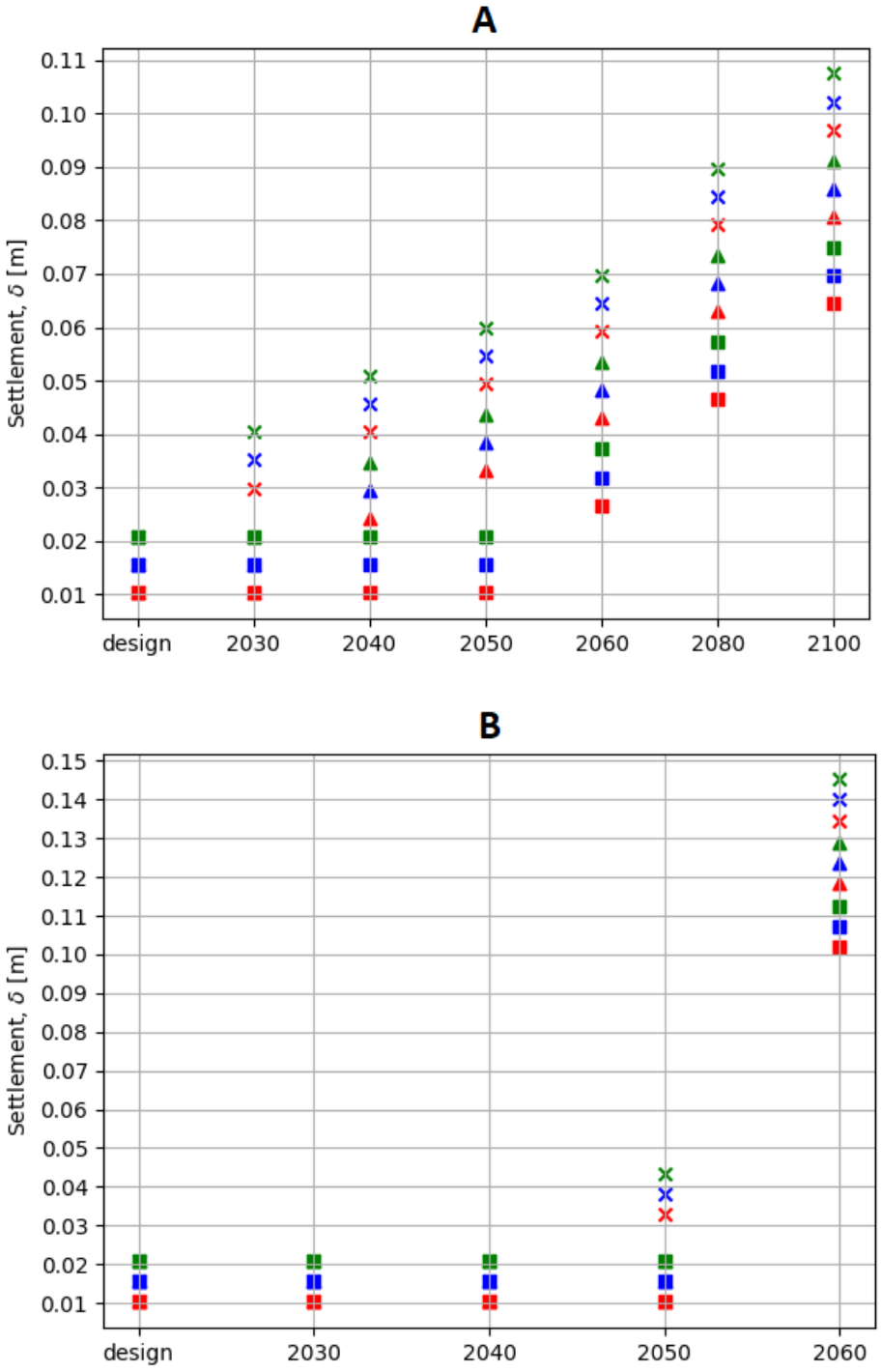

Figure 4.27: Settlement in Clay based on modulus of deformation and melt of ground ice. Active layer thickness is based on analytical (A) and numerical (B) solution. Markers are described in Figure 4.22.

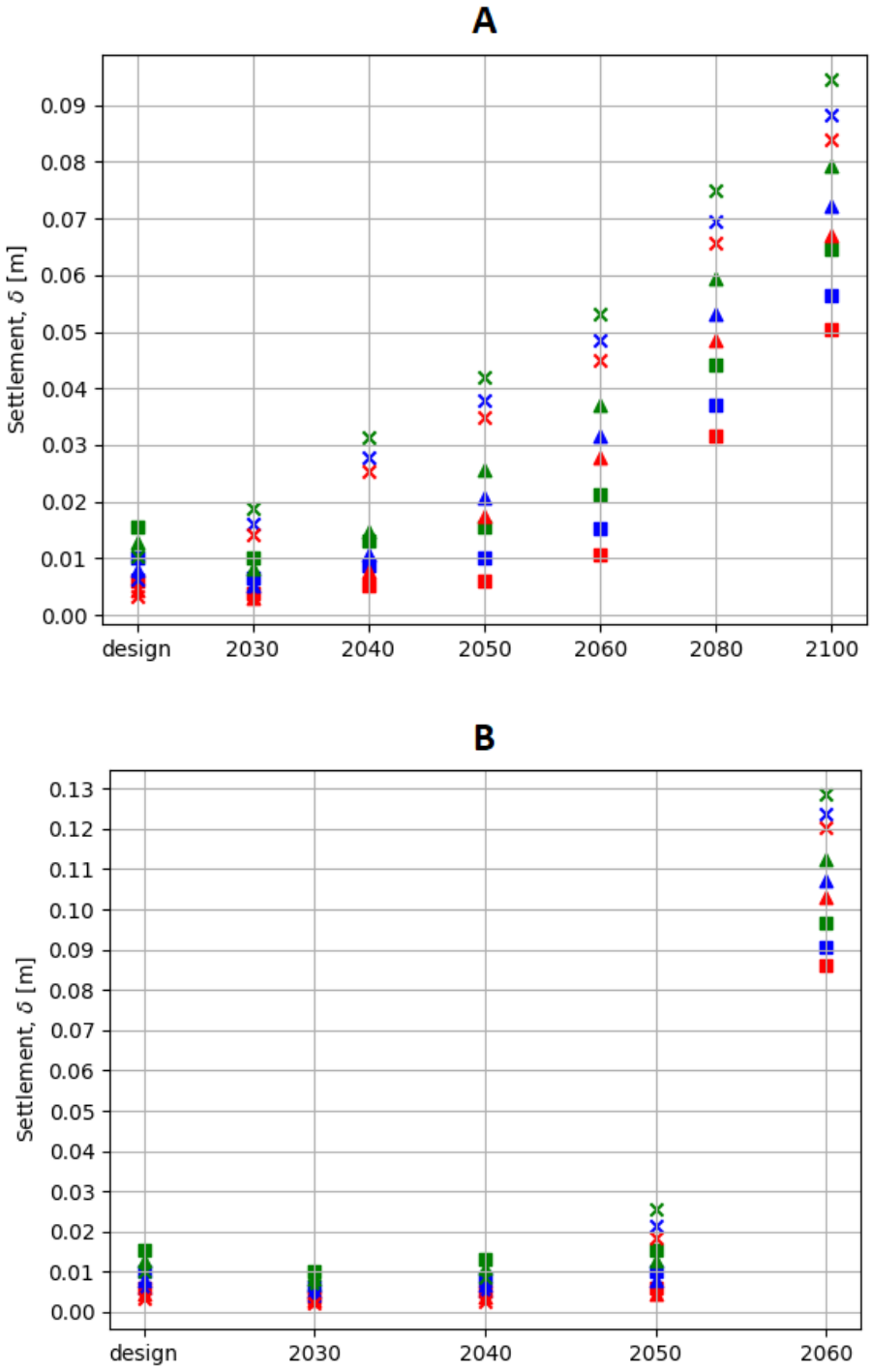

Figure 4.28: Settlement in Clay due to melt of ground ice and creep in frozen soil. Active layer thickness is based on analytical (A) and numerical (B) solution. Markers are described in Figure 4.22.

Chapter 5

Discussion and Conclusion

In this thesis we have studied two different foundation solutions for the cableway posts: authentic foundation solution and use of a modern functional solution, i.e. pile foundation. Adaptation of the authentic solution to a warming climate, i.e. degrading permafrost, was also considered via testing of increased laying depth of the authentic solution (increased foundation depth). In this Section we aim to summarise, discuss and visualize the obtained results.

We have analyzed structures of three different sizes and three different foundation depths. The settlements are calculated due to active layer thicknesses from a design approach with analytical calculation and predicted future scenarios with analytical calculations and numerical simulations. The analysis results in increased settlements for increased active layer depth.

Influence of soil parameters

Assuming an uniform soil is a simplification. In reality the soil has stratigraphy, which may include different soil types with different properties. This may, in particular, affect the thawing depth and settlements. The soil parameters are calculated based on theory from the literature. The parameters are adapted to reports from field investigations in Longyearbyen. The salinity was chosen according to Gilberts report [13], from a depth of 7 m. Salt in the upper layer of the soil might be washed away due to infiltration of water over time. This is also shown in the results from Gilbert [13] in Appendix B. The depth of 7 m was chosen due the expected average depth of a wooden pile. As a simplification, the salinity of 25 ppt was used for the three soil types through all the settlement calculations. For shallow foundation the salinity might be lower as explained above, since salt decrease the strength of frozen

ground it is a conservative assumption.

The thermal diffusivity, used to calculate the trumpet curves in Figure 4.5, Figure 4.6 and Figure 4.7, are based on the average of the frozen α_f and unfrozen α_u thermal diffusivity from Table 4.5 and Table 4.6 as described in [2]. The thermal diffusivity results in high values compared to the reference values in Table 2.7. This results in an increased temperature in the soil and increased thawing depth which differs from the thawing depth calculated by Stephan's Equation and by Temp/W. The plots are not further used, due to the unreliable results but kept in the thesis to illustrate how the temperature may develop through the ground.

Active layer thickness

The design value for the active layer thickness is based on temperatures from the past and an analytical approach with Stephan's equation. The standard approach of design active layer thickness in Section 4.2.2 results in active layer thicknesses:

- SAND: 1.92 m
- SILT: 1.48 m
- CLAY: 1.49 m

The design values should give a service life time of 30 years, but the results from Table 4.8 show that the active layer thickness will increase the design values already after 10 years based on the projected future temperatures from MET [35].

The calculations of the future thawing depth are based on analytical and numerical studies. According to the calculations it is estimated that the active layer might increase up to two meters or more within 2050, depending on the thermal properties of the soil. Increase in ground temperature will lead to increase of the permafrost temperature below and around the foundation, which affects the strength of frozen soil and bearing capacity of foundations.

Results based on the numerical approach (from Table 4.10) shows that from year 2060-2080 there will be drastic change in the active layer thickness. The predicted drastic change of ground temperatures is defined as a tipping point. A tipping point means that the whole permafrost system will change dramatically between these years. Large increase of the ALT will result in a shift

in the hydrological regime of permafrost, with increased amount of water in the soil. The thick unfrozen layer will permit bigger storage of groundwater. Larger quantities of water will warm up the upper part of permafrost. Heat transfer will include a considerable part due to convection. Modelling with Temp/W will not be adequate any longer because it does not capture convective heat transport in this analysis.

It is important to find the timing for such tipping point. We suggest that a thick ALT can be an indicator of it. For example, in our simulations the ALT significantly increases from 4 m to much higher values after year 2060. An active layer depth of 4 m may be considered as realistic value which may be found in the regions of discontinuous permafrost, while higher values of the ALT are related to even warmer permafrost regions, where engineering is not necessary relying on the principles of handling frozen ground, but rather on traditional geotechnics. In other words dealing with such warm permafrost should be avoided if possible due to its low stability. Due to the latter, settlements of shallow foundations until 2060 (i.e. for the ALT thinner than 4 m) might be reasonable. The projection is based on "worst case" weather data and thereby gives conservative values.

Temp/W is used as a numerical approach. Temp/W is better than the analytical approach to simulating accumulating effects. It takes the temperatures for each day and applies them. The weakness of Temp/W is that it exaggerates the effects over many years.

In both analytical and numerical simulation we try to simulate reality but we cannot capture the reality 100 %. We try to approximate reality.

Temperature

The average warming trend in Longyearbyen since the 1980s, based on 30-year mean values, is approximately 0.72 °C/decade [17]. The same trends are shown in Figure 4.3 in Section 4.2.1 based on the temperature from 1976 until today, for a meteorological station at Longyearbyen airport. The temperature trend based on previous temperature measurements presented with linearization, visualise a drastically change in the temperatures at Svalbard. Using a linearization is an approximation, but an easy way to analyse the trends. The decreased ground cooling from warmer temperatures during winter is the main factor causing permafrost warming and thaw in Svalbard [17]. Combination of decreasing air freezing index and increasing thawing index (as shown in section 4.2.3) is a clear signal of warmer climate, and will affect

the stability of existing foundations on permafrost in the region [17]. Similar results were modelled by Instanes [17].

The coldest estimated temperature below the authentic foundation is $-1.6\,^{\circ}\mathrm{C}$ (see Table 4.11), for Clay with foundation depth of 2.5 m in 2030. The temperatures below the foundations are warm and the guarantee that the soil will be in a frozen state is low. If the soil contains salt the freezing depression will decrease the freezing point. Due to the warm permafrost temperatures the soil will not be frozen for high salinities. The shallow foundation need to be in the permafrost (permanently frozen ground) to have sufficient capacity, according to [2]. Therefor, rehabilitation with the authentic solution is not recommended.

Permafrost modelling done by Bekele and Sinitsyn [3] projection based on the same data input (climate projections [35]) as in this report, but with different soil parameters, gave similar results. The three projections for the period until 2050 are quite similar and gives a thawing depth at approximately 2 m.

Cableway posts

The vertically loads on the foundation are assumed to mainly originate from the self weight of the structure and wind actions. The lateral loads due to sloping terrain are not evaluated. The results are presented in terms of settlements.

In Chapter 4 a generalized weight is assumed based on a generalized volume for three different sized cableway posts. During May 2022 two relatively small cableway posts in Adventdalen was rehabilitated. This was a pilot project for SNSK. In this operation they measured the weight of the structure to be 3-5 tons. The assumed weight is higher than the measured weight, which is conservative. For our assumptions with a surface area equal to $1.8\,\mathrm{m}^2$ the big structure (from Table 4.1) approximately equals a weight of 15 tons and the small category equal 7.5 tons. For a 5 ton structure with a safety factor of 1.5 the assumption of 7.5 tons seems reasonable.

Bearing capacity of shallow foundation

The bearing capacity of the three soil types calculated in Section 4.4 are sufficient compared to the pressure of the three different sized structures presented in Table 4.1. As long as the soil is frozen the safety factors are bigger than 3 for all cases.

According to the predicted increase of active layer thicknesses (Section 4.2 and Section 4.3) the foundation depth is recommended to be deeper than the "maximum" foundation depth of 2.5m until year 2050. The temperature regime is quite uncertain and depends on the local site. The predicted temperatures in the permafrost below the foundation (Table 4.11), at 2.5 m in year 2050, are between -1°C and 0°C. This is warm permafrost soil. A small change in the temperature will have a big impact on the capacity.

Settlement of pile foundation

According to the predicted future temperatures, the effective length L_{eff} of a standard pile of 10 m will decrease drastically within year 2050. Instanes [16] and Sinityns [3] reports similar scenarios. The piles will settle less than 5 cm until 2040 (Table 4.21). Soil type Sand and Silt do not have sufficient capacity for a 10 m standard pile after year 2040 due to the increased active layer thickness. Soil type Clay has sufficient capacity until year 2050.

The depth of permanently frozen temperatures below -1°C increases which mean that the effective length of a pile decreases (see Section 4.3). Already at year 2040 the depth of -1°C reaches 5.5 m for sand. Therefore longer piles are recommended. Changing from wooden piles to steel piles will increase the range of pile length. It will also prevent concerns regarding rot.

Settlement of authentic foundation

Comparing the design approach to the predicted future scenarios the settlements in Sand increases the design approach already in year 2040 (except for the analytical approached based on modulus of deformation where the settlements increase the design values already in 2030). For soil type Silt there is a big difference (factor 10) between the settlements calculated due to the modulus of deformation and the creep parameters (see Figure 4.25 and Figure 4.26). The settlements due to the design approach for Silt due to creep gives settlements that is outside the range of acceptable settlements.

This means that based on the design ALT Silt will not have sufficient capacity through the service lifetime (30 years). For soil type Clay the design approach resulted in small settlements, 1-2 cm, which was increased between year 2030 and 2050 depending on the calculation approach (see Figure 4.27 and Figure 4.28).

The maximum predicted settlements of the authentic solution in 2060 vary between 4.5 cm (Figure 4.25) and 38 cm (Figure 4.26). The settlements are calculated based on two different mathematical approaches: modulus of deformation and creep parameters. There are several points that contribute to the difference in the settlement calculations: The modulus of deformation and creep parameters are obtained for different types of soil (no soil is identical). The approaches are based on different types of tests. The modulus of deformation are based on oedometer tests while the creep parameters are obtained from uni axial compression test. Those tests do not correspond one to one to each other.

The settlement increase 10 cm (which is defined as the failure criteria, see Section 2.3.3) at year 2060 for Sand and Clay, and 2040 for Silt.

General requirements

The shallow foundation need to be in the permafrost, which is defined as permanently frozen ground. The ground is assumed to be frozen when the temperatures are below 0 °C, which might not be the case for saline soil. For warm permafrost, which is "plastic frozen" [2], consolidation should be taken into account. For piles the definition of the effective length claims a temperature equal or below −1 °C in frozen soil, to have sufficient adfreeze strength. When the ground temperatures increases, the temperature difference between 0 °C and −1 °C give a telling difference in depth. This is one of the reasons that both the standard piles and the shallow foundation fails around the same time (2040). If the shallow foundation required temperatures equal or below −1 °C to have sufficient capacity, they would fail around year 2030 (see Table 4.11).

For shallow foundation the rehabilitation need to take place during the fall when the thawing depth is deepest, to limit the need of digging in frozen soil. The permafrost is disturbed during the installation process and need to freeze back during the following winter to have sufficient capacity. Piles on the other hand, is not limited by the seasons and can be drilled into the soil through the whole year. Therefore piles is assumed to increase the efficiency of the rehabilitation.

The shallow foundations are more vulnerable to temperature change in the ground, due to the warm permafrost temperatures. Due to the uncertainties of the temperatures below the shallow foundation, piles are recommended. The service life time of a standard pile is also questioned, further investigation of longer piles in steel is recommended.

The size of the settlement might be uncertain due to climate change and variable soil properties. Settlements will occur and most likely uneven settlements as illustrated in Figure 5.1. An uneven settlement of +/− 5 cm (which is defined as an acceptable situation according to Section 2.3.3) will create a remarkable movement of the top of the structure as illustrated in Figure 5.1.

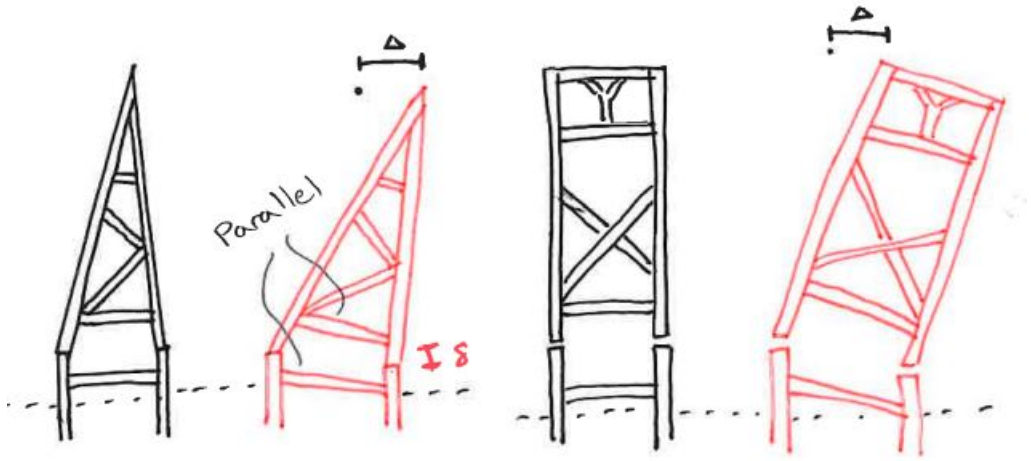

Figure 5.1: The sketch illustrates the effect of uneven settlements (not in scale).

Assuming a frame of 5 m times 5 m and a maximum uneven settlement of 5 cm this will create a movement of 28 cm of the top of a structure for a 28 m high structure. An uneven vertical settlement of 10 cm will cause a movement of the top that will increase half a meter (for a 28 m high structure).

Until now the structures, which is still standing, has stood for several years. That means that the loads need to be in equilibrium and thereby the resistance capacity is bigger than the force that the structures are exposed to (until failure). Even though the structures may have sufficient capacity today, the rehabilitated foundation need to be designed for the future scenarios.

5.1 Further work

For the rehabilitation projects, installation of a thermistor-string in the ground close to the foundation is recommended, in order to be in control of the temperature distribution along the foundation. Data from the installed I-buttons (see Section 3) should be measured and used for more accurate predictions of the surface temperatures close to the cableway posts. The report from the field inspection is recommended used for planning the order of the future rehabilitation projects regarding the cableway posts.

Accurate estimation of material properties is required for a definitive stability evaluation. This thesis highlights the differences in design method, and

calculate settlement due to a "general" situation. The design of a specific cableway post should be based on more accurate material properties for the specific cite. Site investigations and lab test to get in situ soil parameters are therefore recommended.

Bibliography

[1] AMAP. "Arctic Climate Change Update 2021: Key Trends and Impacts. Summary for Policy makers". In: *Working Group of the Arctic Council* 1 (May 2021).

[2] Orlando B. Andersland and Branko Ladanyi. *Frozen Ground Engineering*. 2nd ed. ISBN:0-471-61549-8. John Wiley & Sons, New Jersey, 1986.

[3] Yared Bekele and Anatoly O.Sinitsyn. "SINTEF NOTES 36. Impact of Climate Change on Infrastructure in Longyearbyen. Case study of pile foundations on sloping terrains." In: (2020). Ed. by SINTEF Academic Press. ISBN:978-82-536-1658-2.

[4] Jean-Louis BRIAUD. *Geotechnical Engineering: Unsaturated and Saturated Soil*. 1st ed. John Wiley & Sons, New Jersey, 2013.

[5] Burke et al. *Evaluating permafrost physics in the Coupled Model Intercomparison Proeject 6 (CMIP6) models and their sensitivity to climate change*. Ed. by European Geosciences Union. 2021. URL: `https://tc.copernicus.org/articles/14/3155/2020/`.

[6] Braja M. Das. *Principles of Geotechnical Engineering*. 7th ed. CENGAGE Learning, 2010.

[7] Kulturminneforvalter SNSK Dennis Guhl. *Rapport om restaurering av taubanebukk gruve 5-6 bane ved Alpinbakken*. Tech. rep. Store Norske Spitsbergen Kullkompani, 2019.

[8] Kristin Enevoldsen. "Rehabilitation of Cableway post, Pre-project for master thesis". Prosjektoppgave. 2021.

[9] Anne-Chatrine Flyen and Johan Mattsson. "Bevaring av teknisk industrielle kulturminner, Reparasjon av taubanebukker i Longyearbyen." In: (2018). Ed. by NIKU.

[10] Anne-Chatrine Flyen and Johan Mattsson. "Permafrost og fundamenteringsfohold for kulturminner i Longyearbyen". In: (2017). Ed. by NIKU.

[11] Geostudio. *Thermal modeling with TEMP/W. An Engineering MEthology*. Jan. 2014. URL: https://www.geoslope.com/products/temp-w.

[12] Fag-gruppe for Geoteknikk NTNU. "Introduksjon til GEOTEKNIKK". Kompendium in TBA4100. 2018.

[13] Anatoly O. Sinitsyn Graham L. Gilbert Arne Instanes and Arne Aalberg. *Characterization of two sites for geotechnical testing in permafrost: Longyearbyen, Svalbard*. Tech. rep. 1. Geosciences, Sept. 2019. URL: http://www.aimspress.com/journal/geosciences.

[14] Sarah Theresa Heller. "A numerical simulation of permafrost thermal rgime under a heat pump chilled foundation in Longyearbyen, Svalbard". MA thesis. NTNU and UNIS, 2021.

[15] A.Sorteberg I.Hanssen-Bauer E.J.Førland H.Hisdal S.Mayer A.B.Sandø. *Climate in Svalbard 2100, a knowledge base for climate adaptation*. Tech. rep. 1. ISSN: 2387-3027. Sysselmesteren på Svalbard, Miljøavdelingen, Jan. 2019. URL: http://www.miljodirektoratet.no/M1242.

[16] Arne Instanes. *Coastal permafrost- foundation design Incorporating climate warming scenarios*. Report no. IAS162131-1. Center for reasearch-based Innovation, 2017.

[17] Arne Instanes. "Incorporating climate warming scenarios in coastal permafrost engineering design- Case studies from Svalbard and northwest Russia." In: (2016). Ed. by Cold Regions Science and Technology.

[18] Hilde Tokie Yri Irene Skauen Sandodden. *Kulturminneplan for Svalbard 2012-2023*. Tech. rep. 1. Sysselmesteren på Svalbard, Miljøavdelingen, 2013. URL: https://www.sysselmesteren.no/contentassets/bffbcd7fa7ae42ad8c6c22f047b360b3/kulturminneplan-2013---2023.pdf.

[19] Jochen Köhler. "Lecture K_{01}: Introduction Structural Engineering". NTNU Lecture notes. TBA4125. 2019.

[20] L.T. *Mechanics of Frozen Soils*. 1st ed. Moskow, MAIK "Nauka/Interperiodika", 2002.

[21] Per Kristian Larsen. *Prosjektering av konstruksjoner, laster og bæresystemer*. 2nd ed. Tapir Akademisk forlag, Trondheim, 2008.

[22] Max Konig Matthew Sturm Jon Holmgren and Kim Morris. "The thermal conductivity of seasonal snow". In: (2017). Ed. by Cambridge university press.

[23] Klima- og miljødepartementet. *Kulturminneloven*. Feb. 1979. ISBN: 82-504-1287-7. URL: https://lovdata.no/dokument/NL/lov/1978-06-09-50?q=kulturminneloven.

[24] Klima- og miljødepartementet. *Svalbard Miljøloven*. 7th ed. June 2001. URL: https://lovdata.no/dokument/NL/lov/1925-07-17-11?q=svalbard.

[25] BAF Multiconsult. "Tilnærmet beregning av vindlast taubanebukk". Project: Stabilisering av taubanebukker ordre: 713851. 2017.

[26] Norges geotekniske institutt NGI. *Historiske hendelser*. URL: https://www.ngi.no/Om-NGI/Hvem-er-vi/Historiske-hendelser. (accessed: 23.11.2021).

[27] Standard Norge. "NS-EN 1990:2002+A1:2005+NA:2016 Eurokode: Grunnlag for prosjektering av konstruksjoner". In: *Standard Norge* (2005).

[28] Standard Norge. "NS-EN 1991-1-4:2005+NA:2009 Eurokode 1: Laster på konstruksjoner Del 1-4 Allmenne laster Vindlaster". In: *Standard Norge* (2005).

[29] Standard Norge. "NS-EN 1995-1-1:2004+A1:2008+NA:2010 Eurokode 5: Prosjektering av trekonstruksjoner Del 1-1 Allmenne regler og regler for bygninger". In: (1995).

[30] Standard Norge. "NS-EN 1997-1:2004/AC:2009 + National Annex 2008 Eurocode 7: Geotechnical Design Part 1: General Rules." In: (2008).

[31] Standard Norge. "NS-EN 338:2016 Konstruksjonstrevirke Fasthetsklasser". In: *Standard Norge* (2016).

[32] Arne Instanes Ole Humlum and Johan Ludvig Sollid. "Permafrost in Svalbard: a review of research history climate background and engineering challenges." In: (2003). Ed. by Norsk Polarinstitutt.

[33] Longyearbyen lokalstyre/Norsk Polarinstitutt/Store Norske/Sysselmanen på Svalbard/Telenor. *TopoSvalbard*. webside. Nov. 2021. URL: https://toposvalbard.npolar.no/.

[34] Geo precision. *Thermistor-string*. URL: https://www.thermistor-string.com/. (accessed: 25.05.2022).

[35] Kjetil Isaksen Rasmus E Benestad Kajsa M Parding and Abdelkader Mezghani. "Climate change and projections for Barents region: what is expected to change and what will stay the same?" In: *Environmental Research* 11.5 (2016). URL: https://iopscience.iop.org/article/10.1088/1748-9326/11/5/054017/meta.

[36] Per Kyrre Reymert. “Fra company town til moderne by”. In: *Sysselmannen, miljøvern avdelingen*. 1.1 (Jan. 2013), p. 58.

[37] Norwegian centre for climate service. *Temperature measurements LYR*. URL: https://seklima.met.no/. (accessed: 01.09.2016).

[38] Anatoly Sinitsyn. *PCCH-Arctic*. URL: https://www.sintef.no/prosjekter/2021/pcch-arctic/. (accessed: 26.02.2021).

[39] Svalbard bygg AS Trond Håvelsrud. *Rapport om vedlikehold av taubanebukken ved sykehuset*. Tech. rep. Svalbard bygg AS, 2016.

[40] Aksenov V.I. “"Koeffitsiyenty dlya korrektirovki znacheniy moduley deformatsii, poluchennykh v rezul’tate kompressionnykh ispytaniy morzlykh gruntov (Coefficients for adjusting the values of deformation modulus obtained as a result of compression tests of frozen soils)." (1 (Special issue "The Earth Planet System"))”. In: (2013). Ed. by Electronic Scientific Edition Almanac Space and Time 4.

[41] Aksenov V.I. *Zasolennyye merzlyye grunty arkticheskikh poberezhiy kak osnovaniya sooruzheniy (Saline frozen soils of Arctic coast as bases for structures)*. 1st ed. Moscow, Vse o mire stroitel’stva (Everything about construction world), 2008.

[42] Wikepedia. *Albedo*. URL: https://en.wikipedia.org/wiki/Freezing-point_depression. (accessed: 07.06.2022).

[43] Wikepedia. *Freezing-point depression*. URL: https://en.wikipedia.org/wiki/Albedo. (accessed: 31.05.2022).

[44] Wikepedia. *Solifluction*. URL: https://en.wikipedia.org/wiki/Solifluction. (accessed: 30.05.2022).

Appendix A

Python Code

List of Scripts

Script A.1: Trumpet Curve

```
import matplotlib.pyplot as plt
import pandas as pd
import numpy as np
import math



data=pd.read_csv('MAATMinMaks.csv',header=None)
year=data[2]
MAAT=data[3]
MAAT_maks=data[4]
MAAT_min=data[5]

def A_z1(Year,alpha):
    i=0
```

```
16
17      T_min=[]
18      T_maks=[]
19      while Year!=year[i]:
20          i+=1
21      T_min.append(MAAT_min[i])
22      T_maks.append(MAAT_maks[i])
23      print('Year:',Year, 'T_min is:',T_min[0],'T_maks is:',
        T_maks[0])
24      A_z=[]
25      T_z_pluss = []
26      T_z_minus = []
27      A_s = (T_maks[0] - T_min[0]) / 2
28      T_m = MAAT[i]
29      #z = [0, -0.2, -0.4, -0.6, -0.8, -1, -1.2, -1.4, -1.6,
        -1.8, -2, -2.2, -2.4, -2.6, -2.8, -3, -3.2, -3.4, -3.8,
        -4]
30      z=np.linspace(0,-10.50)
31      p = 365 * 24 * 3600
32      print('T_m is:',T_m,'A_s is:',A_s)
33      k=0
34      while k < (len(z)):
35          A_z_i = A_s * math.exp(z[k] * math.sqrt(math.pi / (
        alpha * p)))
36          A_z.append(A_z_i)
37          T_z_pluss.append(T_m + A_z_i)
38          T_z_minus.append(T_m - A_z_i)
39          k += 1
40
41      return A_z, z, T_z_pluss, T_z_minus, i
42
43
44  def TrumpetPlot(Input,color1,label):
45      z=Input[1]
46      T_z_pluss=Input[2]
47      T_z_minus=Input[3]
48      i=Input[4]
49      plt.rcParams["xtick.top"]=plt.rcParams["xtick.labeltop"]=
        True
50      plt.rcParams["xtick.bottom"] = plt.rcParams["xtick.
        labelbottom"] = True
51      plt.plot(T_z_pluss,z,color1,label=label)
52      plt.plot(T_z_minus,z,color1 )
53      plt.axvline(x=MAAT[i], linestyle='--')
54      plt.axvline(x=0,color='k')
55      plt.xlabel('Temperature [Celsius]')
56      plt.ylabel('Depth [m]')
57      plt.legend()
58      plt.grid(True)
```

```
    plt.title('Temperature profile')


#Creating dataset for Year  with alfa based on T_air_min and
    T_air_maks from seklima.met.no
# dry soil: alpha=2,5*10^-7 m^2/s [Table 2-13 p52 "Frozen
    ground engineering"]
#alpha=0,00000049 m^2/s
#Dense saturated sand: alpha=8*10^-7 m^2/s
#Soft saturated clay: alpha=4*10^-7 m^2/s
#dry sandy soil: alpha=6.95*10^-7 m^2/day

#alpha unit= [m^2/s]
A_1980=A_z1(1980, 8*10**(-7))
A_1990=A_z1(1990, 8*10**(-7))
A_2000=A_z1(2000, 8*10**(-7))
A_2020=A_z1(2020, 8*10**(-7))

#Creating Trumpetcurve plot
TrumpetPlot(A_1980,'b','1980')
TrumpetPlot(A_1990,'m','1990')
TrumpetPlot(A_2000,'r','2000')
TrumpetPlot(A_2020,'c','2020')


plt.show()
```

Script A.2: Plot of MAAT with linearization

```
import matplotlib.pyplot as plt
import pandas as pd
import numpy as np



data=pd.read_csv('MAAT.csv',header=None)
data.head()
year=data[0]
MAAT=data[1]

plt.plot(year,MAAT)
plt.xlabel('Year')
plt.ylabel('Temperature')
plt.title('Mean annual air temperature')
plt.xlim(1976,2100)
linear_model=np.polyfit(year,MAAT,1)
linear_model_fn=np.poly1d(linear_model)
print(linear_model_fn)
x_s=np.arange(1976,2100)
plt.plot(x_s,linear_model_fn(x_s),color="green")
```

```
plt.grid()
plt.show()
```

Script A.3: Soil Parameters

```

class Soil:
    def __init__(self,Name,gamma_d,G_s):
        self.gamma_d=gamma_d
        self.G_s=G_s
        self.Name=Name


    def LatentHeat(self,w_u):
        L=self.rho_d*333700*(self.w-w_u)/100 #Latent heat of water = 333700 J/kg
        self.w_u=w_u
        # Equation 2.5-23 Frozen Ground
        print(self.Name,'with unfrozen watercontent= ',w_u,': Has the Latent heat',L, 'J/m^3', '\n ')
        return L

    def Parameters(self):
        self.rho_w = 1000  # kg/m^3
        self.rho_d=self.gamma_d/9.81
        self.rho_s=self.G_s*self.rho_w # Eq. (2.1-9) Frozen Ground
        self.n=1-self.rho_d/self.rho_s # Eq. (2.1-3) Frozen Ground
        self.e=self.rho_s/self.rho_d-1 # Eq. (2.1-1) Frozen Ground
        #assume fully saturated V_w=V_v

        self.w=self.rho_w/self.rho_s*self.e # Eq. (2.1-4) combined with (2.1-2) Frozen Ground
        self.rho=self.rho_d*(1+self.w) # Eq. (2.1-6) Frozen Ground
        print(self.Name,'\n', self.Name, 'with dry unit weight:',self.gamma_d,'N/m^3 and G_s:',self.G_s,
              'Has the following parameters:\n rho=',self.rho,'kg/m^3 \n Porosity n=',self.n,', \n Water content w=',self.w)
        return self.Name, self.rho, self.rho_d, self.w

    def HeatCapacity(self):

        c_vw=4.187 #MJ/m^3 p.51 Frozen ground
        c_vf=(self.rho_d/self.rho_w)*(0.17+1.0*self.w_u/100+0.5*(self.w-self.w_u)/100)*c_vw # Eq. (2.5-19) Frozen Ground
```

```
34          c_vu=(self.rho_d/self.rho_w)*(0.17 +1*self.w/100)*
    c_vw # Eq. (2.5-18) Frozen Ground
35          self.c_vf=c_vf
36          #c_v=c_m*self
37          #c_m = c_v / self.rho
38          #self.c=c_v
39
40          print('Volumetric heat capacity for',self.Name,'is: \
    n', 'c_vu:',c_vu, 'MJ/m^3 degree \n', 'c_vf:', c_vf, 'MJ/m
    ^3 degree','\n')
41
42      def ThermalDiffusivity(self,k):
43          alpha=k/(self.c_vf)
44          print('Thermal diffusivity for',self.Name,',with
    thermal conductivity equal to',k,'W/mK, is:',alpha,'
    10^(-6) m^2/s \\')
45
46  Sand=Soil('Sand',16000,2.65)
47  Sand.Parameters()
48  Sand.LatentHeat(0)
49  Sand.HeatCapacity()
50  Sand.ThermalDiffusivity(3.2)
51  Sand.LatentHeat(6.4) #4.5
52  Sand.HeatCapacity()
53  Sand.ThermalDiffusivity(3.2)
54  Sand.LatentHeat(5.11)
55  Sand.HeatCapacity()
56  Sand.ThermalDiffusivity(3.2)
57  Sand.LatentHeat(4.54)
58  Sand.HeatCapacity()
59  Sand.ThermalDiffusivity(3.2)
60
61  Silt=Soil('Silt',16000,2.65)
62  Silt.Parameters()
63  Silt.LatentHeat(6.4)
64  Silt.HeatCapacity()
65  Silt.ThermalDiffusivity(1.9)
66  Silt.LatentHeat(5.11)
67  Silt.LatentHeat(0)
68
69  Clay=Soil('Clay',16500,2.7)
70  Clay.Parameters()
71  Clay.LatentHeat(12.4)
72  Clay.HeatCapacity()
73  Clay.ThermalDiffusivity(1.9)
74  Clay.LatentHeat(9.82)
75  Clay.LatentHeat(0)
```

Script A.4: Plot of deformation

```

#Code below is running :
def D_unfrozen(M,delta_P,delta_h):
    return (delta_P/M)*delta_h

M=np.linspace(1500,500,100)

#Plot
plt.title('Deformation due of unfrozen soil below foundation')
plt.xlabel('Modulus of deformation, M')
plt.ylabel('Deformation, ${\delta_{unfrozen}}$')
plt.grid(True)

plt.plot(M,D_unfrozen(M,64,0.5), color='red', label='Big structure')
plt.plot(M,D_unfrozen(M,18,0.5), color='blue', label='Medium structure')
plt.plot(M,D_unfrozen(M,12,0.5), color='green', label='Small structure')
plt.legend()
plt.show()
```

Script A.5: Self weigth of cablewaypost (upper structure)

```
# This script calculate the approximately self weight of the upper structure of a cablewaypost
class Eigen:
    def __init__(self,rho,H,D_c,n_c,B_x,D_b,n_bx,B_y,n_by,L_s,D_s,n_s,L_plate,B_plate,t_plate):
        self.rho=rho
        self.H=H
        self.D_c=D_c
        self.n_c=n_c
        self.B_x=B_x
        self.D_b=D_b
        self.n_bx=n_bx
        self.B_y=B_y
        self.n_by=n_by
        self.L_s=L_s
        self.D_s=D_s
        self.n_s=n_s
        self.L_plate=L_plate
        self.B_plate=B_plate
        self.t_plate=t_plate
    def V(self,D,h):
        return  3.14 * (D / 2) ** 2 * h
    def V_plate(self):
```

```
        return self.L_plate*self.B_plate*self.t_plate
    def TotalVolume(self):
        T_V=self.n_c*self.V(self.D_c,self.H)+self.n_bx*self.V
    (self.D_b,self.B_x)+self.n_by*self.V(self.D_b,self.B_y)+
    self.n_s*self.V(self.D_s,self.L_s)+self.V_plate()
        print('Total volume:',T_V, 'm^3')
        return T_V
    def Eigen_w(self):
        eigen_w=Eigen.TotalVolume(self)*self.rho
        print('The weight of the structure is',eigen_w,'kg')
        return eigen_w
    def Eigen_load(self):
        eigen_load=Eigen.Eigen_w(self)*9.81
        print('The eigenload of the structure is',eigen_load,
    'N, this gives',eigen_load/4,'N on each pile.')
        return eigen_load
#Eigen(rho,H,D_c,n_c,B_x,D_b,n_bx,B_y,n_by,L_s,D_s,n_s,
    L_plate,B_plate,t_plate)

Bukk=Eigen(490,28,0.4,4,5.05,0.15,2,7.9,2,9,0.25,20,5,1,0.2)
Bukk.TotalVolume()
Bukk.Eigen_load()
```

Script A.6: Calculation and plot of future I_f I_t and ALT

```
# -*- coding: utf-8 -*-
"""
Created on Thu Jun 15 07:55:05 2017

@author: yaredbe
Adapted by: Kristin Enevoldsen  spring 2022
"""

import matplotlib.pyplot as plt
import numpy as np
import pylab as py
import pandas as pd
plt.rcParams.update({'font.size': 14})
def activeLayer(files, years, ku, Lf, rd, w, wu, nt, markers,
    title):
  """
  A function to read annual air temperature data and return
    Air freezing index
    Air thawing index
    Active layer thickness
  Inputs to function:
    files: a list of files with air temperature data
    years: years corresponding to the input files
    ku: unfrozen thermal conductivity of soil
    Lf: volumetric latent heat of soil
```

```
    rd: dry soil density
    w: total water content
    wu: unfrozen water content
    markers: list of plot markers for customization
  """

  # Create empty lists to store freezing and thawing indices
  Iaf = []
  Iat = []
  # Create empty lists to store number of freezing and
   thawing days
  Fdays = []
  Tdays = []
  # Create empty list to store applied constant surface
   temperatures
  Ts = []
  # Create empty list for active layer thicknesses
  Zt = []

  df = pd.read_csv(files[0], header=None, delimiter=',')
  daily_mean_temp_all = df[1].tolist()

  for i in range(100):
    daily_mean_temp = daily_mean_temp_all[i*365:(i+1)*365]

    # Freezing and thawing indices based on average daily
   temperaure
    fr = 0.0
    th = 0.0
    fd = 0    # Freezing days
    td = 0    # Thawing days
    for i in range(len(daily_mean_temp)):
        if daily_mean_temp[i] <= 0.0:
            fr += daily_mean_temp[i]
            fd += 1
        elif daily_mean_temp[i] > 0.0:
            th += daily_mean_temp[i]
            td += 1
    Iaf.append(fr)
    Iat.append(th)
    Fdays.append(fd)
    Tdays.append(td)
    Ts.append(th*nt/td)

    # Active layer thickness based on Stefan Solution
    L = rd * Lf * (w - wu)      # Volumetric latent heat
    z = np.sqrt(2 * ku * th * nt * 86400 / L)
    Zt.append(z)

```

```
71    print('Air Freezing Indices:', Iaf)
72    print('Air Thawing Indices: ', Iat)
73    print('Number of Freezing days: ', Fdays)
74    print('Number of Thawing Days: ', Tdays)
75    print('Applied constant surface temperatures: ', Ts)
76    print('Year',range(2000,2100))
77    print('Active layer thicknesses: Zt', Zt[ : :10])
78
79
80    vline = [2022 for i in range(len(Zt))]
81    print('test')
82    py.rcParams['figure.figsize'] = 8, 6
83    plt.figure()
84    plt.plot(years,Iaf,'bo-',mfc='none')
85    plt.plot(vline,Iaf,'k-.')
86    plt.xlabel('Year')
87    plt.ylabel('Air Freezing Index, $I_{af}$ [$^\circ$C $\cdot$
        days]')
88    plt.title(title)
89    plt.grid(True)
90    plt.figure()
91    plt.plot(years,Iat,'bo-',mfc='none')
92    plt.plot(vline,Iat,'k-.')
93    plt.xlabel('Year')
94    plt.ylabel('Air Thawing Index, $I_{at}$ [$^\circ$C $\cdot$
       days]')
95    plt.title(title)
96    plt.grid(True)
97    plt.figure()
98    plt.plot(years,Zt,'bo-',mfc='none')
99    plt.plot(vline,Zt,'k-.')
100   plt.xlabel('Year')
101   plt.ylabel('Active Layer Thickness, $Z_t$ [$m$]')
102   plt.axhline(y=1.5, linestyle='--')
103   plt.axhline(y=2, linestyle='--')
104   plt.axhline(y=2.5, linestyle='--')
105   plt.ylim([0, 4.5])
106   ax=plt.gca()
107   ax.invert_yaxis()
108
109   plt.title(title)
110   plt.grid(True)
111   plt.show()
112
113   return Iaf
114
115 # Input files and data
116 files=['Longyearbyen_Daily_Temps.csv']
117
```

```
118
119 years    = range(2000,2100,1)#create a list 2000 to 2100
120 ku = 3.2          # W/m/K
121 Lf = 334000.0     # J/kg
122 rd = 1800         # kg/m3
123 w  = 0.3
124 wu = 0.0
125 nt = 1.0
126 markers = ['s','o']
127
128 #SAND
129 activeLayer(files, years, 3.2, Lf, 16000/9.81, 0.236, 0.0511,
        nt, markers,'SAND')
130 #SILT
131 activeLayer(files, years, 1.9, Lf, 16000/9.81, 0.236, 0.0511,
        nt, markers,'SILT')
132 #CLAY
133 activeLayer(files, years, 1.9, Lf, 16500/9.81, 0.224, 0.0982,
        nt, markers,'CLAY')
```

Appendix B

Data

Table B.1: Historical temperature data from Svalbard airport [37].

Name	Stnr	Date	MAAT	T_{max}	T_{min}
Svalbard Lufthavn	SN99840	1976	-4.6	14.9	-36
Svalbard Lufthavn	SN99840	1977	-6.7	15.1	-35.9
Svalbard Lufthavn	SN99840	1978	-7.6	14.3	-35.6
Svalbard Lufthavn	SN99840	1979	-7.8	21.3	-43.7
Svalbard Lufthavn	SN99840	1980	-7.2	14.2	-33
Svalbard Lufthavn	SN99840	1981	-7.1	14.3	-38.8
Svalbard Lufthavn	SN99840	1982	-6.5	10.9	-32.7
Svalbard Lufthavn	SN99840	1983	-6.4	17.7	-33.3
Svalbard Lufthavn	SN99840	1984	-3.1	13	-29.3
Svalbard Lufthavn	SN99840	1985	-5.5	16.4	-28.3
Svalbard Lufthavn	SN99840	1986	-6.7	12.8	-46.3
Svalbard Lufthavn	SN99840	1987	-6.8	14.2	-30.1
Svalbard Lufthavn	SN99840	1988	-8.9	14.8	-39.1
Svalbard Lufthavn	SN99840	1989	-6.6	12.8	-33.4
Svalbard Lufthavn	SN99840	1990	-3.9	15.9	-28.7
Svalbard Lufthavn	SN99840	1991	-5.1	13.6	-27.3
Svalbard Lufthavn	SN99840	1992	-5.1	13.7	-38.2
Svalbard Lufthavn	SN99840	1993	-6.1	16.6	-34.7
Svalbard Lufthavn	SN99840	1994	-6	12.1	-33.6
Svalbard Lufthavn	SN99840	1995	-6	13.9	-33.6
Svalbard Lufthavn	SN99840	1996	-5	16.5	-35.7
Svalbard Lufthavn	SN99840	1997	-6	18.1	-36.8
Svalbard Lufthavn	SN99840	1998	-6.2	18.9	-35.3
Svalbard Lufthavn	SN99840	1999	-3.9	18.3	-25.8
Svalbard Lufthavn	SN99840	2000	-4	13.7	-29.7
Svalbard Lufthavn	SN99840	2001	-4.6	17.3	-28.8
Svalbard Lufthavn	SN99840	2002	-4.3	16.1	-30.6
Svalbard Lufthavn	SN99840	2003	-6.1	14.4	-30.3
Svalbard Lufthavn	SN99840	2004	-4.3	18.5	-31.4
Svalbard Lufthavn	SN99840	2005	-3	16.8	-31.1
Svalbard Lufthavn	SN99840	2006	-1.7	13	-22.1
Svalbard Lufthavn	SN99840	2007	-2.5	14.1	-24.2
Svalbard Lufthavn	SN99840	2008	-4	12.4	-23.9
Svalbard Lufthavn	SN99840	2009	-3.7	14.8	-32
Svalbard Lufthavn	SN99840	2010	-4.1	13.3	-24.8
Svalbard Lufthavn	SN99840	2011	-3.4	17.1	-31.5
Svalbard Lufthavn	SN99840	2012	-2	13	-23.7
Svalbard Lufthavn	SN99840	2013	-3.5	15	-26.3
Svalbard Lufthavn	SN99840	2014	-2.1	12.2	-20.6
Svalbard Lufthavn	SN99840	2015	-2	17.9	-26.9
Svalbard Lufthavn	SN99840	2016	-0.1	14.5	-18.5
Svalbard Lufthavn	SN99840	2017	-2.2	13.3	-23.5
Svalbard Lufthavn	SN99840	2018	-1.8	15.2	-20.8
Svalbard Lufthavn	SN99840	2019	-3.4	16.1	-25.4
Svalbard Lufthavn	SN99840	2020	-3.4	21.7	-29.9
Svalbard Lufthavn	SN99840	2021	-2.9	12.4	-24

Data er gyldig per 20.02.2022 (CC BY 4.0). Meteorologisk institutt (MET)

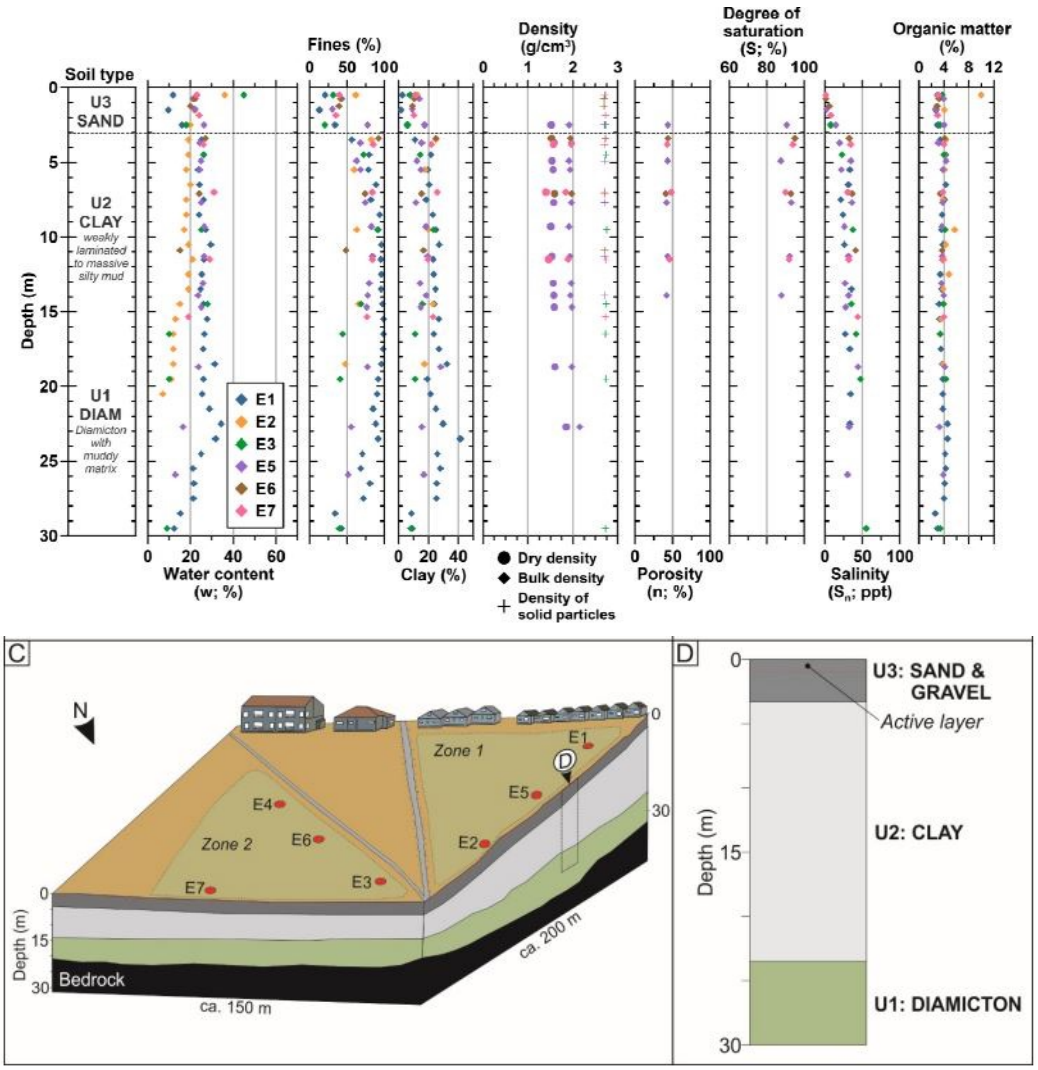

Figure B.1: Soil type and index parameters from soil investigation at UNIS EAST. Adapted from [13].

Таблица 7.10

Значение угла внутреннего трения φ и сцепления С мерзлых грунтов при различных температурах и засоленностях.

Salinization
NB! Not salinity

C_long-term

kPA

Засоленность, $D_{экв}$, %	Температура T,°C											
	−1		−2		−3		−4		−6		−8	
	φ°	$C_{дл}$, кПа	φ°	$C_{дл}$, кПа	φ°	$C_{дл}$, кПа	φ°	$C_{дл}$, кПа	φ°	$C_{дл}$, кПа	φ°	$C_{дл}$, кПа
Clay Глина и тяжелые суглинки (W = 58%, i > 0,2, ρ =1,65 г/см³)												
0	1	98	–	148	1	176	2	203	4	242	6	280
0,5	2	24	2	34	3	56	4	85	6	136	10	184
1,5	–	–	–	–	5	11	6	26	8	52	13	80
Clay Глина и тяжелые и суглинки (W = 38%, i < 0,2, ρ = 1 80 г/см³)												
0	5	115	6	156	8	178	10	198	14	223	17	252
0,5	7	42	10	51	12	69	13	93	17	131	20	172
1,5	9	32	11	32	15	29	17	45	20	60	24	76
Silt Супеси (W = 28%, i < 0,2, ρ = 1,90 г/см³)												
0	16	129	17	164	18	185	22	193	25	196	30	197
0,2	16	50	17	88	18	118	18	141	23	144	25	147
0,8	–	–	–	–	22	10	25	8	27	19	28	27
Fine Sand Пылеватые пески (W = 23%, ρ = 1,95 г/см³)												
0	31	99	32	119	33	141	34	160	37	199	40	222
0,1	29	28	30	41	31	56	32	61	34	68	36	73
0,2	–	–	29	22	30	28	30	32	31	38	32	42

312

Figure B.2: Friction angle and cohesion for frozen soil [41]

Appendix C

Fieldwork

This appendix contain

- Installation of i-buttons
- Installation of time laps cameraes
- Snow depth measurements

General and specific requirements and details for installations of both, i-buttons and time-lapse cameras are given in the applications to authorities. Those applications had three level of approval, i.e. owner of the cases study objects (Kings Bay or SNSK)/Recommendation of the Governor at Svalbard/and final approval from Riksantikvaren. All approval documents are identical from the technical point of view, i.e. the same plans for installations are presented in all of those documents. One, however, shall use the approval (with attached plans and locations) from Riksantikvaren as that is the legally confirmed document.

	Område og navn på objektet	**ID -nummer i Askeladden -databasen**
1.	Bukk nr 32 - Taubane 3	**158619-32**
2.	Taubanesentralen (in Longyearbyen)	**87889-6**
3.	Bukk nr 5 - Taubanelinje 2b	**158986-5**
4.	Bukk nr 6 - Taubanelinje 1b	**158657-6**
5.	Bukk nr 6 - Taubane delstrekning gruve 5 og 6	**87889-14**
6.	Bukk nr 34 - Taubane delstrekning gruve 5 og 6	**87889-43**
7.	Bukk nr 16 - Taubane delstrekning gruve 5	**87889-63**
8.	Bukk 7 - Taubane delstrekning gruve 6	**87889-112**
9.	Bukk 8 - Taubane delstrekning gruve 6	**87889-111**
10.	Taubanesentralen, Bygning I (Hiorthamn)	**93040-6**
11.	Boligbrakke - Bygning G (Hiorthamn)	**146668-7**

	GPS coordinates	**Number of i-buttons**	**Time laps camera**
1.	33X E512630 N8684553	2	No
2.	33X E514041 N8683404	3	Yes
3.	33X E513997 N8681535	5	No
4.	33X E513275 N8681726	4	No
5.	33X E514779 N8682885	2	No
6.	33X E517047 N8681233	5	No
7.	33X E517778 N8679886	5	No
8.	33X E520513 N8678451	2	No
9.	33X E520456 N8678498	2	No
10.	33X E515929 N8686184	2	Yes
11.	33X E515973 N8686605	6	yes

Table C.1: Overview fieldwork.

SNOW Measurements 04.04.2022. Kristin Enevoldsen and Irene Isaksen

[cm]

Cableway post	Coordinates	A	B-Nord	C-Nord	B-East	C-East	B-South	C-South	B-Vest	C-Vest
Bukk nr 32 - Taubane 3 (Burmaveien)	33X E512630 N8684553	0	2	Inn a hill	18, ice	0	1, ice	2	2	0
Bukk nr 6 - Taubane delstrekning gruve 5 og 6 (Byen, Gruvedalen)	33X E514779 N8682885	0	13	0	0	12	0	19	0	13
Bukk nr 34 - Taubane delstrekning gruve 5 og 6 (isdammen)	33X E517047 N8681233	0	0	10	22	0	20	10	34	20
Bukk nr 16 - Taubane delstrekning gruve 5 (Endalen)	33X E517778 N8679886	43	34	53	52	57	28	35	61	106
Endalen, en nord for nr 16	33X E...835 N...976	58	45	36	59	14	19	31	24	30
Bukk 7 - Taubane delstrekning gruve 6 (advendtdalen)	33X E520513 N8678451	8	15	8	23	14	14	0	42	19
Bukk 8 - Taubane delstrekning gruve 6 (advendtdalen)	33X E520456 N8678498	8	8	41	42	37	24	32	41	30
Bukk 9 ? Advendtdalen	33x E..... 407, N...541	1	32	31	13	22	25	28	21	48
Bukk nr 5 - Taubanelinje 2b (Nybyen)	33X E513997 N8681535	0	0	58	10	0	2	0	0	0

Could not access this cableway post due to avalanche risk.

Cableway post	Coordinates	A	B-Nord	C-Nord	B-East	C-East	B-South	C-South	B-Vest	C-Vest
Bukk nr 6 - Taubanelinje 1b (Huset)	33X E513275 N8681726	-	-	-	-	-	-	-	-	-
Taubanesentralen (in Longyearbyen)			33X E514041 N8683404		Blå 5		Blå 8	Blå 11	Lilla rund	
					0	0	0	0		

Figure C.1: Results from snow measurements.

Appendix D

Calculations Pre-project

In this appendix the theory behind the calculation of the wind is presented in Section D.1 and bearing capacity for the rehabilitated cableway post presented in Section X are introduced followed by calculations of the weight of the structure in Section D.2.1 which is presented in Table 4.1. The load combination is calculated in Section D.2.3. The theory and calculations are adapted from the preproject for this thesis [8].

D.1 Wind

The wind climate is determined by meteorological conditions; circulations in the atmosphere driven by density-induced convection, thermal convection, and the Coriolis effect. To be able to describe the wind conditions at a regional and local level, it is necessary to take into account the topography of the area, the viscosity of the air and the frictional forces at the surface of the terrain. Wind velocity is a stochastic process that varies in both time and space [21]. Simplifications are necessary to enable wind design. The wind velocity is decomposed into a mean wind velocity v_m, which is constant over a period of 10-30 min, and a fluctuating turbulent component. The Norwegian Meteorological Institute measures the wind at a height 10 m from the terrain surface and includes the mean values of wind velocity and wind direction over a period of 10 minutes [21].

Eurocode 1-1-4 describes wind actions on a structure and how to calculate the forces involved. The equations from the Eurocode used to calculate the forces exerted by wind on a structure, are presented and described in this section.

Eurocode 1-1-4 presents different methods of calculating the horizontal wind force exerted on a structure, one of which can be seen in Equation D.1.

$$F_w = c_s c_d \cdot c_f \cdot q_p(z_e) \cdot A_{ref} \tag{D.1}$$

Here, c_s, c_d and c_f are force coefficients related to the structure itself, q_p represents the wind pressure, which is dependent on height z over the surface, and A_{ref} is the reference area of the lattice structure projected onto the wind.

The coefficient c_s takes into account the effect of wind actions from non-simultaneous occurrences of peak wind pressure on the surface of the structure. Coefficient c_d takes into account the effect of the vibrations of the structure due to turbulence [28]. The values for c_s and c_d are defined in Section 6 of Eurocode 1-1-4. Coefficient c_f takes into account the solidity of the structure and the direction of the incoming wind onto the structure.

The reference area for the lattice structure, A_{ref}, is shown in Equation D.2.

$$A_{ref} = \varphi \cdot A_c \tag{D.2}$$

Area A_c is the enclosed area, and the solidity ratio, φ, is presented in Equation D.3

$$\varphi = \frac{A}{A_c} \tag{D.3}$$

where area A is the projected area of the structure.

The wind pressure $q(z)$ is expressed as:

$$q(z)_p = k_1 \cdot k_2 \cdot k_3 \cdot c_{dir}^2 \cdot c_{alt}^2 \cdot c_{season}^2 \cdot c_{prob}^2 \cdot q_{p0}(z) \tag{D.4}$$

The probability factor c_{prob} is used when the return period differs from 50 years. The level factor c_{alt} depends on the region, height above sea level and the base wind velocity. The national annex of the Eurocode divides Norway into three different regions. The factor k_1 consider wind acceleration due to slopes and hills. Factors k_2 and k_3 are factors which are defined in the guidance of the Eurocode 1-1-4. For simplicity they are set to equal 1.

Eurocode 1-1-4 presents different graphs for the base wind pressure $q_{p,0}$ for different base values of the wind velocity $v_{b,0}$. Figure D.1 presents this graph when the basic wind velocity $v_{b,0}$ equals 30 m/s. The Figure shows how the base wind pressure $q_{p,0}$ varies with respect to the height for the different terrain categories. The Eurocode has divided the terrain parameters into five different terrain categories.

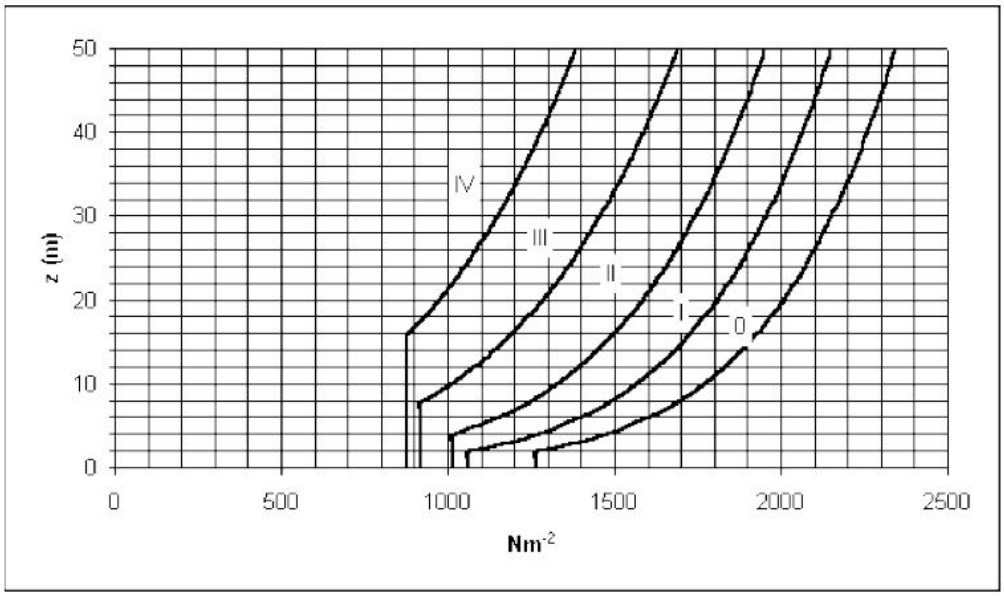

e) Grunnverdi for hastighetstrykk fra vindkast $q_{p0}(z)$ for $v_{b,0}$= 30 m/s

Figure D.1: Wind velocity pressure $q_{p,0}$ as a function of altitude z, using terrain categories ranging from 1-4, when the wind velocity $v_{b,0} = 30m/s$. Illustration from Figure V.1(e) of EC-1-1-4 [28].

Figure D.2 shows how the wind velocity pressure q_p is calculated for tall structures, where the height is more than double of the width of the structure.

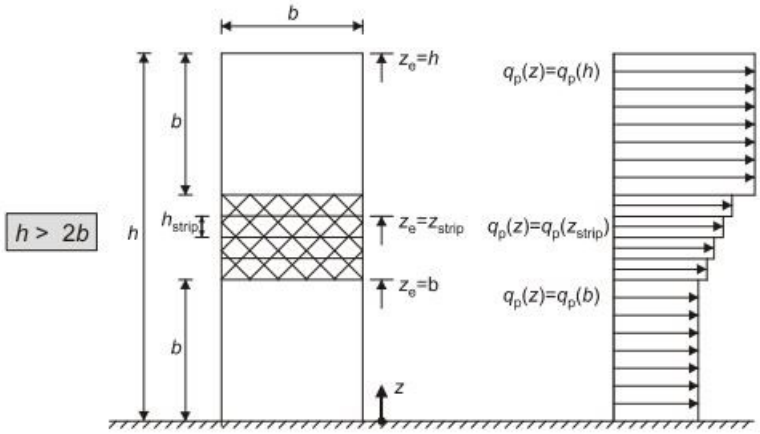

Figure D.2: Reference height, z_e, with respect to height, h and width, b. The corresponding wind velocity pressure profile is shown on the right. Adapted from Figure 7.4 in EC 1-1-4 [28]).

The force coefficient of lattice structures, c_f used in Equation D.1, is expressed by Equation D.5.

$$c_f = c_{f,0} \cdot \psi_\lambda \tag{D.5}$$

The expression includes the end-effect factor ψ_λ, found in Eurocode 1-1-4 Section 7.13, and the force coefficient of structures, or structural elements, without free-end flow, denoted as $c_{f,0}$. The force coefficient without free-end flow $c_{f,0}$ depends on Reynolds number, which is described by Equation D.6.

$$Re = \frac{D \cdot v_m(z)}{\nu} \tag{D.6}$$

Reynolds Number depends on the diameter of the element D, the mean wind velocity v_m presented i Equation D.7 and the air viscosity ν.

$$v_m(z) = c_r(z) \cdot c_o(z) \cdot v_b \tag{D.7}$$

The mean wind velocity v_m is effected by the roughness $c_r(z)$, an orography factor c_o and the basic wind velocity v_b, described in Equation D.9. The roughness factor $c_r(z)$ is presented in Equation D.8.

$$c_r(z) = k_r \cdot ln(\frac{z}{z_0}) \tag{D.8}$$

Factor k_r is a terrain factor, z is the height above ground and z_0 is the roughness height. The terrain factor k_r and roughness height z_0 depend on what type of terrain the structure is located in.

The base wind velocity v_b used in Equation D.7 is presented in Equation D.9.

$$v_b = c_{dir} \cdot c_{season} \cdot v_{b,0} \tag{D.9}$$

The basic wind velocity v_b is effected by a direction factor c_{dir} and seasonal factor c_{season}. The reference wind velocity $v_{b,0}$ is estimated by local data, values are presented in the national annex in Eurocode 1-1-4. The reference wind velocity has a return period of 50 years.

To find the force coefficient $c_{f,0}$ used in Equation D.5, Figure D.3 is used. The force coefficient $c_{f,0}$ depends on the solidity ratio φ from Equation D.3 and Reynolds number from Equation D.6.

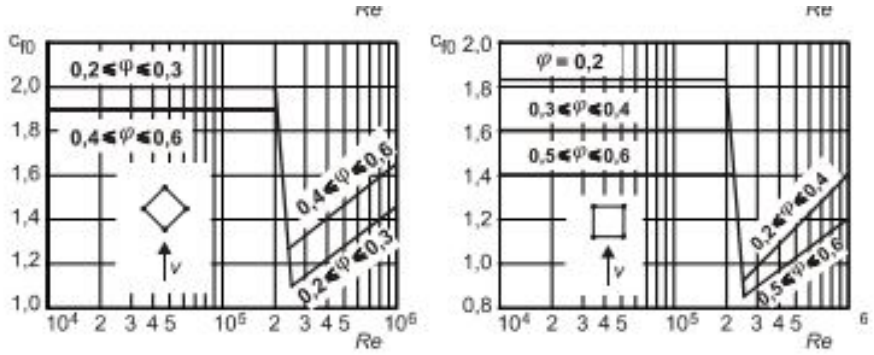

Figure D.3: Force coefficient $c_{f,0}$ for plane spatial lattice structure with members of circular cross-section with respect to Reynolds number Re and the solidity ratio φ. Plot adapted from Figure 7.35 in EC1-1-4 [28].

Another way to calculate the horizontal wind force exerted on a structure, as expressed in Equation D.1, can be seen in Equation D.10.

$$F_w = F_{w,e} + F_{w,i} = c_s c_d \sum_{surface} w_e \cdot A_{ref} + \sum_{surface} w_i \cdot A_{ref} \tag{D.10}$$

Factors c_s and c_d are the same components used in Equation D.1 and A_{ref} is the area from Equation D.2. The additional components used in Equation D.10 are the external surfaces pressure w_e, presented by Equation D.11, and wind pressure acting on an internal surface w_i, obtained from Equation D.12.

$$w_e = q_p(z_e) \cdot c_{pe} \tag{D.11}$$

$$w_i = q_p(z_i) \cdot c_{pi} \tag{D.12}$$

The pressure coefficient for external (c_{pe}) and internal (c_{pi}) pressure coefficient depends on the approach angle of the wind. Figure D.4 illustrates the direction of the wind normal to a surface. The figure also shows how the structure is divided into different zones depending on the position with respect to the wind direction.

The pressure coefficient for external pressure c_{pe} varies between $c_{pe,1}$ and $c_{pe,10}$. Values for $c_{pe,1}$ are intended for design of small elements and fixings with an area per element of 1 m^2 or less such as cladding elements and roofing elements [28]. Values for $c_{pe,10}$ may be used for the design of the overall load bearing structure of buildings [28]. Equation D.13 presents the internal pressure coefficient c_{pi}, for structures when the area of the opening face is at least three times the area of the openings in the remaining faces.

$$c_{pi} = 0,90 \cdot c_{pe} \tag{D.13}$$

D.2 Load combinations

The structure undergoes permanent actions G and variable actions Q. Permanent loads are represented with mean values and variable loads with extreme value with 50 years return period. For ultimate limit state the load combination is presented in Equation D.14.

$$F_{d,ULS} = \gamma_G \cdot G_k + \gamma_{Q,1} \cdot Q_{k,1} + \gamma_{Q,i} \cdot \psi_{0,i} \cdot Q_{k,i} \tag{D.14}$$

The index k is the characteristic value, the value without safety factors. Factor $\psi_{0,wind}$ is a combination value and is used when a structure is exposed

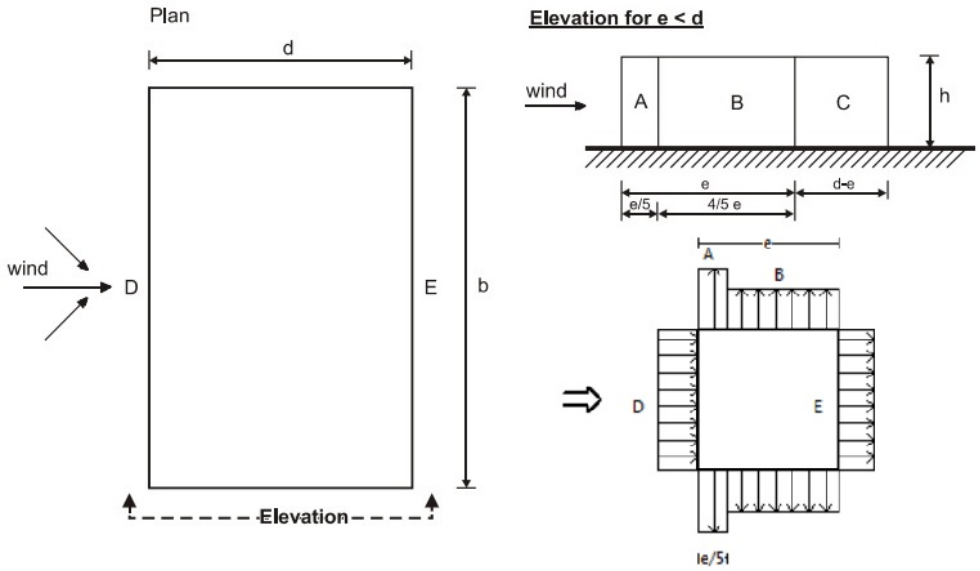

Figure D.4: Illustrates how the structure is divided into zone A, B, C, D and E depending on the position with respect to the wind direction. The left figure shows a horizontal cross-section. The upper right figure shows a vertical cross-section. The lower right figure shows how the pressure acts on the different surfaces. The Figure is adapted from Figure 7.5 in EC1-1-4[28] and from [25].

to more than one variable load. The combination factor $\psi_{0,wind}$ is used since the chance of max load for two or more variable loads at the same time is low. Factor γ is a partial safety factor and depends on the type of load and if the load is favourable or not, as shown in Table D.1.

Table D.1: Partial factors for favorable and unfavorable permanent (G) and variable (Q) loads. The values are adapted from NS-EN 1990: Basis of structural design [27].

Factor	Value	Ref. NS-EN 1990
$\gamma_{G,unfavorable}$	1.2	Table NA.A1.2(A)
$\gamma_{G,favorable}$	0.9	Table NA.A1.2(A)
$\gamma_{Q,i,favorable}$	0.0	Table NA.A1.2(A)
$\gamma_{Q,1,unfavorable}$	1.5	Table NA.A1.2(A)
$\gamma_{Q,i,unfavorable}$	1.5	Table NA.A1.2(A)
$\psi_{0,wind}$	0.6	Table NA.A1.1

D.2.1 Loads from self-weight

The self-weight of the upper structure is the density of the material multiplied with the volume of the structure. Figure D.5 shows a sketch of the cableway post with labels of the dimensions, used in the following calculation.

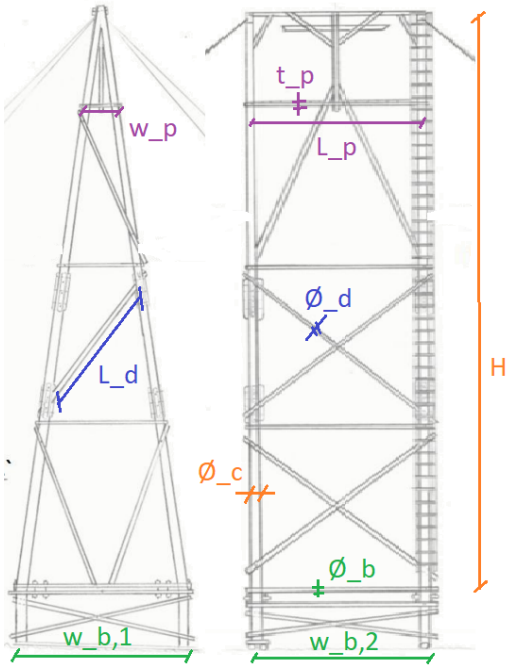

Figure D.5: Sketch of a cableway post showing both the front view and the side view of the structure. Labels are added. d is the diameter of the element, w is the width, L is the length and H is the height. The indexes b, c, d and p represent beam, column, diagonal and plate element. The figure is adapted from [7].

Table D.2 gives the structural data of the cableway post. The length and number of the diagonals are an average of the typical diagonals in the structure.

Table D.2: The first column shows the dimensions marked in Figure D.5. The values of the dimensions are shown in column two. In the third column the number of elements are presented.

	Value[m]	number
d_b x $w_{b,1}$	0.15 x 5.05	2pc
d_b x $w_{b,2}$	0.15 x 7.90	2pc
d_p x L_p x t_p	1.00 x 5.00 x 0,20	1pc
T_c x h	0,40 x 28.00	4pc
d_d x L	0.25 x 9.00	20pc

The structural data gives a total volume of 24.54 m^3 for the cableway post. In this calculation, strength class C30 is assumed. The strength classes for softwood are added from NS-EN 338 [31]. C30 gives a density equal to $\rho_{mean} = 460\,kg/m^3$ [31] and hence a self weight equal to $G_k = 110.7kN$. Divided by four piles, this yields a self-load of 27.7 kN for each pile, assuming they share the load equally.

D.2.2 Eurocode 1-1-4 Wind

The wind calculation in this section follows the description from Section D.1, Eurocode 1-1-4. A summary of some of the parameters used in the calculation is presented in Table D.3.

Table D.3: Parameters from Eurocode 1-1-4 [28]

Parameter, wind		Ref. in EC 1-1-4
$v_{b,0}$	$30m/s$	NA4.2
H_0	400 m	Table NA.4(901.2)
H_{topp}	1000 m	Table NA.4(901.2)
c_{dir}	1.0	Table NA.4(901.4)
c_{season}	1.0	NA.4.2(2)P(901.3)
c_{alt}	1.0	Table NA.4(901.3)
c_{prob}	1.0	Figure V.1(e)
k_r	0.17	Table NA4.1
k_l	1.0	NA 4.3.3(901.2)
z_0	0.01 m	Table NA4.1
z_{min}	2 m	Table NA4.1

The cableway post is situated close to the coast, as well as in an area without trees or shrubs. This corresponds to the definition of terrain category 1 in the standard. The reference wind velocity $v_{b,0}$ on Svalbard is 30 m/s [NA.4.2]. The directional factor c_{dir} is equal to 1.0 according to Table NA.4(901.4). Since the rehabilitation has a long time perspective (more than one season), wind is not reduced due to the season, thus the seasonal factor c_{season} is 1.0. From Equation D.9 the base wind velocity v_b is equal to 30 m/s.

Hence, the terrain category is 1, the terrain factor k_r equal to 0.17, roughness length z_0 equal to 0.01m and minimum height z_{min} equal to 2 m according to NA.4.3.3(901.2) [28]. The terrain factor c_o adjusts for the effect the terrain has at the wind velocity. For simplicity $c_o = 1,0$ is used. Since the roughness factor $c_r(z)$ depends on the height above ground z, as shown i Equation D.8, the mean wind velocity v_m also changes due to the height, as shown i Equation D.7. The calculations are performed as described in Section D.1 and Python code used to get the results are shown in Appendix **??**. Figure D.6 shows a plot of the calculated mean wind velocity v_m.

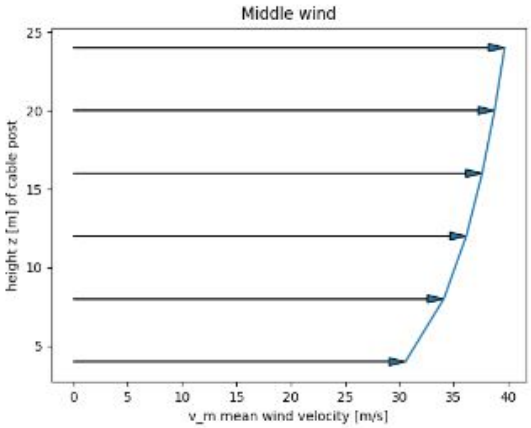

Figure D.6: Mean wind velocity v_m with respect to the height z, using parameters from Table D.3. Here we see that the velocity decreases as the height decreases.

Svalbard is defined as region 3, with $c_{alt} = 1{,}00$. The base wind pressure $q_{p,0}$, for terrain category 1 from Figure D.1, with Δz equal to 4 m is presented in Table D.4. As long as the required design return period is 50 years; c_{prob} is equal to 1.0.

Table D.4: Base wind pressure $q_{p,0}$ from Figure D.1 with respect to the height z of the structure.

z [m]	$q_{po}(z)$ [N/m^2]
0	1060
4	1490
8	1500
12	1630
16	1720
20	1810
24	1880
28	1930

When calculating the wind pressure $q_p(z)$, the structure was considered comprised from multiple parts, as described in Figure D.2. Table D.5 summarizes the calculations of the wind pressure $q_{p,0}(z)$.

The wind pressure $q_{p,0}(z)$ in the upper part ($\Delta z = 5$ m from top) is equal to 1930 N/m^2, with $q_{p,0}$ from Table D.4 at $z_e = \text{h} = 28$ m. For the lower part

($\Delta z = 5$m from ground), $q_{p0}(z = b \approx 5\,m) = 1492.5\,\mathrm{N/m^2}$. The middle part is equal to $\Delta z = 28 - 5 - 5 = 18\,\mathrm{m}$ and divided into three equal parts with $h_{strip} = 6\,m$.

Table D.5: Base pressure values for specific heights according to Figure D.2.

z[m] from ground	$q_{p,0}(z)$[N/m^2]	Δz [m]
28	1930	5
23	1862.3	6
17	1742.5	6
11	1597.5	6
5	1492.5	5

The average of the base wind velocity from Table D.5 is

$$q_{p,0} = \frac{1}{h} \sum q_{p,0}(z) * \Delta z = 1725.94\,\mathrm{kPa}$$

Since the structure is located in a slope, the factor k_1 is assumed to be $1,15$ from Figure V.2 in EC1-1-4. Equation D.4 gives a wind pressure q_p equal to 1985 kPa.

Table D.6 presents the external pressure from Equation D.11 on the zones presented in Figure D.4.

Table D.6: The external pressure coefficients $c_{pe,1}$ and $c_{pe,10}$ are from Table 7.1 in EC1-1-4 [28]. The external pressure, w_e, is calculated from Equation D.11. Value D is the pressure in front of the structure, A and B on the sides and E is the suction behind the element as illustrated in Figure D.4.

	A	B	D	E
$c_{pe,10}$	-1.20	-0.80	0.80	-0.70
w_e [MPa]	-2.38	-1.59	1.59	-1.39
$c_{pe,1}$	-1.40	-1.10	1.0	-0.70
w_e [MPa]	-2.78	-2.18	1.98	-1.39

Equation D.12 and Equation D.1 with $c_{pe,10}$ equal to 0.8, give an internal pressure w_i equal to 1.57 MPa.

The structure can be characterised as a lattice structure. The dimensions of the structure are height 28 m and width 5.05 m. The enclosed area A_c(h·b) is equal to 141.4 m^2. The projected area of the structure is 31.15 m^2. Equation D.3 gives a solidity ratio φ equal to 0.22. From Equation D.2, the reference

area A_{ref} is 31.15 m^2.

The end-effect factor ψ_λ is equal to 1.0 for slender structures (when the ratio $\frac{height}{diameter}$ is larger than 25). The force coefficient $c_{f,0}$ depends on Reynolds number Re described by Equation D.6. The kinematic viscosity of air is $1.5 \cdot 10^{-5}$ m^2/s, the diameter is set to be 0.3 m, and the velocity is estimated to be 37.9 m/s. The Reynolds number is thereby calculated to be $7.94 \cdot 10^5$. The force coefficient c_{f0} from Figure D.3 is approximately 1.4. Equation D.5 gives $c_f = 1.4$.

The total wind force from Equation D.10, with external pressure w_e equal to 2.09 MPa and inner pressure $w_i = 1.57$ MPa is:

$$F_w = 116.8\,\text{kN}$$

The wind force from Equation D.1 with c_f equal to 1.4, area A_{ref} equal to 31.15m^2 and both coefficients c_s and c_f equal to 1.0 and wind pressure q_p equal to 1985 kPa becomes:

$$F_w = 86.6\,\text{kN}$$

D.2.3 Load Summary

In this section we will compare the calculated loads in this report with the calculated loads in the calculation report 713851 from Multiconsult [25]. The comparison is presented in Table D.7.

Table D.7: Force G_k is the permanent self-weight. Force $F_{w,1}$ is the wind load from Equation D.10 and force $F_{w,2}$ is the wind load from Equation D.1. Force Q_k is the wind load from Multiconsult's calculation report [25].

Load	This report	Multiconsult [25]
$G_k[kN]$	110.7	115.3
$F_{w,1}[kN]$	116.8	-
$F_{w,2}[kN]$	86.6	-
$Q_k[kN]$	-	88.2

The calculation of G_k depends of the density. In this report it is assumed strength class C30 with density ρ_{mean} equal to $460kg/m^3$. Multiconsult has assumed C45 which has a higher density, ρ_{mean} equal to $490kg/m^3$. This may be one of the reasons for the different load values.

The wind force F_w can be calculated from force coefficients with use of Equation D.10, $F_{w,1}$, or from pressure coefficients with use of Equation D.1, $F_{w,2}$. The calculation of the horizontal wind force Q_k done by Multiconsult used the wind pressure. The main differences in the calculation of the wind force in this report compared to Multiconsults report are the use of factor k_1 in Equation D.4 and the use of the force coefficient c_f in Equation D.1.

The values from Multiconsult's report are used in the further calculations. Figure D.7 shows a sketch of how the horizontal wind force creates a bending moment in the structure.

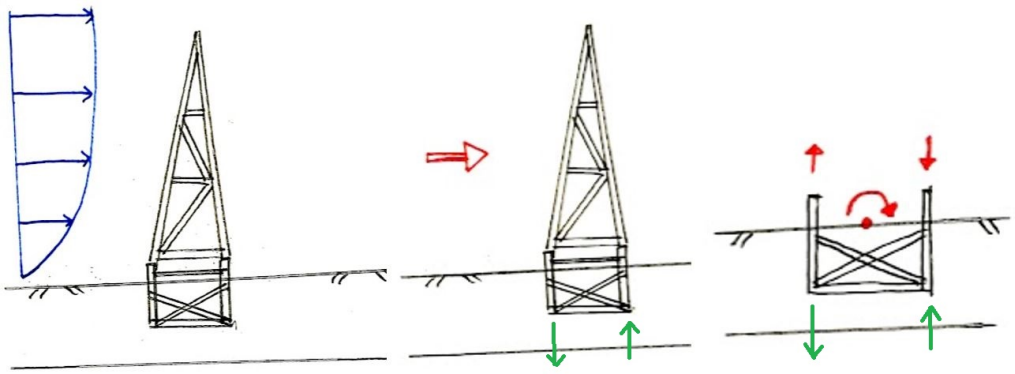

Figure D.7: Sketch of a cableway post exposed to a horizontal wind load. The blue distributed force in the left represents the wind pressure. The red arrow in the middle represents the resulting horizontal wind load. The green arrows represent the response loads in the foundation piles due to the wind load. The right sketch illustrates the bending moment in the foundation.

Assumed that the wind force Q_w, equal to $88.2kN$, attacks in the middle of the structure with a height h of $28m$, it will create a bending moment:

$$M = Q_w \cdot \frac{h}{2} = 1234.8\,\text{kNm}$$

As shown in Figure D.7, the bending moment creates an axial force in the foundation piles. The compression and tension forces act in two piles. Assuming a width w of 5m the axial force in each pile is:

$$N_{Q,k} = \frac{M}{w \cdot 2} = 158\,\text{kN}$$

The self-weight G_k acts vertically in the mass center of the structure and gives an axial load in the piles. The permanent axial load, from self-weight of 115.3kN, in each of the four piles is:

$$N_{G,k} = 29.2\,\text{kN}$$

The dimensional axial load due to the permanent self-weight and the variable wind load is calculated from Equation D.14. With safety factors

γ from Table D.1, the dimensional axial tension and compression load in a foundation pile are:

$$N_{tension,d} = -\gamma_{G,favourable} \cdot N_{G,k} + \gamma_{Q,1,unfavorable} \cdot N_{Q,k} = 158.8\,\text{kN}$$

$$N_{compression,d} = \gamma_{G,unfavourable} \cdot N_{G,k} + \gamma_{Q,1,unfavorable} \cdot N_{Q,k} = 220.2\,\text{kN}$$

D.2.4 Bending moment in the supporting piles

The horizontal wind load creates a local bending moment in the foundation. Figure D.8 illustrates how the moment is transferred to the supporting pile for the temporary structure and creates bending moments in the piles.

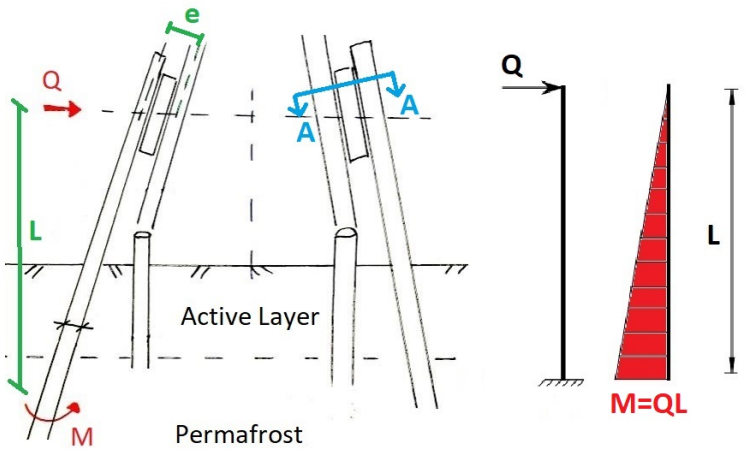

Figure D.8: The figure on the right shows how to calculate the bending moment for a fixed-ended beam. On the left is a sketch of the temporary structure subjected to an axial force N and a horizontal force Q. In the calculation in this section the axial force is not included.

For this calculation it is assumed that the supporting piles are fixed in the permafrost layer. For simplicity the piles are calculated as vertical piles. The distance H between the horizontal wind load Q and the fixed end is assumed to be 3 m. With a horizontal load equal to 22 kN for each pile, the bending moment in the fixed end of a pile is:

$$M = Q \cdot H = 66\text{kNm}$$

D.2.5 Moment of torsion in the supporting piles

Figure D.9 shows a sketch of the temporary design with supporting piles parallel to the original columns.

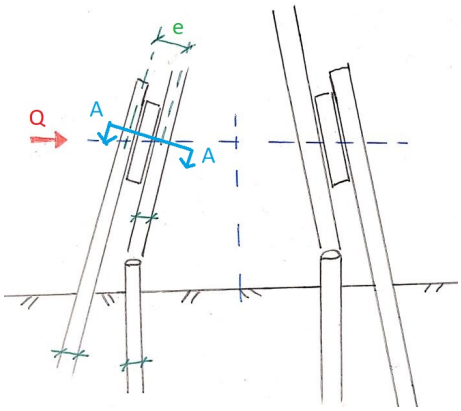

Figure D.9: The figure shows a sketch of the rehabilitation situation with a horizontal wind load Q. The eccentricity e between the supporting pile and the original column is marked in the sketch. A cross-section A-A is marked in blue.

If the wind, marked with a horizontal red arrow, acts as shown in Figure D.9, the wind load gives shear and bending moment in the structure. But the wind might change direction and act normal to the sketch. This will create a moment of torsion in the cross-section A-A marked in the sketch as shown in Figure D.10.

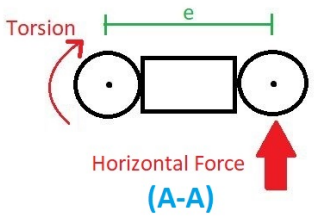

Figure D.10: Illustration of imposed torsion when the force has an eccentricity to the cross-section. The figure is in the xy-plane. The shear and axial forces are not shown in this figure.

The distance between the supporting pile and chord in post is approximately 0.4 m [7]. The eccentricity e is the distance between the center of the two

piles. Assuming diameter of $300mm$ for original pile and $200mm$ for supporting pile the eccentricity e is approximately 0.6 m. The horizontal wind load Q_w of 88.2 kN gives a horizontal force F_h of 22 kN in each pile.

The moment of torsion T in the supporting pile due to the horizontal wind load F_h for each pile, is:

$$T = F_h \cdot e = 13\,\text{kNm}$$

Kristin Enevoldsen

Rehabilitation of Cableway Posts, Longyearbyen

NTNU
Norwegian University of
Science and Technology

UNIS
The University Centre in Svalbard